Engineering of phosphoserine aminotransferase and new metabolic pathways for microbial production of 1,3-propanediol and 1,2,4-butanetriol from sugar

Vom Promotionsausschuss der
Technischen Universität Hamburg

zur Erlangung des akademischen Grades
Doktor der Naturwissenschaften (Dr. rer. nat.)

genehmigte Dissertation

von
Yujun Zhang

aus
Shandong, China
2020

Gutachter:

Prof. Dr. An-Ping Zeng

Prof. Dr. Andreas Liese

Prüfungsausschussvorsitzender:

Prof. Dr. Frerich Keil

Tag der mündlichen Prüfung:

17. Februar 2020

Acknowledgements

First of all, I would like to sincerely thank my supervisor, Prof. Dr. An-Ping Zeng, for giving me the opportunity to learn at the Institute of Bioprocess and Biosystems Engineering, and for his support, guidance, patience and trust during the past four years. The knowledge and experience that I have gained will be valuable for my career.

I would like to express my gratitude to Prof. Dr. Andreas Liese for being a member of my thesis committee and for his helpful comments and suggestions about my thesis. I would also like to thank the Chair of the committee, Prof. Dr. Frerich Keil.

I would like to thank Dr. Chengwei Ma for his work in protein engineering and protein structure analysis. I also thank my master student M. Sc. Antu Thomas for working on 1,2,4-butanetriol pathway. I would also like to thank Dr. Lin Chen for the construction of a homoserine-producing *E. coli*. I would also like to thank Dr. Wei Wang and Anna Gorte for giving me helpful supports on the identification of some key components by HPLC and GC, and Dr. rer. nat. Heike Frerichs and Dipl.-Ing. Andrea Simon from the *Zentrallabors Chemische Analytik* in TUHH for helping me with the GC-MS analyses. Many thanks to Sukanya R. Sekar, Sibel Ilhan, and Ludwig Selder for their help with the English and the German language in writing this thesis. Without their generous support, it would be difficult for me to finish everything in a relatively easy way.

I would also like to express my gratitude to other IBB members that were always willing share their experience with me and supported me in many ways: Dr. Uwe Jandt, Dr. Wael Sabra, Mrs. Cornelia Hoffmann, Jan Sens, Olaf Schmidt, Jan Bomnüter, Birgit Stacks, Dr. Feng Geng, Dr. Libang Zhou, Dr. Lifu Song, Jin Guo, Minliang Chen, Yongfei Liu, Dr. Rebekka Schmitz, Dr. Tyll Utesch, Dr. Anibal Mora, Dr. Christin Groeger, Yaeseong Hong, Philipp Arbter, Cornelius Jacobi, Jonas Heuer. I am grateful to Prof. Dr.-Ing. Ralf Pörtner and all the members of his group.

In the end, I would like to thank my friends and family for their love and support throughout this thesis work.

Abstract

1,3-Propanediol (1,3-PDO) is an important chemical compound with lots of applications in the fields of polymers, cosmetics, food and pharmaceutical. The significant advances of metabolic engineering in the past thirty years have made it possible to develop efficient industrial strains to synthesize 1,3-PDO from different resources. A milestone for microbial production of 1,3-PDO is the DuPont Tate & Lyle process from sugar via glycerol. To circumvent the use of expensive vitamin B_{12} in the 'glucose-glycerol-PDO' process, a completely new homoserine-derived 1,3-PDO pathway was developed by Chen et al. (2015) in our lab. In this pathway, 1,3-PDO is produced from L-homoserine via three heterologous enzymatic reactions. The bottleneck step is the first deamination step of L-homoserine to 4-hydroxy-2-oxobutanoic acid (HOBA).

In this work, a phosphoserine aminotransferase (SerC) from *E. coli* was investigated and engineered to achieve the crucial deamination of L-homoserine. To alter the substrate specificity of SerC from L-phosphoserine to L-homoserine, a computation-based rational method was firstly implemented. Key residues responsible for the substrate binding specificity were identified by calculating the binding free energy based on molecular dynamics simulations and this was followed by *in silico* site-directed saturation mutagenesis. After three rounds of screening, a few candidates were selected and experimentally verified. The specific activity of the best mutant, SerC(R42W-R77W), was improved by 4.2-fold towards L-homoserine in comparison to the wild type, while its activity towards the natural substrate L-phosphoserine was decreased by 43-fold.

However, the improvement of SerC is still not satisfactory. Considering the limitations of rational design, other screening strategies have also been developed in order to achieve better mutants of SerC. Apart from the method of site-directed mutagenesis, random mutagenesis and semi-rational design method were also used to generate larger

and more diverse libraries of mutants. Afterwards, three different strategies were employed to screen the mutant libraries: a) generation and use of glutamate-dependent auxotrophic strain; b) GDH-coupled photometric detection; and c) mercaptopyruvate sulfurtransferase (MPST)-coupled colorimetric screening. Finally, a better mutant SerC(R42W-R77W-R329P) was identified. This mutant showed an increased activity towards L-homoserine by 5.5-fold compared to the wild type and its activity towards L-phosphoserine was completely deactivated. With 3 mM L-homoserine as the substrate, the K_m of SerC(R42W-R77W-R329P) was decreased by 68-fold compared to that of the wild type.

To examine the performance of the improved SerC, the complete "homoserine to 1,3-PDO" pathway was constructed by combining SerC with pyruvate decarboxylase (PDC) and alcohol dehydrogenase (YqhD) and introduced into *E. coli*. To enhance the L-homoserine supply, a homoserine-producing strain was constructed by overexpressing aspartate kinase III (LysC) and homoserine dehydrogenase (MetL) with a medium-copy plasmid. In addition, the genes *ldh*A and *adh*E encoding lactate dehydrogenase and aldehyde/alcohol dehydrogenase, respectively, were also removed from the *E. coli* genome to increase NADH supplementation and decrease byproduct formation under oxygen-limited conditions. Finally, the engineered recombinant *E. coli* was tested for 1,3-PDO production in both shake flask and fed-batch fermentation. The mutant strain, S147, was able to produce 3.03 g/L 1,3-PDO after 62 h of fermentation, which is 13-fold higher than the wild type strain (S144, 0.24 g/L).

Given the largely improved performance of the engineered SerC for 1,3-PDO production, a new pathway for 1,2,4-butanetriol (BT) biosynthesis, was also constructed from L-homoserine. BT is best-known as a precursor for the production of 1,2,4-butanetriol trinitrate (BTTN), which is of interest as propellant and energetic plasticizer. The new BT pathway involves five consecutive enzymatic reactions catalyzed by four heterologous enzymes, including an engineered SerC, a lactate dehydrogenase, a 4-hydroxybutyrate CoA-transferase and an aldehyde/alcohol

dehydrogenase. Implementation of this new pathway in an engineered *E. coli* resulted in a production of up to 19.6 ± 5.9 mg/L BT in fed-batch fermentations, which is much higher than that (120 ng/L) reported in literature for the production route from L-malate.

In summary, different strategies were employed to develop SerC with an increased activity towards L-homoserine and mutants with improved performance were successfully identified. By integrating these SerC mutants into the homoserine-derived 1,3-PDO pathway and the new BT pathway, their production can be dramatically increased. These studies also provide a basis for developing potential microbial processes for other homoserine-derived biosynthetic pathways.

Zusammenfassung

1,3-Propandiol (1,3-PDO) ist eine wichtige chemische Substanz, die vielfältige Anwendung im Bereich der Polymere, Kosmetika und Pharmazie findet. Die maßgeblichen Entwicklungen des Metabolic Engineering in den letzten 30 Jahren ermöglichen die Entwicklung effizienter Stämme für die Produktion von 1,3-PDO aus verschiedenen Ausgangsstoffen. Ein Meilenstein in der mikrobiellen Produktion von 1,3-PDO ist der Prozess von DuPont & Tate and Lyle, der ausgehend von Zuckern über Gylcerol verläuft. Um die Verwendung des teuren B_{12} Vitamins im Zucker-Glycerol-PDO Prozess zu vermeiden, wurde von Chen et al. (2015) ein komplett neuer Stoffwechselweg entwickelt, in dem die PDO Generierung über L-Homoserin erfolgt. In diesem Stoffwechselweg wird 1,3-PDO mittels dreier heterologer enzymatischer Reaktionen aus L-Homoserin gewonnen. Der Engpass dieses Stoffwechselweges ist die erste Deaminierung von L-Homoserin zu 4-Hydroxy-2-oxobutansäure (HOBA).

In dieser Arbeit wurde eine Phosphoserineaminotransferase (SerC) aus *E. coli* untersucht und so modifiziert, dass die notwendige Deaminierung von L-Homoserin erzielt wird. Um die Substratspezifität von SerC von L-Phosphoserin zu L-Homoserin zu ändern, wurde eine rationale computergestützte Methode angewandt. Die entscheidenden Reste von SerC, die verantwortlich sind für die Substratspezifität, wurden identifiziert, indem die freie Bindungsenergie über Moleküldynamiksimulationen bestimmt wurde. Anschließend wurde eine ortsgerichtete Mutagenese *in-silico* durchgeführt. Nach insgesamt drei Screeningdurchgängen wurden die vielversprechendsten Kandidaten ausgewählt und experimentell verifiziert. Die spezifische Aktivität bezüglich L-Homoserin der am besten geeigneten Mutante, SerC(R42W-R77W), wurde um das 4,2-fache verbessert im Vergleich zum Wildtyp, wobei die spezifische Aktivität von L-Phosphoserin um das 43-fache gesenkt wurde.

Jedoch ist die Verbesserung von SerC noch nicht zufriedenstellend. Durch die

Limitationen des rationalen Design-Konzepts, war es notwendig auch andere Mutation und Screening Methoden zu entwickeln, um bessere SerC Mutanten zu erzeugen. Neben der ortsgerichteten Mutagenese wurden auch die zufällige Mutagenese und die semi-rationale Design Methode angewandt, um eine größere und diversere Mutantenbibliothek zu generieren. Im Anschluss wurden drei verschiedene Strategien benutzt, um die Mutantenbibliothek zu screenen:

a) Konstruktion und Anwendung eines glutamatabhängigen auxotrophen Stammes
b) GDH gekoppelte photometrische Detektion
c) Mercaptopyruvatsulfurtransferase (MPST) gekoppeltes kolorimetrisches Screening

Schlussendlich wurde eine verbesserte SerC Mutante identifiziert (R42W-R77W-R329P). Diese Mutante zeigte im Vergleich zum Wildtyp eine 5,5-fach erhöhte Aktivität bezüglich L-Homoserin und keine Aktivität gegenüber L-Phosphoserin. Die K_M Konstante von SerC (R42W-R77W-R329P) wurde um das 68-fache gesenkt im Vergleich zum Wildtyp bei einer Substratzugabe von 3 mM L-Homoserin.

Um die Leistung der verbesserten SerC Mutante zu untersuchen, wurde der komplette Stoffwechselweg von L-Homoserin zu 1,3-PDO konstruiert, indem SerC mit einer Pyruvatdecarboxylase (PDC) und Alkoholdehydrogenase (YqhD) kombiniert und in *E. coli* eingebracht wurde. Die Bereitstellung von L-Homoserin als Substrat wurde dadurch verbessert, dass ein homoserinproduzierender Stamm konstruiert wurde, indem eine Aspartatkinase III (LysC) und eine Homoserindehydrogenase (MetL) mit einem medium-copy Plasmid überexprimiert wurden. Zusätzlich wurden die codierenden Gene *ldhA* für die Lactatdehydrogenase und *adhE* für die Aldehyd/Alkoholdehydrogenase aus dem Genom von *E. coli* entfernt, um die NADH Bereitstellung zu fördern und die Bildung von Nebenprodukten unter sauerstofflimitierten Bedingungen zu senken. Schlussendlich wurde der gentechnisch veränderte rekombinante *E. coli* Organismus in Schüttelkolben und fed-batch

Kultivierungen auf 1,3-PDO Produktion untersucht. Der mutante Stamm von *E. coli* (S147) erzielte eine 1,3-PDO Konzentration von 3,03 g/L nach 62 h Kultivierung. Dies ist 13mal höher als die Endkonzentration des Wildtypstammes (S144, 0,24 g/L).

Aufgrund der stark gesteigerten Leistung der gentechnisch veränderten SerC Mutante für die 1,3-PDO Produktion wurde ein neuer Stoffwechselweg für die biosynthetische Erzeugung von 1,2,4-Butantriol (BT) ausgehend von L-Homoserin konstruiert. BT ist am bekanntesten als Ausgangsstoff für die Herstellung von 1,2,4-Butantrioltrinitrat (BTTN), was als Treibstoff und Weichmacher verwendet wird. Der neue Stoffwechselweg umfasst fünf konsekutive enzymatische Reaktionen, die von vier heterologen Enzymen katalysiert werden. Darunter befindet sich eine gentechnisch veränderte SerC Mutante, eine Lactatdehydrogenase, eine 4-Hydroxybutyrat-CoA-transferase und eine Aldehyd/Alkoholdehydrogenase. Das Einbringen dieses Stoffwechselweges in *E. coli* erzielte einen Produkttiter von 19,6 ± 5,9 mg/L BT in einer fed-batch Kultivierung, was deutlich höher, als der in der Literatur veröffentlichte Wert von 120 ng/L ausgehend von L-Malat, ist.

Zusammenfassend kann man sagen, dass verschiedenste Strategien angewandt wurden, um eine SerC Mutante mit einer erhöhten Aktivität gegenüber L-Homoserin zu entwickeln und diese erfolgreich identifiziert werden konnten. Indem diese SerC Mutanten in den Homoserin basierten 1,3-PDO und den neuartigen BT Stoffwechselweg eingebaut wurden, konnte die jeweilige Produktionsleistung drastisch erhöht werden. Diese Untersuchungen bilden zudem die Grundlage für die Entwicklung potenzieller mikrobieller Produktionswege, die ebenfalls auf biosynthetischen L-Homoserin basierten Stoffwechselwegen fußen.

TABLE OF CONTENTS

Abbreviations

AAAs	aromatic amino acids
AKIII(LysC)	aspartate kinase III
AMG	alpha methyl-L-glutamic acid
APAD	acetylpyridine adenine dinucleotide
AroG	3-deoxy-D-arabino-heptulosonate-7-phosphate synthase
AspC	aspartate transaminase
BT	1,2,4-butanetriol
BTTN	1,2,4-butanetriol trinitrate
Cas9	Cas protein 9
CGSS	growth-coupled and sensor-guided *in vivo* screening
CRISPR	Clustered Regularly Interspaced Short Palindromic Repeats
CRISPRi	CRISPR interference
crRNA	CRISPR RNA
DHAP	dihydroxyacetone phosphate
DHB	2,4-dihydroxybutarate
E. coli	*Escherichia coli*
FACS	fluorescene-activated cell sorting
FDA	Food and Drug Administration
GDH	glutamate dehydrogenase
GOGAT	glutamine synthetase-glutamate synthase
HOBA	4-hydroxy-2-oxobutanoate
MD	molecular dynamics
MM/GBSA	molecular mechanics/generalized Born surface area
MSA	multiple sequence alignment
N20	a user-defined 20-bp complementary region
PAM	protospacer-adjacent motif
PBPM	position-based prediction method

PDC	pyruvate decarboxylase
PEP	phosphoenolpyruvate
PLP	pyridoxal phosphate
PPP	pentose phosphate pathway
PTS	phosphotransferase system
PTT	polytrimethylene terephthalate
RMSD	root-mean-square deviations
RMSF	root-mean-square fluctuations
SASA	solvent-accessible surface area
SerC	phosphoserine transaminase
sgRNA	single synthetic guide RNA
SucD	succinate semialdehyde dehydrogenase
tracrRNA	trans-activating crRNA
VDW	van der Waals
YqhD	alcohol dehydrogenase
1,2-PDO	1,2-propanediol
1,3-PDO	1,3-propanediol
1,4-BDO	1,4-butanediol
2,3-BDO	2,3-butanediol
3-HPA	3-hydroxypropionaldehyde
4-HB	4-hydroxybutyrate
4HBd	4-hydroxybutyrate dehydrogenase

CHAPTER 1 Introduction and objectives

1.1 Introduction

Oil, natural gas and coal are the primary raw materials for bulk chemicals, polymers and many other products that improve our overall living standard. However, the environment problems caused, volatile fossil-energy price and the non-renewable fossil feedstocks have led to growing concerns in society and push people to search and develop more sustainable processes for value-added chemicals from renewable feedstocks. In recent years, industrial biotechnology offers a sustainable approach to manufacturing chemicals from renewable feedstocks instead of petroleum-based raw materials.

Microorganisms have evolved over billions of years to utilize a broad range of renewable feedstocks, including carbohydrates, glycerol, fatty acids and even one-carbon (C1) compounds, for chemical production. In the past thirty years, significant advances in enzyme engineering, metabolic engineering, synthetic biology and computational systems biology allow us to exploit and speed up the application of microorganisms, such as *Escherichia coli* (*E. coli*) and *Saccharomyces cerevisiae*, for production of bulk chemicals. Major achievements in recent years include microbial productions of amino acids like L-valine (Park et al., 2007), L-threonine (Lee et al., 2007), L-lysine (Becker et al., 2011) and L-arginine (Park et al., 2014), bulk chemicals like 1,3-propanediol (Nakamura and Whited, 2003), 1,4-butanediol (Yim et al., 2011) and succinic acid (Lee et al., 2006) and the antimalarial drug artemisinin (Paddon et al, 2013).

1.1.1 Bioproduction of 1,3-propanediol

1,3-Propanediol (1,3-PDO) is an important chemical compound with many applications in polymers, cosmetics, food and pharmaceutical industries (Saxena et al., 2009; Kaur

et al., 2012; Zeng and Biebl, 2002) (Figure 1.1). Currently, 1,3-PDO is mainly used in the manufacture of polytrimethylene terephthalate (PTT). The superior characteristics of PTT lead in turn to a drastic rise in the demand of 1,3-PDO (Kurian, 2005; Kraus, 2008; Zeng and Sabra, 2011; Kaur et al., 2012; Zeng, 2019). To date, several routes have been developed for the synthesis of 1,3-PDO, including the chemical routes from acrolein (Lawrence and Sullivan, 1972) or ethylene oxide (Brown et al., 2000). However, high pressure and temperature, expensive catalysts and toxic intermediates limit their applications in industrial scale.

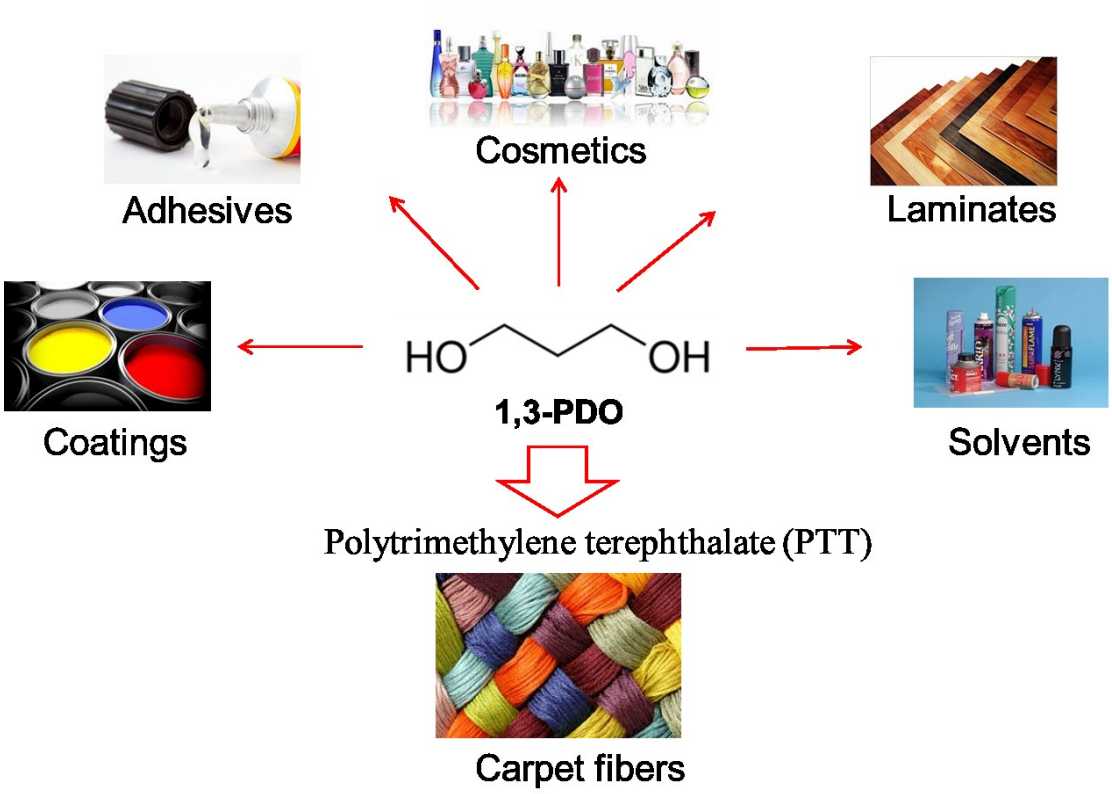

Figure 1.1. Structure of 1,3-propanediol (1,3-PDO) and its applications.

It has been known for a long time that 1,3-PDO can be produced from glycerol in some bacterial strains, like *Clostridium pasteurianum* (Groeger et al., 2016; Schmitz et al., 2019; Utesch et al., 2019;), *Klebsiella pneumonia* (Tong et al., 1991), *Citrobacter freundii* (Boenigk et al., 1993), *Clostridium butyricum* (Biebl, 1991), *Enterobacter agglomerans* (Barbirato et al., 1995) and *Lactobacillus brevis* (Schütz and Radler,

1984). However, no natural strains have been discovered to convert glucose directly to 1,3-PDO (Cameron et al., 1998). Therefore, most studies focus on the 'glycerol to 1,3-PDO' or 'glucose to 1,3-PDO via glycerol' pathways. Among them, the state-of-the-art achievement was the DuPont Tate & Lyle process (Nakamura and Whited, 2003). In their process, a heterologous carbon pathway that diverts carbon from dihydroxyacetone phosphate (DHAP) to 1,3-PDO was introduced into an engineered strain. The heterologous carbon pathway involved genes from *S. cerevisiae* for glycerol production from DHAP and the genes from *K. pneumoniae* for 1,3-PDO production from glycerol. This recombinant *E. coli* reached a final 1,3-PDO concentration of 135 g/L using glucose as the substrate. The productivity was 3.5 g/L/h and the efficiency of substrate conversion reached 51%. However, the glycerol-dependent pathway suffers from the requirement of exogenous addition of coenzyme B_{12} into the reactor because of the B_{12}-dependent GDHt used in this pathway. To circumvent patents associated with the glucose-glycerol-PDO pathway, alternative pathways which are glycerol-independent and thus do not require the addition of coenzyme B_{12} are desired for the biosynthesis of 1,3-PDO.

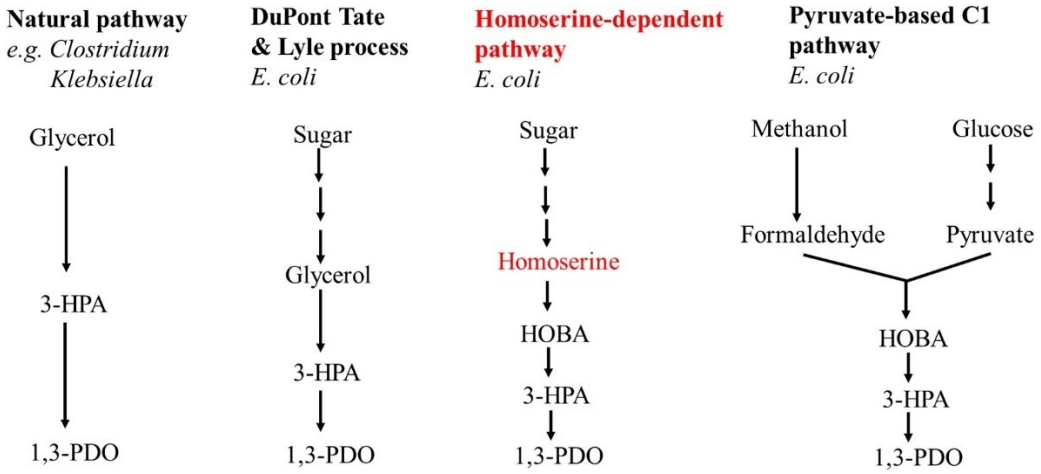

Figure 1.2. Natural and synthetic metabolic pathways for 1,3-PDO production reported in literature. 3-HPA: 3-hydroxypropionaldehyde; HOBA: 4-hydroxy-2-oxobutanoate; 1,3-PDO: 1,3-propanediol; C1: one-carbon. (Adapted from Figure 1 in Celińska 2015)

Recently, a completely new homoserine-derived pathway has been developed for

microbial 1,3-PDO production, which is realized by extending the L-homoserine biosynthesis pathway via three heterologous enzymatic reactions: (i) deamination of L-homoserine to 4-hydroxy-2-oxobutanoic acid (HOBA) using an engineered glutamate dehydrogenase (GDH); (ii) decarboxylation of HOBA into 3-hydroxypropionaldehyde (3-HPA); and (iii) reduction of 3-HPA into 1,3-PDO (Chen et al., 2015; Geng et al., 2017) (Figure 1.2). As a new pathway, the capability of 1,3-PDO production is hampered by the deamination step of L-homoserine to HOBA. Although there are several natural transaminase and dehydrogenase reported in literature exhibiting certain ability of utilizing L-homoserine, their poor catalytic performance still limits their usage in this non-natural synthetic metabolic pathway (Chen et al., 2015; Soucaille, 2012; Walther et al., 2018; Frazão et al., 2018; Zhong et al., 2019).

More recently, Wang et al. (2019) demonstrated a pyruvate-based C1 metabolic pathway to synthesize 1,3-PDO from methanol or formaldehyde and glucose (Figure 1.2). The production of 1,3-PDO was 508.3 ± 9.1 and 32.7 ± 0.8 mg/L when formaldehyde and methanol were used as co-substrate of glucose, respectively.

1.1.2 Bioproduction of 1,2,4-butanetriol

1,2,4-Butanetriol (BT) is a compound with many applications in pharmaceuticals, polymer materials and military field (Bhoge et al., 2012; Niu et al., 2003). Among the various applications, BT is best-known as a precursor for the production of 1,2,4-butanetriol trinitrate (BTTN) in the military field. BTTN can be used as propellant and energetic plasticizer. It is less hazardous, more thermally stable, less shock sensitive, and less volatile than nitroglycerin (Abdel-Ghany et al., 2013; Niu et al., 2003; Sun et al., 2016). BTTN is also used in the synthesis of growth factors (Xu et al., 2004) and other pharmaceutical compounds that have antiviral and anticancer applications (Solladie et al., 1998; Sato et al., 2003).

BT is traditionally manufactured by reducing esterified malic acid using $NaBH_4$ under harsh conditions (Ikai et al., 2005; Bal'zhinimaev et al., 2017). This chemosynthetic

route produces a variety of byproducts and for each ton of BT synthesized, multiple tons of byproducts are generated (Frost and Niu, 2011). As a result, more economical and environmentally safer, biosynthetic techniques have recently been examined for BT production.

Microbial synthesis of BT from D-xylose or L-arabinose was firstly reported by Niu et al. (2003). In this new pathway, D-xylose was first oxidized to D-xylonic acid by *Pseudomonas fragi*. Then D-xylonate dehydratase from *E. coli* was employed for the conversion of D-xylonic acid into D-3-deoxy-glyceropentulosonic acid. Subsequently, D-3-deoxy-glyceropentulosonic acid was converted to D-3,4-dihydroxybutanal by benzoylformate decarboxylase isolated from *Pseudomonas putida* and then transformed to BT by alcohol dehydrogenases from *E. coli*. Li et al. (2014) designed a new artificial pathway for biosynthesis of BT from glucose. This novel BT pathway consists of six heterologous enzymatic reactions starting from L-malate and 2,4-dihydroxybutarate (DHB) is an important intermediate in this pathway. Since the formation of DHB can be achieved by the reduction of HOBA, BT is a possible end-product derived from L-homoserine. As a key step in this novel “homoserine to BT” pathway, the production of BT is also considered to be strongly dependent on the deamination of L-homoserine to HOBA.

1.1.3 Strategies for strain development

To get rid of the limitations of wild type enzymes, two complementary strategies can be employed in enzyme engineering: directed evolution and rational design. Directed evolution of enzymes can be achieved by introducing random mutations in protein sequences (e.g. Error-prone PCR) (Chen and Arnold, 1993; Bloom and Arnold, 2009; Romero and Arnold, 2009; Chen and Zeng, 2016). Though no structural information is needed in this method, a large number of mutants have to be screened and this makes it laborious and time-consuming. Normally, a cheap, fast and reliable high-throughput screening is necessary when the directed evolution approach is employed. Rational

design takes advantage of the knowledge of enzyme 3D structure, function and catalytic mechanism to modify the amino acid sequence of a protein using site-directed mutagenesis (Lutz, 2010; Bommareddy et al., 2014; Chen and Zeng, 2016). The advantages of rational design include a significant reduction of the mutant library size, an increased probability of beneficial mutations, less efforts and time-saving for screening. This is especially advantageous when the protein structure is reported and no high-throughput screening method for engineered enzymes exists.

To date, *E. coli* is the most widely used host organism for production of many complex compounds and serves as the prime prokaryotic genetic model because of its well-characterized genetics, well-adapted to the laboratory environment and Food and Drug Administration (FDA)-approved status for human applications (Marisch et al., 2013; Tang and Zhao, 2009). Though the wild type *E. coli* has no capacity to produce 1,3-PDO, *E. coli* has become the most thoroughly exploited heterologous system for 1,3-PDO production. L-Homoserine, as a metabolic intermediate and precursor for 1,3-PDO and BT, is used for the biosynthesis of L-threonine and L-methionine and does not accumulate during the cultivation of wild type *E. coli*. Thus, specific studies into the construction of homoserine-producing strain based on rational metabolic engineering of *E. coli* should be conducted. Li et al. (2016) successfully constructed a high homoserine-producing strain from the wild type *E. coli* W3110 via several strategies, such as blocking the competing and degradation pathways, deregulating feedback inhibition and increasing export fluxes. The resulting strain could produce 39.54 g/L L-homoserine in fed-batch fermentation, indicating its potential use in the new “homoserine to 1,3-PDO” and “homoserine to BT” pathways.

1.2 Objectives

The main goal of this thesis is to further optimize the new homoserine-derived 1,3-PDO pathway and construct a non-natural homoserine to BT pathway using glucose as the substrate. Specifically, the challenge is to improve the activity of phosphoserine

transaminase (SerC) towards L-homoserine and at the same time to deactivate its activity towards its natural substrate L-phosphoserine. The engineered SerC should help to achieve a more efficient deamination of L-homoserine to HOBA, which is the bottleneck of both the homoserine-derived 1,3-PDO pathway and the BT pathway.

For this purpose, a computation-based rational approach should be first used to alter the substrate specificity of SerC from L-phosphoserine to L-homoserine. In this approach, molecular dynamics simulations and virtual screening are to be combined to predict mutation sites. To obtain a suitable mutant SerC, directed evolution methods are to be applied to build large mutant libraries and new screening strategies are to be developed.

Strain development is necessary for the 1,3-PDO and BT production after an improved SerC is obtained. As the starting material, sufficient supplement of L-homoserine *in vivo* is necessary. To avoid the production of byproducts such as ethanol and lactate, some genetic modifications on *E. coli* are desired. Finally, the performance of the obtained mutant(s) of SerC are to be studied in bioreactor for 1,3-propanediol and BT production, respectively.

CHAPTER 2 Theoretical and technological background

This section is a short review of metabolic engineering of *E. coli*, protein design for industrial strain development and engineering of *E. coli* for 1,3-PDO and BT production. Strategies used for protein design are described, as well as the status of the 1,3-PDO and BT biosynthesis in *E. coli*.

2.1 Metabolic engineering of *E. coli* for biosynthesis

2.1.1 *E. coli* as a host strain

As a gram-negative, facultative anaerobic bacterium, *E. coli* has become one of the best studied organisms over the past century. *E. coli* is an ideal platform host for both laboratory and industrial purposes because of its advantages for metabolic engineering.

Firstly, *E. coli* has a short doubling time and can easily adapt to different growth conditions. Secondly, well studied biochemistry and physiology of *E. coli* and many efficient genetic manipulation tools make it the first choice as a host strain. In *E. coli*, there are extensive regulatory mechanisms controlling various metabolic pathways. In addition to the metabolic network itself, these extensive regulatory mechanisms also play a crucial role in metabolic engineering. In the following part, some regulation mechanisms and features in *E. coli* physiology that are relevant to metabolic engineering will be discussed.

E. coli can utilize several compounds such as glucose, xylose and glycerol as carbon sources. Compared to glucose, the uptake of xylose by *E. coli* is significantly slower, and the anaerobic use of glycerol as substrate may need additional reducing equivalents to support redox-balanced production pathways for compounds such as ethanol or succinate (Dien et al., 2003; Dharmadi et al., 2005; Zeng, 2019). The rapid utilization of glucose depends on the phosphoenolpyruvate (PEP)-carbohydrate phosphotransferase system (PTS). PTS imports and phosphorylates glucose using PEP

as the phosphoryl group donor and provides a driving force for sugar uptake by converting PEP to pyruvate. Therefore, two pools of metabolites are generated during this process. One pool is the metabolites derived from PEP, including those of pentose phosphate pathway, the upper glycolysis and the TCA cycle. The other pool is the metabolites derived from pyruvate, including compounds derived from acetyl-CoA. There is a thermodynamic barrier between these two pools. The overproduction of a metabolite either from PEP-derived pool or pyruvate-derived pool may face limitations for its maximum yield, due to the availability of PEP or loss of carbon from pyruvate to acetyl-CoA step (Pontrelli et al., 2018).

As a facultative anaerobic bacteria, *E. coli* can grow and metabolize glucose with or without oxygen. With oxygen, *E. coli* can efficiently produce ATP using reducing equivalents via oxidative phosphorylation, which is favorable for its growth. While in the absence of oxygen, ATP production will be severely limited. The TCA cycle will be downregulated, leading to an incomplete oxidation of the carbon source. Under these conditions, fermentation byproducts such as ethanol, lactate, acetate and succinate are produced (Koebmann et al., 2002). The conversion of pyruvate to acetyl-CoA is catalyzed primarily by two separate reactions: pyruvate dehydrogenase, works under aerobic conditions producing one molecule of NADH and CO_2 and pyruvate formate-lyase, works under anaerobic conditions producing formate.

When engineering *E. coli* for production of desired chemicals, especially producing reduced compounds under anaerobic conditions, it is very important to make sure that sufficient cofactors are supplied. Several methods have been demonstrated for this purpose. For example, increasing NADH supply by the oxidization of formate into CO_2 using NAD^+-dependent formate dehydrogenase (Berríos-Rivera et al., 2002), changing enzyme's preference of NADH and NADPH through protein engineering (Brinkmann-Chen et al., 2013; Cahn et al., 2018) or deleting certain genes to divert carbon flux (Siedler et al., 2011).

2.1.2 Strategies and tools for metabolic engineering

Metabolic engineering has become more and more important in developing microbial cell factories for the biosynthesis of value-added chemicals. Various metabolic engineering strategies and tools have been employed for strain development. They include construction of novel metabolic pathways (Chen et al., 2015), fine-tuning and control of gene expression (Yim et al., 2011), genome engineering (Chae et al., 2015), directed cell evolution (LaCroix et al., 2015) and improving the tolerance to certain chemicals (Park et al., 2014), and so on (Figure 2.1).

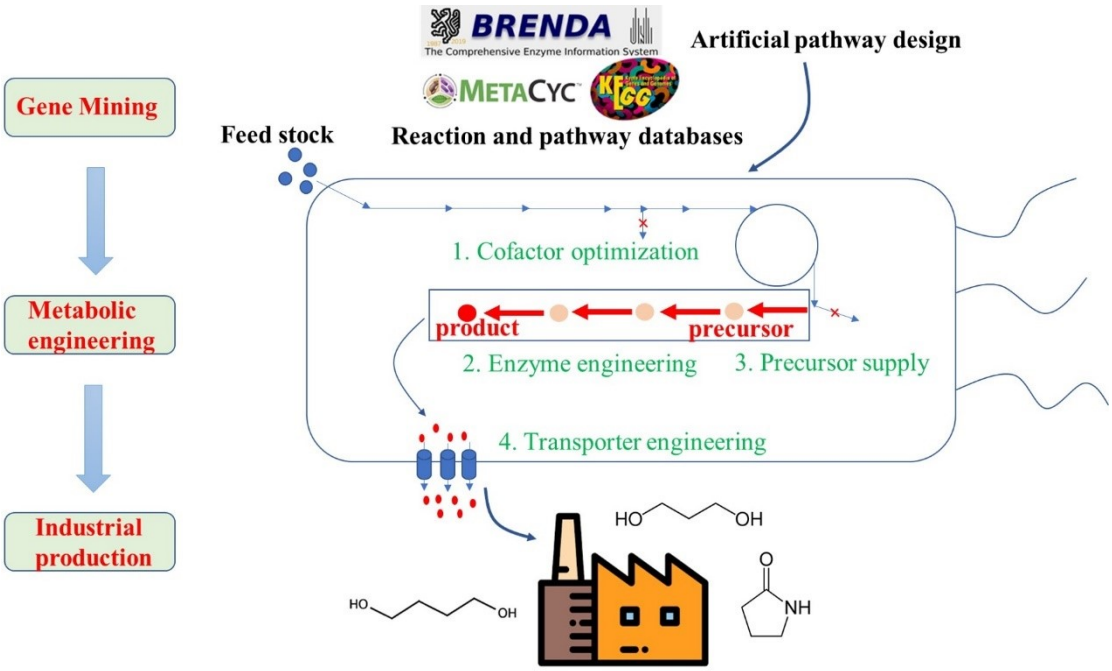

Figure 2.1. Simplified scheme of developing microbial cell factories.

To construct a novel metabolic pathway in *E. coli*, one approach is to combine genes from different organisms and design a new set of metabolic pathways to produce desired product. The host strain *E. coli* only provides precursors and cofactors from its own primary and secondary metabolisms, and the precursors are subsequently converted to the target product through the expression of the heterologous genes.

To modify the genome of *E. coli*, several genetic tools can be used. The lambda red

recombination system based on homologous recombination of linear fragments is a well-known and classic way for genome modification (Datsenko and Wanner, 2000). CRISPR/Cas9 is a new and fast-growing strategy for genomic modification (Cong et al., 2013; Qi et al., 2013; Kim et al., 2017; Cress et al., 2017; Chen et al., 2019). These two methods will be described in details in the following section.

While gene deletions give a reliable genetic manipulation in cells, it also means a removal of gene expression. But in reality, transcriptional regulation for modulate expression is necessary for metabolic engineering. The most commonly used approach to adjust the gene expression is to replace its native promoter with a foreign one. However, the promoter replacement based on homologous recombination is labor- and time-consuming and suffers from low throughput. Currently, many new RNA-based strategies have been developed to control gene expression, such as the use of riboswitches (Zhou and Zeng, 2015), CRISPR interference (CRISPRi) (Cress et al., 2017), small transcriptional activating RNAs (STARs) (Chappell et al., 2017) and synthetic small regulatory RNAs (sRNAs) (Na et al., 2013). Riboswitches are natural RNA elements that regulate gene expression by binding a ligand. Zhou and Zeng (2015) generated a synthetic lysine-ON riboswitch from a natural *E. coli*-sourced lysine-OFF riboswitch and it was successfully used for improving L-lysine production in *Corynebacterium glutamicum*. CRISPRi is a genetic technique that allows for sequence-specific repression of gene expression in cells. In one study, CRISPRi was used to down-regulate the competing pathways to enhance butanol production (Kim et al., 2017).

2.1.3 Recent progress in strain engineering

2.1.3.1 Amino acids production

Amino acids, such as L-lysine, L-tryptophan, L-threonine and L-methionine, are important bioproducts with many industrial applications in pharmaceutical, animal feed, nutritional supplements as well as cosmetic fields (Zhou et al., 2011; Zhao et al., 2011;

Chen and Zeng, 2017). Microorganisms generally do not produce amino acids in surplus by regulating cellular metabolism. However, after great advance in metabolic engineering in the 1990s, microbial processes for producing amino acids from *E. coli* have increasingly been developed and commercialized (Baez-Viveros et al., 2004; Sprenger, 2007; Chavez-Bejar et al., 2008; Chen and Zeng, 2017). The rational engineering of the complex and highly regulated metabolic network combined with the advances of omics technology and genome-scale computational biology have replaced the traditional random mutagenesis and selection procedures in strain development. To date, all 20 amino acids can be produced using *E. coli* and several of them have been commercialized.

The L-threonine biosynthesis pathway involves five enzymatic reactions starting from L-aspartate in *E. coli*. The key step for L-threonine formation is the first step catalyzed by three aspartate kinase isoenzymes (AKI, AKII and AKIII). AKI encoded by *thr*A gene is inhibited by L-threonine and its synthesis is repressed by L-threonine and L-isoleucine. The synthesis of AKII (encoded by the *met*L gene) is repressed by L-methionine. AKIII encoded by *lys*C is inhibited by L-lysine. The AKI and AKII are bifunctional enzymes with both aspartate kinase activity and homoserine dehydrogenase activity. Lee et al (2009) removed the negative regulation of both feedback inhibition and transcriptional attenuation regulation by targeted metabolic engineering. On the basis of that, the target genes needed to be engineered were further identified using transcriptome profiling combined with *in silico* flux response analysis. Then their expressions were controlled at desirable levels accordingly. Finally, the engineered *E. coli* achieved a production of 82.4 g/L L-threonine in fed-batch fermentations, with a significant high yield of 0.393 g L-threonine/g glucose.

2.1.3.2 Bioproduction of diols

Short chain diols such as 1,3-propanediol (1,3-PDO) (Nakamura and Whited, 2003; Zeng and Sabra, 2011; Zhang et al., 2017), 1,2-propanediol (1,2-PDO) (Lee, et al.,

2016), 1,4-butanediol (1,4-BDO) (Yim et al., 2011), 1,3-butanediol (1,3-BDO) (Chen and Liu, 2016) and 2,3-butanediol (2,3-BDO) (Kim et al., 2017) are of great interest as platform chemicals. Owing to their unique structures, they are widely used as monomer for the synthesis of polymers. Currently, a variety of metabolic engineering strategies have been developed for the microbial production of diols. Among the various diols, the microbial production of 1,3-PDO in an engineered *E. coli* developed by DuPont Tate & Lyle is the most successful case. They created an industrial *E. coli* overproducing 1,3-PDO from glucose by introduction of glycerol pathway from *S. cerevisiae* and 1,3-PDO pathway from *K. pneumonia* (Nakamura and Whited, 2003). The resulting strain can produce 1,3-PDO with a titer of 135 g/L. However, except for some patents, little detailed scientific literature about this work has been published (Emptage et al., 2003).

1,4-BDO and 2,3-BDO are important C4 diols platform chemicals which can be used to manufacture polymers, solvents and fine chemicals. There are chemical routes or biotechnological pathways for 2,3-BDO production (Zeng and Sabra, 2011), whereas 1,4-BDO production only comes from fossil fuel stocks. As the development of synthetic biology and systematic metabolic engineering, renewable feedstocks-based biosynthesis of 1,4-BDO was realized by engineered *E. coli* (Yim et al., 2011). Yim et al. (2011) used an accurate genome-scale metabolic model of *E. coli* and biopathway prediction algorithms were employed to broadly survey and prioritize specific 1,4-BDO pathways that were predicted to lead to an optimal performance. In addition, metabolic engineering strategies for balancing energy and redox needs, and for elimination of potentially toxic byproducts were employed. Finally, the authors introduced and optimized two heterologous pathways for 1,4-BDO production in *E. coli*. The first heterologous pathway is the biosynthesis of 4-hydroxybutyrate (4-HB) from glucose. It starts from the TCA-cycle intermediate succinate, which is activated as succinyl-CoA by succinyl-CoA synthetase. Then the CoA derivative is converted to 4-HB via two sequential reduction steps catalyzed by CoA-dependent succinate semialdehyde dehydrogenase (SucD) and 4-hydroxybutyrate dehydrogenase (4HbD), respectively.

Both SucD and 4HbD are from *Porphyromonas gingivalis*. The second heterologous pathway is the conversion of 4HB to 1,4-BDO in *E. coli*, requiring two reduction steps, catalyzed by 4-hydroxybutyryl-CoA transferase from *P. gingivalis* W83 and aldehyde/alcohol dehydrogenase from *C. acetobutylicum*. The resulting strain can produce 1,4-BDO from glucose with a titer up to 18 g/L.

2.1.4 Metabolic engineering of *E. coli* for 1,3-propanediol production

1,3-PDO biosynthesis pathways have been intensively studied and are the targets of various patents or patent applications. As described above, the DuPont Tate & Lyle developed 1,3-PDO production process from glucose in a recombinant *E. coli* and it is so far the most successful commercial bio-based route. Given the importance and significance of this process, little detailed scientific literature about this work was disclosed and only patents were published. Using similar approaches, other research groups have constructed various *E. coli* strains for 1,3-PDO production from glucose via glycerol (Wang et al., 2007; Kaur et al., 2012). However, the addition of expensive coenzyme B_{12} into the medium during the cultivation is a serious disadvantage. Therefore, alternative pathways that are independent of coenzyme B_{12} for 1,3-PDO production are needed.

Wang et al. (2019) demonstrated a pyruvate-based C1 metabolic pathway for the biosynthesis of 1,3-PDO from methanol or formaldehyde and glucose. This novel pathway consists of four major enzymatic reactions: i) the oxidation of methanol to formaldehyde using a methanol dehydrogenase; ii) aldol condensation of formaldehyde with pyruvate into HOBA using 2-keto-4-hydroxybutyrate aldolase; iii) decarboxylation of HOBA to 3-HPA using a branched-chain alpha-keto acid decarboxylase, and iv) reduction of 3-HPA to 1,3-PDO using a NADH-dependent 1,3-PDO oxidoreductase. The feasibility of this novel 1,3-PDO pathway was confirmed both *in vitro* and in *vivo*. The formation of 1,3-PDO was significantly improved by reducing formate formation through knockout of the corresponding *frmA* gene.

A new homoserine-derived pathway for microbial 1,3-PDO production was reported (Soucaille and Boisart, 2012; Boisart, 2013; Chen et al., 2015; Chen et al., 2016). In their work, 1,3-PDO production was achieved by extending the L-homoserine biosynthesis pathway with three heterologous enzymatic reactions. The bottleneck of this pathway is the first step, the deamination of L-homoserine to 4-hydroxy-2-oxobutanoatec (HOBA) catalyzed by an engineered GDH. The yield of 1,3-PDO is quite low due to the limited activity of GDH toward L-homoserine. To improve the activity of GDH, Geng et al. (2017) used a position-based prediction method (PBPM) to re-engineer the active site of SerC for L-homoserine. Generally, the catalytic efficiency of an enzyme depends on the position of the substrate within its binding pocket (Malisi et al., 2012). Based on this, PBPM was proposed to re-engineer the binding pocket of enzymes towards a non-natural substrate. After identification of key residues that determine the substrate specificity, prediction of mutants with a higher activity towards L-homoserine was conducted by PBPM. Experimental results indicated that the specific activity of the obtained best mutant K92V was increased from 171 to 1328 μU/mg.

Except for dehydrogenase, several natural transaminases are also reported to be able to catalyze L-homoserine (Soucaille and Boisart, 2012; Walther et al., 2018; Frazão et al., 2018; Zhong et al., 2019). Zhong et al. (2019) combined aspartate transaminase (AspC) from *E. coli* with pyruvate decarboxylase (PDC) from *Zymomonas mobilis* and alcohol dehydrogenase (YqhD) from *E. coli* together and constructed an engineered *E. coli* which can produce 0.32 g/L 1,3-PDO from glucose. The titer of 1,3-PDO was further increased to 0.49 g/L by introducing a point mutation into the *pdc* gene and to 0.63 g/L by constructing a fusion protein between AspC and PDC.

As a positive candidate, the phosphoserine aminotransferase (SerC) from *E. coli* is investigated and engineered through protein engineering strategies in cooperation with Metabolic Explorer (France). The use of SerC for catalyzing L-homoserine into HOBA was firstly reported in their patents (Soucaille and Boisart, 2012; Boisart, 2013). SerC

belongs to the subgroup IV aminotransferases. Its natural substrate L-phosphoserine shows a very high similarity in structure to L-homoserine. More importantly, the 3D structure of SerC reported in literature makes it possible to take the advantage of rational design in order to alter the substrate specificity of SerC (Zhang et al., 2019).

Apart from engineering the dehydrogenase or transaminase to improve its activity toward L-homoserine, other metabolic engineering methods are also considered in the above-mentioned studies to increase the final production of 1,3-PDO. One strategy is to increase the supply of L-homoserine. Therefore, a homoserine-producing plasmid is introduced into *E. coli*. This plasmid can enhance the production of L-homoserine by overexpressing the genes of *lys*C and *met*L, which are key enzymes in the homoserine biosynthesis pathway in *E. coli*. To alleviate the consumption of L-homoserine *in vivo*, the *thr*B gene in the threonine biosynthesis pathway is deleted.

2.1.5 Metabolic engineering of *E. coli* for 1,2,4-butanetriol production

The biosynthesis of 1,2,4-butanetriol has been achieved using microorganisms from D-xylose and L-arabinose (Niu et al., 2003). The biotransformation process occurs in four steps catalyzed by four different enzymes (Figure 2.2). The first oxidation step is the conversion of D-xylose to D-xylonic acid catalyzed by D-xylose dehydrogenase (XDG) or L-arabinose to L-arabinonic acid by L-arabinose dehydrogenase (ADG). The second step is the dehydration of D-xylonic acid or L-arabinonic acid to the corresponding D- or L-3-deoxy-glyceropentulosonic acids, catalyzed by D-xylonate dehydratase (XDT) or L-arabinonate dehydratase (ADT), respectively. Then the D- or L-3-deoxy-glyceropentulosonic acids are decarboxylated by benzylformate decarboxylase (BFD) to form D- or L-3,4-dihydroxybutanal, which are converted to the corresponding D- or L-1,2,4-butanetriol enantiomer by dehydrogenase (DH) in the last step.

Thereafter, a series of genetic engineering strategies were employed to improve the production of BT from xylose in an engineered *E. coli* (Frost and Niu, 2011; Cao et al., 2015; Lu et al., 2016; Wang et al., 2018; Jing et al., 2018). Cao et al. (2015) constructed

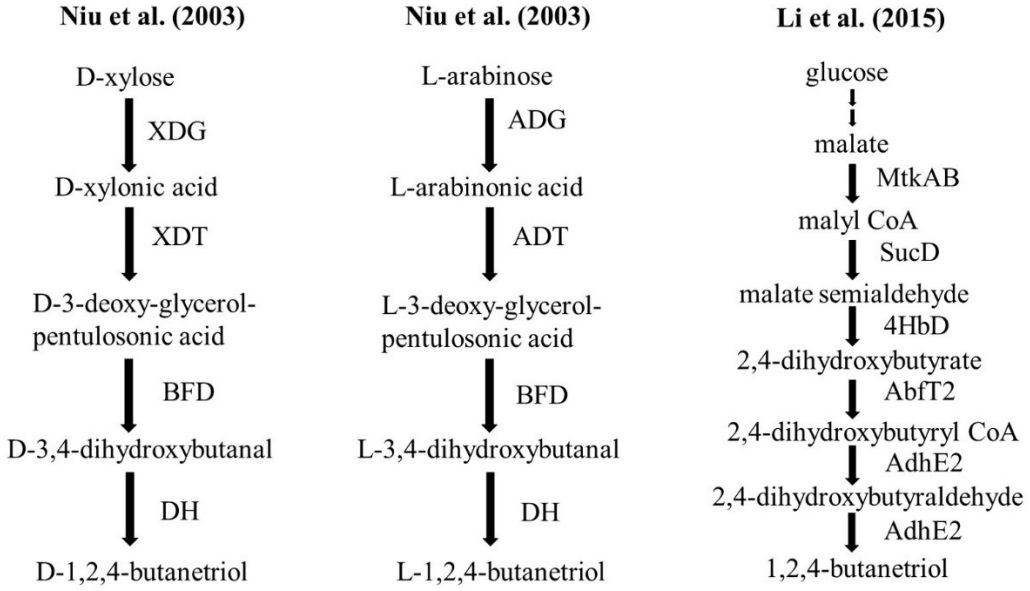

Figure 2.2. Biosynthetic pathways for 1,2,4-butanetriol production reported in literature. XDG: D-xylose dehydrogenase; XDT: D-xylonate dehydratase; BFD: benzylformate decarboxylase; DH: dehydrogenase; ADG: arabinose dehydrogenase; ADT: L-arabinonate dehydratase; MtkAB: malate thiokinase; SucD: succinate-semialdehyde dehydrogenase; 4HbD: 4-hydroxybutyrate dehydrogenase; AbfT2: 4-hydroxybutyrate CoA-transferase; AdhE2: bifunctional aldehyde/alcohol dehydrogenase.

an engineered strain by optimizing the co-expression of enzymes involved in the BT pathway from different microorganisms and blocking the competitive pathways that are responsible for xylose metabolism in *E. coli*. This resulted in up to 3.92 g/L of BT from 20 g/L of xylose under fed-batch conditions. In the study by Wang et al. (2018), BT pathway was optimized with the gene homolog screening strategy. Six aldehyde reductases, four 2-keto acid decarboxylases and four D-xylonate dehydratases were screened. The co-expression of these enzymes in recombinant *E. coli* led to 3.4 g/L BT production when using corncob hydrolysates as the substrate. Jing et al. (2018) modified the recombinant *E. coli* by multi-strategy to increase BT production. First, the 2-keto acid reduction pathway was disrupted by deleting the genes *yia*E and *ycd*W, resulting in the increase of BT titer and yield by 19% and 41%, respectively. Second,

the expression of *xyl*A gene was interfered by antisense RNA to balance the carbon flux for cell growth and BT accumulation. Finally, two decarboxylases from different sources were applied to improve BT titer and a 72% increase of BT titer (10.03 g/L) was achieved.

In addition, BT production using plant cell factories has also been reported (Abdel-Ghany et al., 2013). In this study, the authors cloned native bacterial genes or codon optimized synthetic genes into a binary vector and the vector was stably transformed into Arabidopsis plants. The transgenic plants expressing bacterial genes involved in BT synthesis produced up to 20 μg of BT per gram of soil-grown plants.

Glucose can be used as a preferred substrate for cell growth in BT biosynthesis. As a proof of concept, Li et al. (2015) designed a novel BT biosynthetic pathway from glucose via L-malate. This biosynthetic pathway was achieved through six sequential enzymatic reactions (Figure 2.2). After testing several combinations of enzymes for the pathway, five enzymes were finally chosen and co-expressed in *E. coli*. They were malate thiokinase (MtkAB), succinate-semialdehyde dehydrogenase (SucD), 4-hydroxybutyrate dehydrogenase (4HbD), 4-hydroxybutyrate CoA-transferase (AbfT2) and bifunctional aldehyde/alcohol dehydrogenase (AdhE2). Finally, 120 ng/L BT was detected in the fermentation using glucose as the sole carbon source.

2.2 Protein engineering for biosynthesis

2.2.1 Methods of protein engineering

Directed evolution is a procedure mimicking Darwinian evolution to move the evolution process into laboratories and speed it up. For enzymes, directed evolution is based on the combination of appropriate random gene mutagenesis, mutant enzymes expression and high-throughput screening or selection for desired properties. The process can be iterated until the desired improvement has been reached. A wide range of tools and techniques have been developed, including error-prone PCR which

introduces random point mutations into the gene of interest, and DNA shuffling techniques which is *in vitro* recombination of homologous genes (Chen and Arnold, 1993; Bornscheuer et al., 2012). The advantage of directed evolution is that it does not require detailed information of structure-function relationships and that mutations at unexpected positions far from the active site can also be introduced. However, the size of the mutant library is usually quite large and a high number of mutants need to be screened, which is time- and labor-consuming (Chen, 2001; Hart and Waldo, 2013).

With the availability of an increasing number of protein structures and biochemical data and the development of computational methods, enzyme engineering now is developing from directed evolution to rational design, a knowledge-driven process. In rational design, protein structures, biochemical data and deep understanding of the catalytic mechanism are evaluated to predict mutations that can affect the properties of the enzyme. The advantage of rational design method is the increased probability of getting beneficial mutations and a significant reduction of the library size, which means much less effort and time in the screening step. Semi-rational design is the combination of rational protein design and random mutagenesis. It uses the structural information of protein and the understanding of catalytic mechanism to identify key amino acids in the active site region, then do random mutagenesis or site-saturation mutagenesis at the target positions (Reetz et al., 2006; Abrahamson et al., 2012; Chen and Zeng, 2016). One example of application is the iterative cycles of CASTing (the Combinatorial Active-site Saturation Test). The adjacent residues whose side chains form part of the substrate-binding pocket were organized into two or three groups. Saturation mutagenesis was applied simultaneous for each group to create libraries that were subsequently screened. The best hit of each group was used as template for the next round of mutagenesis. The process was continued until the desired improvement was reached (Reetz et al., 2006).

2.2.2 Strategies for rational protein design

There are two widely used strategies to investigate sequence-structure-function relationships for rational protein design: statistical approaches to analyze protein families or mutant libraries, and molecular modelling methods to study the interaction of protein with ligands or substrates (Figure 2.3) (Bornscheuer and Pohl, 2001; Pleiss, 2011; Prier and Arnold, 2015; Ebert and Pelletier, 2017).

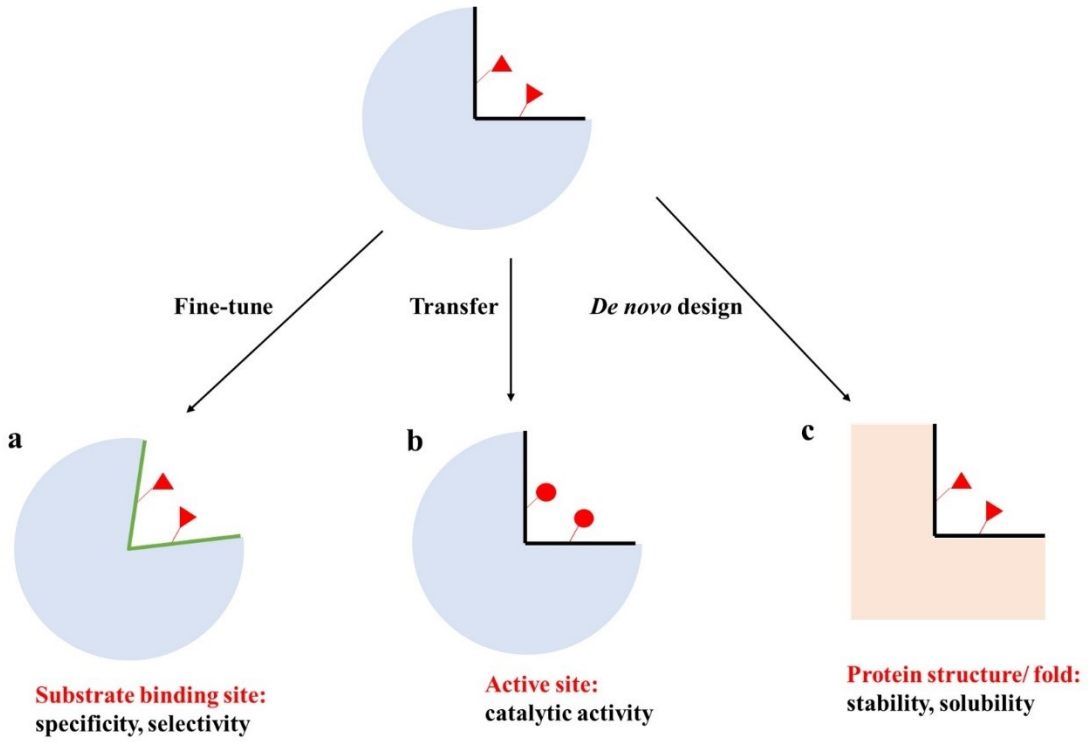

Figure 2.3. Protein design strategies: a) fine-tuning (e.g. of the substrate binding site); b) transfer from another enzyme (e.g. of the active site); c) *de novo* design (e.g. of the protein structure/fold). (Adapted from Figure 2 in Pleiss 2011)

Multiple sequence alignment (MSA) is a useful tool for the identification of conserved and variables sites within a protein family which are of structural and functional importance. Statistical methods utilize the rapidly growing sequence databases such as GenBank (Benson et al., 2010) and advanced programs such as Clustal W (Thompson et al., 1994) to carry out MSA so as to identify conserved or consensus sequences. These sequences are usually important for the function and structure of enzymes. Analyzing these results is useful to predict mutations that can improve catalytic activity, stability, or alter substrate specificity. Statistical methods of sequence analysis are also very

efficient in analyzing mutant libraries. For example, based on the statistical analysis of lots of mutants, a quantitative sequence-function relationship could be established to identify hotspot regions which are proved to be beneficial (Fox et al., 2007; Bornscheuer et al., 2012).

Molecular modelling methods are based on the known protein structure, no matter it is experimentally determined or modelled from other protein. The final goal of molecular modelling is to predict the biophysical and /or biochemical properties of enzymes based on the enzyme structure, the chemical properties of its components (amino acids, cofactors, metal ions) and the environment (pH, temperature, solvent, protein concentration, interaction with interfaces) (Pleiss, 2011; Bornscheuer et al., 2012; Ebert and Pelletier, 2017). The major modeling tools include homology modeling, docking, QM-based methods and molecular dynamics simulations. Modelling of the enzyme-substrate complex by molecular docking methods has been successfully used to invert the enantioselectivity of a carbonyl reductase (Zhu et al., 2008) and increase catalytic activity towards a given substrate (Lee et al., 2009).

2.2.2.1 Molecular dynamics simulation

Biological functions are the results of time dependent interactions between molecules and these interactions occur at the interfaces such as protein-ligand and protein-protein. The laboratory macroscopic observables are related to the microscopic behavior at atomic level. Molecular dynamics (MD) simulations can calculate the time dependent (and independent) microscopic behavior of a molecule. It enables us to understand the flexibility characteristics of biomolecules and how they affect each other. The classic MD is based on Newton's equations of motion. For a system of N interaction atoms, the force on each atom is given by:

$$F_i = m_i a_i = m_i \frac{d^2 r_i}{dt^2} \qquad i = 1 \ldots N \tag{1}$$

$$F_i = -\frac{\partial U}{\partial r_i} \tag{2}$$

Where F_i is the force on atom i; m_i is the mass of atom i; a_i is the acceleration of atom i; r_i is the coordinate of atom i; U is the potential energy function of the system; t is time; and N labels the number of atoms in the system.

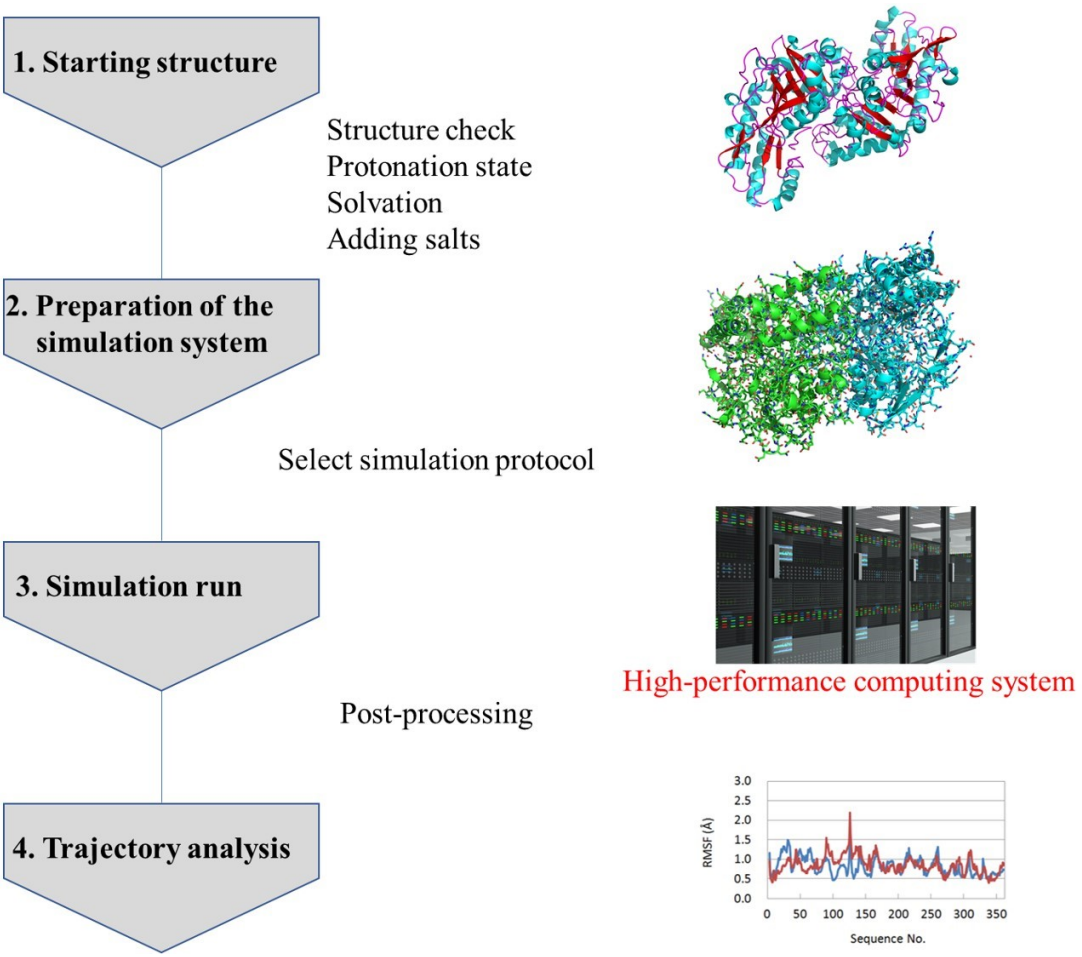

Figure 2.4. Molecular dynamics simulations process.

A MD simulation starts with the selection of a suitable solvent model and boundary conditions. Then after the steps of initializing the particle positions and velocities, it follows with calculating forces from the particle positions and solving Netwon's eqns. of motion (integrate). The results are analyzed via post-processing. A brief description of MD simulation process is illustrated in Figure 2.4.

There are many simulation softwares that can carry out MD simulations, such as AMBER (Case et al., 2005), NAMD (Phillips et al., 2005), CHARMM (Brooks et al., 1983). These programs are widely used today since the increasing availability of protein structures and improvements of computational power, especially via the use of GPUs, have made the MD simulation possible to achieve time scales compatible with biological processes. At present, when routine simulations are close to the microsecond scale, ligand binding or conformational changes can be effectively simulated.

2.2.2.2 Calculation of binding free energy

During the MD simulations, the position and orientation of the ligand are possible to change, and due to these changes, the binding affinity and the binding free energies are likely to be changing constantly. Therefore, calculating these energies helps to understand each movement of the ligand. The molecular mechanics/generalized Born surface area (MM/GBSA) approach, which is implemented in the AMBER program, can be applied to compute the binding free energy ($G_{binding}$) of the protein-ligand complex (Kollman et al., 2000). In this method, a very simple equation is used to calculate the binding free energy of the ligands which is as below:

$$\Delta G_{binding} = G_{water}(complex) - [G_{water}(protein) + G_{water}(ligand)] \quad (3)$$

For each frame of the simulation, the calculations of the van der Waals (VDW) energy, electrostatic energy, polar solvation energy and solvent-accessible surface area (SASA) energy are carried out to achieve the binding energy of the ligand.

2.2.3 Strategies for screening and selection

As for directed evolution of enzymes, a successful protein engineering requires two aspects, genetic diverse mutant library and high-throughput screening or/and selection method. Normally, the steps of searching for mutants with desired properties are the most difficult ones, because a poorly chosen approach could result in many false-

positive variants or variants remaining unidentified. A good screening or selection method could considerably increase the chance of obtaining target mutants with desired properties and reduce the time and cost. High-throughput screening methods refer to evaluation of individual mutants for the desired property using microtiter plates (He et al., 2011; Xiao et al., 2015), digital imaging (Koné et al., 2008) and fluorescence-activated cell sorting (FACS) (Yang and Withers, 2009). High-throughput selection methods automatically eliminate 'bad' variants by linking cell growth with acquired enzyme function, such as growth complementation (Zhang et al., 2010; Chen et al., 2019) and plasmid/phage display (Speight et al., 2001; Park et al., 2011). Herein, the methods of microtiter plates and growth complementation will be discussed in the following sections.

2.2.3.1 Microtiter plates

Microtiter plate-based screening is the most commonly applied method in identifying desirable variants (Leemhuis et al., 2009; Reetz, 2016; Kato and Hanyu, 2018). Cells transformed with mutant library are grown in microtiter plates with a single transformant per well. The variants are evaluated for the desired property in a second plate after cell lysis. The original microtiter plate is stored as back-up. For certain enzymatic reactions, the consumption of substrates or formation of products can be easily visualised with eyes or monitored using a plate reader if it involves changes of colour or fluorescence. These assays are very convenient and efficient for screening. However, the dependence of chemistry and the availability of suitable substrates make it not generally applicable for all enzymatic reactions. Normally, the throughput is also low compared to other selection methods. By taking advantage of automation, the traditional screening process of microtiter plate can be streamlined and sped up by reducing plate preparation time (Xiao et al., 2015; Porter et al., 2016).

2.2.3.2 Growth Complementation

The growth complementation method depends on a direct correlation between cell

survival and the desired enzyme property. Since it deals with the entire library simultaneously, its screening size is majorly limited by the transformation efficiency. Cells are transformed with mutant library and cultivated in a certain selective medium, in which only strains containing mutations with desired properties can survive (Esvelt et al., 2011; Bouzon et al., 2017; Chen et al., 2019). Recently, Chen et al. (2019) developed a method by integrating CRISPR/Cas9-facilitated engineering of the target gene with growth-coupled and sensor-guided *in vivo* screening (CGSS) for protein engineering. The CGSS method was successfully employed to improve the resistance of 3-deoxy-D-arabino-heptulosonate-7-phosphate synthase (AroG) to L-phenylalanine (Phe) and the L-tryptophan (Trp) production was increased by 38.5% in a fed-batch fermentation when the obtained mutant was used in an engineered Trp producing *E. coli*. In this CGSS method, an aromatic amino acids (AAAs)-auxotrophic strain was used as a platform and CRISPR/Cas9 system was employed to efficiently integrate variants of *aro*G gene into the chromosome of AAAs-auxotrophic strain. In the presence of a high Phe concentration, AAAs-auxotrophic strains harboring AroG mutations that are resistant to Phe can survive. The Trp production in these strains can be further monitored by Trp biosensor.

2.3 Chromosome engineering

2.3.1 Overview of lambda red recombineering in *E. coli*

The phage lambda-derived red recombination system is a powerful tool for making precisely defined deletions, insertions and point mutations in *E. coli*. Unlike yeast, which has efficient DNA double-strand break and repair recombination pathway (Szostak et al., 1983), *E. coli* is not readily transformed by linear DNA fragments due to the degradation of DNA by intracellular RecBCD exonuclease (Yu et al., 2000). To obtain efficient recombination of linear DNA, lambda red recombineering system is introduced into *E. coli*. The lambda red recombineering system has three components: Exo, Beta and Gam. All three are needed for recombineering with a dsDNA (double-

stranded DNA) substrate. However, for a modification with an ssDNA (single-stranded DNA) substrate, only Beta is required. The Gam protein encoded by the *gam* gene prevents the endogenous RecBCD and SbcCD nucleases from digesting the linear DNA introduced into *E. coli* (Murphy, 1991). The Exo protein is a 5' to 3' dsDNA-dependent exonuclease, which degrades the 5'-ending strand of dsDNA, while the 3'-ending strand is preserved, generating a 3'-ssDNA overhang (Hillyar, 2012). The Beta binds to the ssDNA created by Exo and facilitates recombination by promoting its annealing to a complementary ssDNA target in the cell.

All three lambda red genes are assembled into one plasmid (e.g. pKD46), generating a mobile recombineering system with a tight regulation of expression (Figure 2.5). Promoters commonly used to control expression of *gam*, *exo* and *bet* genes include arabinose-inducible pBAD promoter, IPTG-inducible lac promoter and endogenous phage pL promoter.

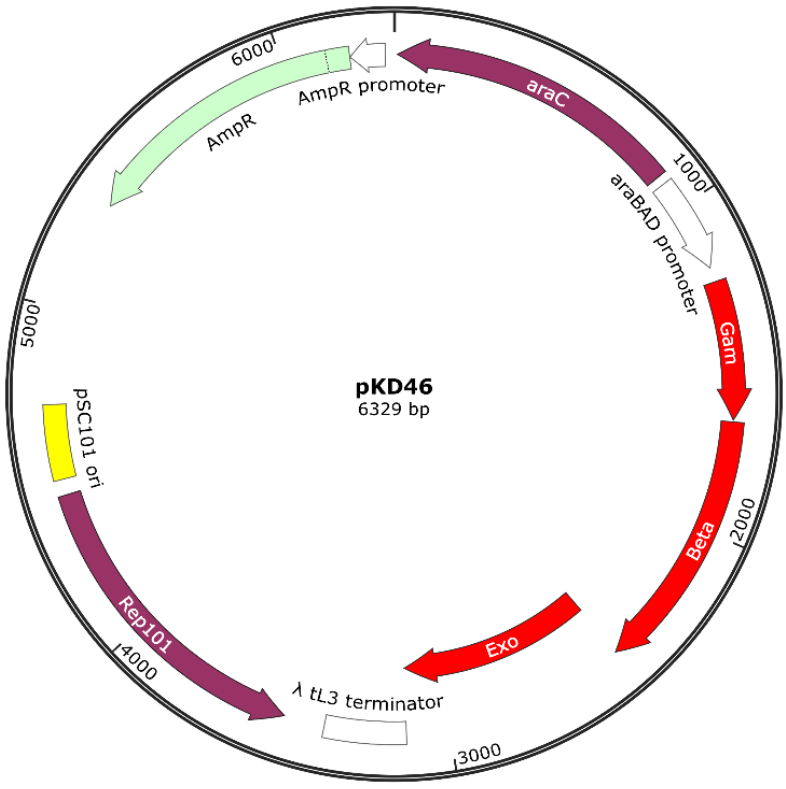

Figure 2.5. The plasmid pKD46 harboring the lambda red recombination system under the arabinose-inducible pBAD promoter. pKD46 sequence: GenBank AY048746.

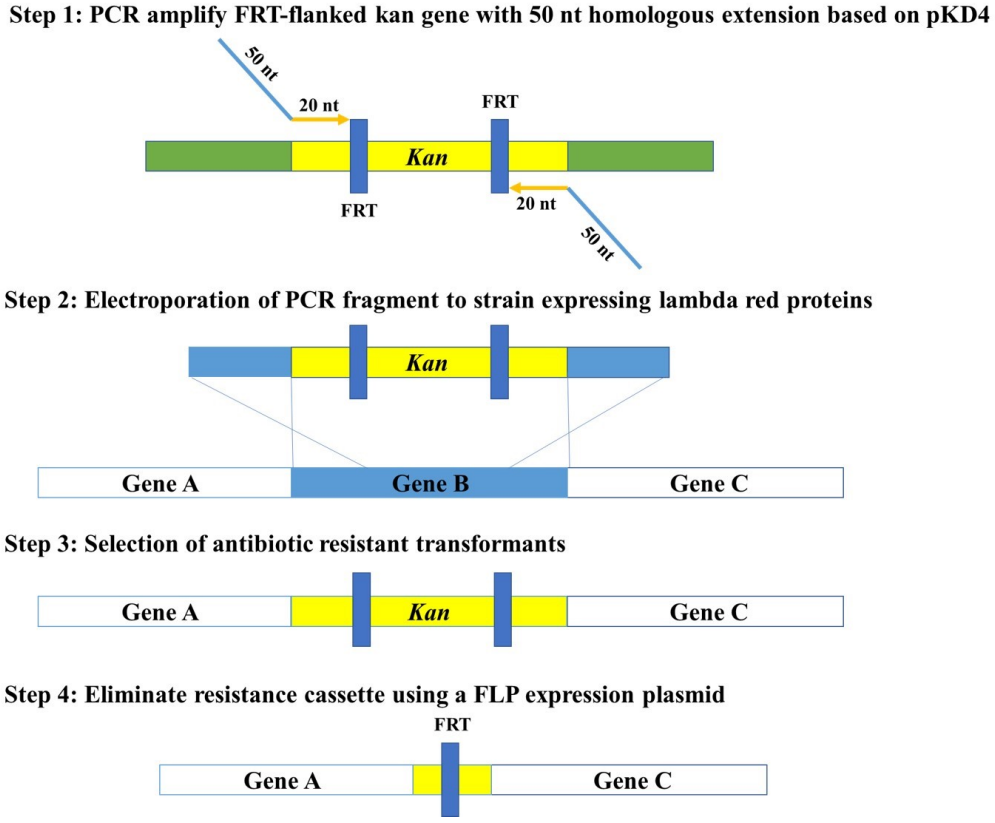

Figure 2.6. Overview of using lambda red recombineering system to replace a target gene with an antibiotic resistance cassette. This diagram is adapted from Figure 1 in Datsenko and Wanner (2000).

The basic strategy of lambda red recombineering in *E. coli* is illustrated in Figure 2.6: In Step 1, PCR fragments are amplified using pKD4 as template with primers including 20-nt priming sequences and 50-nt homology extensions; In Step 2, *Dpn*I is used to digest the PCR products, which are then purified and transformed into *E. coli* carrying pKD46; In Step 3, the antibiotic-resistant transformants are selected; In Step 4, resistance cassette is eliminated using a FLP expression plasmid pCP20; The final step is to get rid of the helper plasmid and verify its loss. pCP20 is resistant to both ampicillin and chloramphenicol and contains a temperature-inducible flp gene which can remove the FRT-flanked resistance gene and the FLP helper plasmid simultaneously when cultivated at 43 °C (Cherepanov and Wackernagel, 1995).

2.3.2 Application of CRISPR in *E. coli*

Nowadays, CRISPR, shorted from Clustered Regularly Interspaced Short Palindromic Repeats, has rapidly become the most popular genome engineering technology in several prokaryotes and eukaryotes because of its comparative simplicity and adaptability.

The type II CRISPR/Cas system from *Streptococcus pyogenes* utilizes a dual guide RNA system to guide the nuclease Cas protein 9 (Cas9) to the target of any DNA sequence, known as a protospacer, which is adjacent to a protospacer-adjacent motif (PAM) (Figure 2.7). The dual guide RNA system is a trans-activating crRNA (tracrRNA) complexing with a CRISPR RNA (crRNA) (Deltcheva et al., 2011). In genome editing cases, a single synthetic guide RNA (sgRNA) was created by fusing the crRNA (a user-defined 20-bp complementary region, N20) and tracrRNA sequences together into a single RNA chimera by creating a loop at the end of the duplex region (Jinek et al., 2013; Cong et al., 2013), allowing the sgRNA to be expressed from a plasmid for gene editing. By using sgRNA, one can change the genomic target of the Cas9 by simply changing the N20 sequence in the sgRNA. In *E. coli*, the CRISPR/Cas9 system has been demonstrated to control gene expression via a nuclease-deficient Cas9 protein (Jinek et al., 2012; Qi et al., 2013), apply allelic exchange with efficiency as high as 65% ± 14% (Jiang et al., 2013) and realize a variety of precise genome modifications with a highest efficiency of 100% (Jiang et al., 2015).

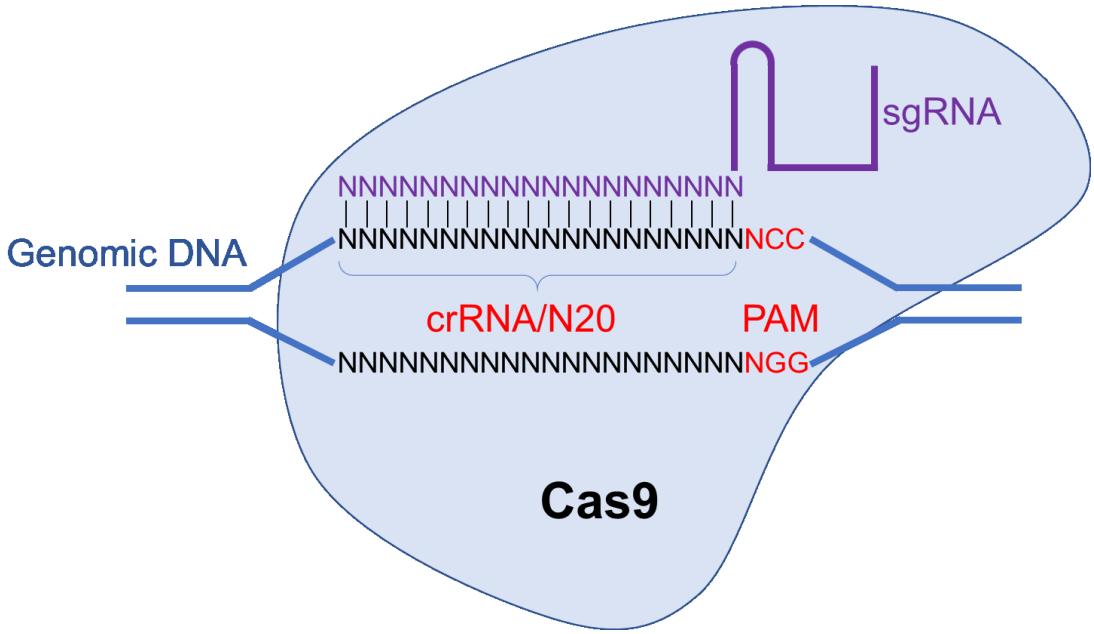

Figure 2.7. Illustration of Cas9 nuclease programmed by the sgRNA complex.

In the study by Jiang et al. (2015), a two-plasmid based CRISPR/Cas9 system was designed to apply a precise genome editing, including gene insertions and knockouts. The two-plasmid systems separate the Cas9 and the sgRNA in pCas plasmid and pTarget plasmid respectively (Figure 2.8). The pCas plasmid contains the Cas9 gene from *S. pyogenes* MGAS5005 with its native promoter, the temperature-sensitive replicon repA101(ts) from plasmid pKD46, the lambda red genes (*gam*, *exo*, *bet*) under the P_{araB} promoter and a sgRNA targeting the pMB1 replicon in pTarget plasmid. The pTarget plasmid consists of the sgRNA with N20 sequence, pMB1 replicon, and the donor DNA for recombination. As illustrated in Figure 2.8, the pCas plasmid is electroporated into *E. coli* in the first day. The resulting strain with the existence of L-arabinose is made into electrocompetent cells and then introduced with the plasmid pTarget. In the following day, curing the pTarget plasmid is achieved by inducing the expression of pCas plasmid with IPTG. The resulting engineered *E. coli* with pCas plasmid can go another round of genome editing or be cured to get rid of pCas plasmid by growing overnight at 37 °C.

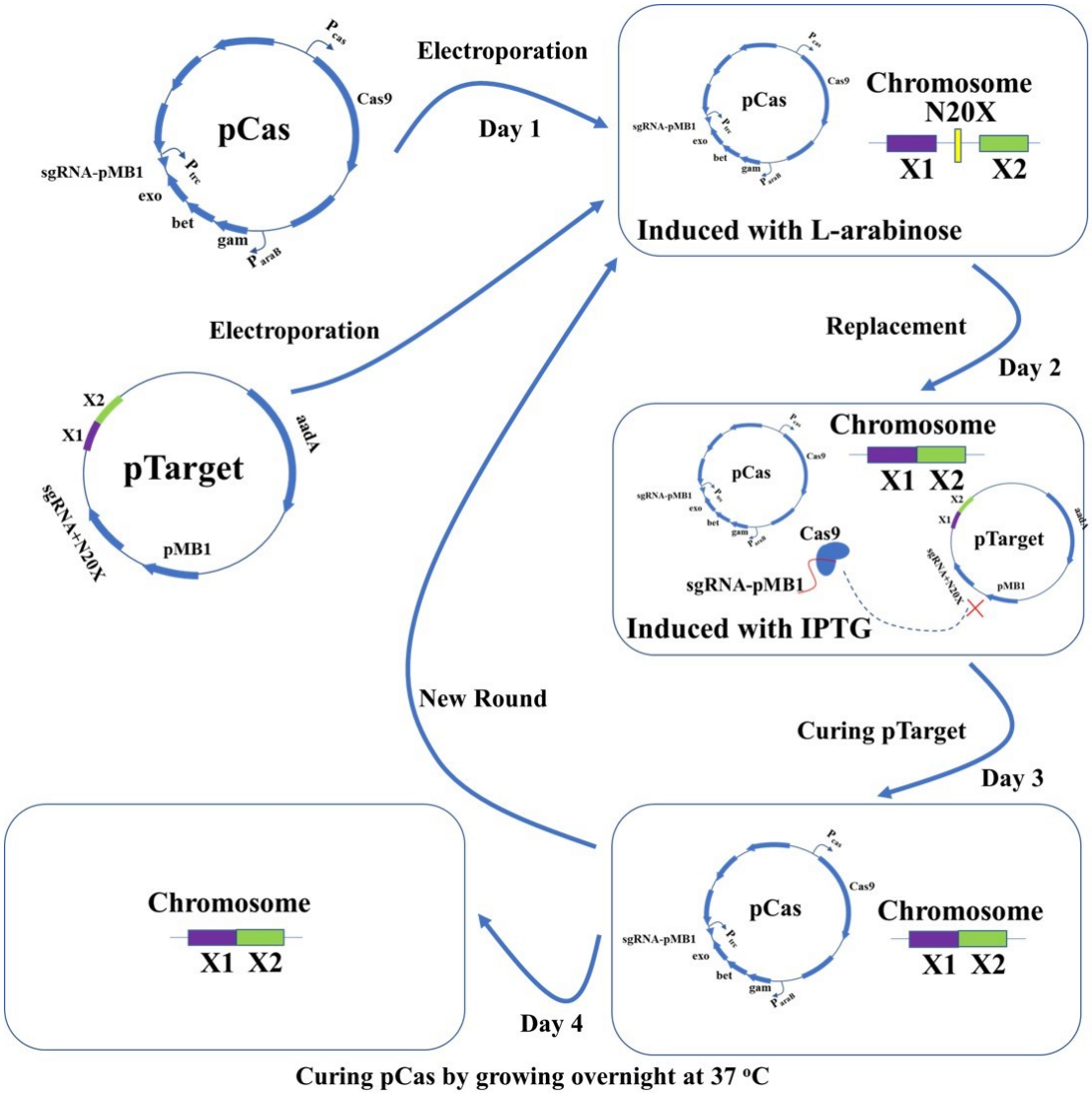

Figure 2.8. Detailed diagram of two-plasmid based CRISPR/Cas9 system for genome editing.

CHAPTER 3 Materials and methods[1]

3.1 Chemicals

Analytical grade chemicals and L-glutamic dehydrogenase were purchased from Sigma-Aldrich (München, Germany) or from Carl Roth GmbH (Karlsruhe, Germany). Other enzymes and molecular biology reagents were from Thermo Fisher Scientific GmbH (Karlsruhe, Germany), Takara Bio Europa S.A.S. (Saint-Germain-en-Laye, France) or NEB (New England Biolabs, USA). Bacterial strains and DNA were purchased from DSMZ (Braunschweig, Germany). Plasmid carrying the gene of wild type SerC was obtained from Metabolic Explorer Co. (France).

3.2 Strains, plasmids and primers

3.2.1 Strains

The main strains used in this study are listed in Table 3.1.

Table 3.1: List of strains used in this study

Strains	Genotype	Source
HOM002	MG1655 △*thr*B	Chen et al., 2015
Stellar™ Competent Cells	F-, endA1, supE44, thi-1, recA1, relA1, gyrA96, phoA, Φ80d lacZΔ M15, Δ(lacZYA-argF) U169, Δ(mrr-hsdRMS-mcrBC), ΔmcrA, λ-	TaKaRa
BL21 (DE3)	fhuA2 [lon] ompT gal (λ DE3) [dcm] ΔhsdS λ DE3 = λ sBamHIo ΔEcoRI-B int::(lacI::PlacUV5::T7 gene1) i21 Δnin5	New England Biolabs
S66	*E. coli* BL21 △*ser*C △*gdh*A △*glt*B △*glt*D	This study
S87	HOM002 pMely	This study
S128	HOM002 pZA-SerC(R42W-R77W)-PDC-YqhD	This study
S129	HOM002 pZA-SerC(WT)-PDC-YqhD	This study
S144	S87 pZA-SerC(WT)-PDC-YqhD	This study

[1] Parts of this chapter are taken or slightly modified from Zhang et al. (2019).

continues…

S147	S87 pZA-SerC(R42W-R77W)-PDC-YqhD	This study
S310	S87 △*adh*E △*ldh*A	This study
S311	S87 △*adh*E △*ldh*A pZA-SerC(WT)-PDC-YqhD	This study
S312	S87 △*adh*E △*ldh*A pZA-SerC(R42W-R77W)-PDC-yqhD	This study
S164	S87 pZA-SerC(R42W-R77W)-Ldh(Q85C)-AbfT2-AdhE2	This study
S171	S87 pDHPL-SerC(R42W-R77W)-Ldh(Q85C)-AbfT2-AdhE2	This study
S313	S87 △*adh*E △*ldh*A pDPHL-SerC(R42W-R77W)-Ldh(Q85C)-AbfT2-AdhE2)	This study
S314	S87 △*adh*E △*ldh*A pZA-SerC(R42W-R77W)-Ldh(Q85C)-AbfT2-AdhE2)	This study
S317	S87 △*adh*E △*ldh*A pZA-SerC(R42W-R77W-R329P)-PDC-yqhD	This study
S318	S87 pZA-SerC(R42W-R77W-R329P)-PDC-yqhD	This study

3.2.2 Plasmids

The main plasmids used in this study are tabulated in Table 3.2.

Table 3.2: List of plasmids used in this study.

Plasmids	**Characteristics**	**Sources**
pET28a (+)	pET vector	Novagen
pET28a-SerC	pET28a encoding wild type SerC from *E. coli*	METEX Co.
pET28a-SerC(H41Q)	pET28a-SerC derivative with H41Q mutation	This study
pET28a-SerC(H41Y)	pET28a-SerC derivative with H41Y mutation	This study
pET28a-SerC(H41K)	pET28a-SerC derivative with H41K mutation	This study
pET28a-SerC(R42W)	pET28a-SerC derivative with R42W mutation	This study
pET28a-SerC(R42Q)	pET28a-SerC derivative with R42Q mutation	This study
pET28a-SerC(R42K)	pET28a-SerC derivative with R42K mutation	This study
pET28a-SerC(R42E)	pET28a-SerC derivative with R42E mutation	This study
pET28a-SerC(R42V)	pET28a-SerC derivative with H42V mutation	This study
pET28a-SerC(R42S)	pET28a-SerC derivative with H42S mutation	This study
pET28a-SerC(R42T)	pET28a-SerC derivative with H42T mutation	This study
pET28a-SerC(R77T)	pET28a-SerC derivative with R77Tmutation	This study

continues…

continues…

pET28a-SerC(R42W-R77W)	pET28a-SerC derivative with R42W and R77W mutations	This study
pET28a-SerC(R42W-R77T)	pET28a-SerC derivative with R42W and R77T mutations	This study
pET28a-SerC(R42W-R77S)	pET28a-SerC derivative with R42W and R77S mutations	This study
pET28a-SerC(R42W-R77I)	pET28a-SerC derivative with R42W and R77I mutations	This study
pET28a-SerC(R42W-R77E)	pET28a-SerC derivative with R42W and R77E mutations	This study
pET28a-SerC(R42W-R77Q)	pET28a-SerC derivative with R42W and R77Q mutations	This study
pET28a-SerC(R42W-R329H)	pET28a-SerC derivative with R42W and R329H mutations	This study
pET28a-SerC(R42W-R329Q)	pET28a-SerC derivative with R42W and R329Q mutations	This study
pET28a-SerC(R42W-R329G)	pET28a-SerC derivative with R42W and R329G mutations	This study
pET28a-SerC(R42S-R329Q)	pET28a-SerC derivative with R42S and R329Q mutations	This study
pET28a-SerC(R42S-R77W)	pET28a-SerC derivative with R42S and R77W mutations	This study
pET28a-SerC(R42V-R329H)	pET28a-SerC derivative with R42V and R329H mutations	This study
pET28a-SerC(R42V-R77W)	pET28a-SerC derivative with R42V and R77W mutations	This study
pET28a-SerC(R42V-R77T)	pET28a-SerC derivative with R42V and R77T mutations	This study
pET28a-SerC(R42A-R77Q)	pET28a-SerC derivative with R42A and R77Q mutations	This study
pET28a-SerC(R42A-R77W)	pET28a-SerC derivative with R42A and R77W mutations	This study
pET28a-SerC(R42H-R77W)	pET28a-SerC derivative with R42H and R77W mutations	This study
pET28a-SerC(R42T-R77W)	pET28a-SerC derivative with R42T and R77W mutations	This study
pET28a-SerC(R42L-R77S)	pET28a-SerC derivative with R42L and R77S mutations	This study
pET28a-SerC(R42W-R77W-H328Y)	pET28a-SerC derivative with R42W, R77W and R328Y mutations	This study

continues…

continues…

pET28a-SerC(R42W-R77W-H328L)	pET28a-SerC derivative with R42W, R77W and R328L mutations	This study
pET28a-SerC(R42W-R77W-H328E)	pET28a-SerC derivative with R42W, R77W and R328E mutations	This study
pET28a-SerC(R42W-R77W-H328K)	pET28a-SerC derivative with R42W, R77W and R328K mutations	This study
pET28a-SerC(R42W-R77W-R329H)	pET28a-SerC derivative with R42W, R77W and R329H mutations	This study
pET28a-SerC(R42W-R77W-R329Q)	pET28a-SerC derivative with R42W, R77W and R329Q mutations	This study
pET28a-SerC(R42W-R77W-R329P)	pET28a-SerC derivative with R42W, R77W and R329P mutations	This study
pET28a-SerC(R42W-R77W-T240S)	pET28a-SerC derivative with R42W, R77W and T240S mutations	This study
pET28a-SerC(R42W-R77W-F238S)	pET28a-SerC derivative with R42W, R77W and F238S mutations	This study
pET28a-SerC(R42W-R77W-I154G)	pET28a-SerC derivative with R42W, R77W and I154G mutations	This study
pET28a-SerC(R42W-R77W-F46L)	pET28a-SerC derivative with R42W, R77W and F46L mutations	This study
pET28a-SerC(R42M-R77W-D164A)	pET28a-SerC derivative with R42M, R77W and D164A mutations	This study
pZA-gdhA-pdc-yqhD	plasmid pZA encoding GDH, PDC and YqhD	Chen et al., 2015
pZA-serC(WT)-pdc-yqhD (referred as pZAWT)	plasmid pZA encoding wild type SerC, PDC and YqhD	This study
pZA-serC(R42W-R77W)-pdc-yqhD (referred as pZAX)	plasmid pZA encoding SerC(R42W-R77W), PDC and YqhD	This study
pZA-serC(R42W-R77W-R329P)-pdc-yqhD	plasmid pZA encoding SerC(R42W-R77W-R329P), PDC and YqhD	This study
pZA-serC(WT)	plasmid pZA encoding wild type SerC	This study
pZA-serC(R42W-R77W)	plasmid pZA encoding SerC(R42W-R77W)	This study
pET22b-EcSse	plasmid pET22b encoding Sse from *E. coli*	This study
pMely	plasmid pMely encoding MetL and LysC	Chen, 2016
pETDuet-SerC(R42W-R77W)-Sse	plasmid pETDuet encoding SerC(R42W-R77W) and Sse	This study

continues…

continues…

pZA-SLAA	plasmid pZA encoding SerC(R42W-R77W), Ldh(Q85C), AbfT2 and AdhE2	This study
pDPHL-SLAA	plasmid pTrc99A encoding SerC(R42W-R77W), Ldh(Q85C), AbfT2 and AdhE2	This study

3.2.3 Primers

The main primers used in this study are listed in Table 3.3-3.5. According to the aim of study, primers are categorized into: a) SerC protein engineering; b) *E. coli* genome engineering; c) plasmids construction for 1,3-PDO pathway and BT pathway.

Table 3.3: Primers used for engineering SerC protein

Primers	**Sequence (5' to 3')**
SerC-H41K-F	gtgatggaagtgagtaagcgtggcaaagag
SerC-H41K-R	ctctttgccacgcttactcacttccatcac
SerC-R42W-F	atggaagtgagtcactggggcaaagagttcatt
SerC-R42W-R	aatgaactctttgccccagtgactcacttccat
SerC-H41Y-F	gtgatggaagtgagttaccgtggcaaagag
SerC-H41Y-R	ctctttgccacggtaactcacttccatcac
SerC-R42K-F	atggaagtgagtcacaagggcaaagagttcatt
SerC-R42K-R	aatgaactctttgcccttgtgactcacttccat
SerC-R42E-F	atggaagtgagtcacgagggcaaagagttcatt
SerC-R42E-R	aatgaactctttgccctcgtgactcacttccat
SerC-R42Q-F	atggaagtgagtcaccagggcaaagagttcatt
SerC-R42Q-R	aatgaactctttgccctggtgactcacttccat
SerC-H41Q-F	gtgatggaagtgagtcagcgtggcaaagag
SerC-H41Q-R	ctctttgccacgctgactcacttccatcac
SerC-R42W-R77I-F	catggcggtggtatcggtcagtttgctgcg
SerC-R42W-R77I-R	cgcagcaaactgaccgataccaccgccatg
SerC-R42W-R77T-F	catggcggtggtaccggtcagtttgctgcg
SerC-R42W-R77T-R	cgcagcaaactgaccggtaccaccgccatg
SerC-R42W-R77S-F	catggcggtggttccggtcagtttgctgcg

continues…

continues…

SerC-R42W-R77S-R	cgcagcaaactgaccggaaccaccgccatg
SerC-R42W-R77E-F	catggcggtggtgagggtcagtttgctgcg
SerC-R42W-R77E-R	cgcagcaaactgaccctcaccaccgccatg
SerC-R42W-R329G-F	ctgaaaggtcacggtgtggtcggcggaatg
SerC-R42W-R329G-R	cattccgccgaccacaccgtgacctttcag
SerC-R42W-R77W-F	catggcggtggttggggtcagtttgctgcg
SerC-R42W-R77W-R	cgcagcaaactgaccccaaccaccgccatg
SerC-R42W-R329H-F	ctgaaaggtcaccatgtggtcggcggaatg
SerC-R42W-R329H-R	cattccgccgaccacatggtgacctttcag
SerC-R42W-R329Q-F	ctgaaaggtcaccaagtggtcggcggaatg
SerC-R42W-R329Q-R	cattccgccgaccacttggtgacctttcag
SerC-H328L-F	catgcactgaaaggtctccgtgtggtcggcgga
SerC-H328L-R	tccgccgaccacacggagacctttcagtgcatg
SerC-H328Y-F	catgcactgaaaggttaccgtgtggtcggcgga
SerC-H328Y-R	tccgccgaccacacggtaacctttcagtgcatg
SerC-H328E-F	catgcactgaaaggtgaacgtgtggtcggcgga
SerC-H328E-R	tccgccgaccacacgttcacctttcagtgcatg
SerC-H328K-F	catgcactgaaaggtaagcgtgtggtcggcgga
SerC-H328K-R	tccgccgaccacacgcttacctttcagtgcatg
SerC-H328W-F	catgcactgaaaggttggcgtgtggtcggcgga
SerC-H328W-R	tccgccgaccacacgccaacctttcagtgcatg
R42-NNK-F	atggaagtgagtcacnnkggcaaagagttcatt
R42-NNK-R	aatgaactctttgccmnngtgactcacttccat
R77-NNK-F	catggcggtggtnnkggtcagtttgctgcg
R77-NNK-R	cgcagcaaactgaccmnnaccaccgccatg
H41-F	gtgatggaagtgagtnnkcgtggcaaagagttc
H41-R	gaactctttgccacgmnnactcacttccatcac
W102-F	tatgttgatgccggttacnnkgcggcaagtgccatt
W102-R	aatggcacttgccgcmnngtaaccggcatcaacata
T153-F	tattgcccgaatgaannkatcgatggtatcgccatc
T153-R	gatggcgataccatcgatmnnttcattcgggcaata

continues…

continues…

I154-F	tgcccgaatgaaaccnnkgatggtatcgccatcgac
I154-R	gtcgatggcgataccatcmnnggtttcattcgggca
N239-F	aacggctccatgtttnnkacgccgccgacatttgc
N239-R	gcaaatgtcggcggcgtmnnaaacatggagccgtt
T240-F	aacggctccatgtttaacnnkccgccgacatttgcc
T240-R	ggcaaatgtcggcggmnngttaaacatggagccgtt
R335-F	cgtgtggtcggcggaatgnnkgcttctatttataac
R335-R	gttataaatagaagcmnncattccgccgaccacacg
Y339-F	atgcgcgcttctattnnkaacgccatgccgctg
Y339-R	cagcggcatggcgttmnnaatagaagcgcgcat
M237-N239-F	cgataacggctccnnktttnnkacgccgccgacatt
M237-N239-R	aatgtcggcggcgtmnnaaamnnggagccgttatcg
F238-T240-F	taacggctccatgnnkaacnnkccgccgacatttgc
F238-T240-R	gcaaatgtcggcggmnngttmnncatggagccgtta
Y101-W102-F	tatgttgatgccggtnnknnkgcggcaagtgccatt
Y101-W102-R	aatggcacttgccgcmnnmnnaccggcatcaacata
T153-I154-F	tgcccgaatgaannknnkgatggtatcgccatcgac
T153-I154-R	gtcgatggcgataccatcmnnmnnttcattcgggca
Q197-K198-F	atttacgctggcgcgnnknnkaatatcggccc
Q197-K198-R	gggccgatattmnnmnncgcgccagcgtaaat
N239-T240-F	taacggctccatgtttnnknnkccgccgacatttgc
N239-T240-R	gcaaatgtcggcggmnnmnnaaacatggagccgtta
H328-R329-F	cttcatgcactgaaaggtnnknnkgtggtcggcggaatg
H328-R329-R	cattccgccgaccacmnnmnnacctttcagtgcatgaag
S9-G10-P11-F	tcttcaattttagtnnknnknnkgcaatgctaccggc
S9-G10-P11-R	gccggtagcattgcmnnmnnmnnactaaaattgaaga
BamHI-SerC-F	cgcggatccgatggctcaaatcttcaattttagttctggt
HindIII-SerC-R	cccaagcttttaaccgtgacggcgttcgaactcaaccat
Nco I-serC-F	catgccatggctcaaatcttcaattttagttctg
Xho I-SerC-R	ccgctcgagaccgtgacggcgttcgaactcaac
Sse-NdeI-F	gggaattccatatgtccacgacatggtttgtaggagccgactgg
Sse-XhoI-R	ccgctcgagtttcactggctcaaccggtaaatctgcccg

Table 3.4: Primers used for *E. coli* genome engineering

Primers	Sequence (5' to 3')
V-serC-F	atgaaggcgttcgatctccaccgtatggcat
V-serC-R	tcaccacgcgtgcaggaaatataatcatcgc
serCpkD4-F	tcgcaatcgattgaccgcgggttaatagcaacgcaacgtggtgaggggaagtgtaggctggagctgcttc
serCpkD4-R	gaaataaaaaccccacaggctggctgtggggattaagcaaaatttcggcaatgggaattagccatggtcc
V2-gltBD-F	accgcctgctgatacatagaacgcagcacct
V2-gltBD-R	ttgccgatgggaattctgcagatggtgtctgc
gdhApKD4-F	acataaacaacataagcacaatcgtattaatatataagggttttatatctgtgtaggctggagctgcttc
gdhApKD4-R	tgtgcccatttgtaggcctgataagcgtagcgccatcaggcatttacaacatgggaattagccatggtcc
gltBD-F	tattaaccgatgcgaaaaggacaacaaggggcgaatgcgaggcgcgcgtgtgtaggctggagctgcttc
gltBD-R	gagaatttcagcgccgactcttttctgaggaggcggcgctgggacagagcatgggaattagccatggtcc
gdhA2-F	tggagtcattcctcaaccatgtccaaaagcgc
gdhA2-R	catcgcatcggcaaccttcacaaaaccggc
gltB-F	atgacacgcaaaccccgtcgccacgctctttctgtgccc
gltD-R	ttaaacttccagccagttcataataccgtctgccgcctt
1N20-*ldh*A	gctcagtcctaggtataatactagttcagctcttccagcaccggggttttagagctagaaatagcaagttaaaata aggctagtccg
1pTarget-R	actagtattatacctaggactgagctagctgtcaag
2pTarget-F	cgaggtgaagacgaaagggcctcgtgatacg
2pTarget-R	aaaaaagcaccgactcggtgccacttttc
2UpldhA-F	agtcggtgctttttaatttgccacggcaaatcgagc
2DownldhA-R	ttcgtcttcacctcgttttcgcttttgtgtcccccacatcagcg
3pTgL-Fra-F	ggggaattgtgagcggataacaattcccgggagaaggagatatacatatgagtgtgattgcgcaggca
3pTgL-Fra-R	ttcgttcgggcaggtttactcaaacaaattactatgcagtttttgcacc
3pTgL-Vec-F	acctgcccgaacgaactgg
3pTgL-Vec-R	cgctcacaattcccctacacattatacgagccgatgattaattgtcaaactgttttgtgctataaacggcgagt
1N20-adhE	gctcagtcctaggtataatactagtatctgcagcagccagagcgggttttagagctagaaatagcaagttaaaata aggctagtccg
2UpadhE-F	agtcggtgctttttataaggttgaaaagacgcgctgacaatacgc
2DownadhE-R	ttcgtcttcacctcgcagcagtttctcgatcttagcagcagtacg
adhE-Check-F	atcttgcttacgccacctggaagtgacgcat
LdhA-Check-F	atgaaactcgccgtttatagcacaaaaca
LdhA-Check-R	cctggaatgcaggggagcggcaagat

Table 3.5: Primers used for plasmids in 1,3-PDO pathway and BT pathway

Primers	Sequence (5' to 3')
FpZA-serC.R	ttaaagaggagaaagatggctcaaatcttcaattttagttctggt
FpZA-serC.F	ttcttaaagttgttaaccgtgacggcgt
VpZA-serC.R	ctttctcctctttaatgaattcggtcagtgc
VpZA-serC.F	taacaactttaagaaggagatatacatatgtataccgtgg
p15Aori-R	gatgcttgtcaggggggcggagcctatggaaa
Catpromoter-R	ggtgaaagttggaacctcttacgtgccgatca
AbfT2-fragment.FOR	gcagttaaaaactaaaactttaagaaggagatatacatatgcaatggcaagaactttaccgtc
AbfT2-fragment.REV	atgcctctagagtcattattcgaagcgtcggcggatttcc
AbfT2-vector.FOR	tgactctagaggcatcaaataaaacgaaagg
AbfT2-vector.REV	ttagtttttaactgcagaagcaaattcttctttagca
AdhE2-fragment.FOR	cgacgcttcgaataaaactttaagaaggagatatacatatgaaagttacaaatcaaaaa gaactaaaac
AdhE2-fragment.REV	atgcctctagagtcattaaaatgattttatatagatatccttaagttc
AdhE2-Vector-REV	ttattcgaagcgtcggcgga
V-abfT2-F	aggcagcttctgagtcgatcgggtacgaa
V-adhE2-F	ctggtaccggttcagaggcaacacctttg
pDPHL-Vec.FOR	tctagagtcgacctgcaggca
pDHPL-Vec.REV	atgtatatctccttcttcattagaattccatggtctg
pDPHL-Fra.FOR	gaaggagatatacatatggctcaaatcttcaattttagttctggt
pDPHL-Fra.REV	caggtcgactctagattaaaatgattttatatagatatccttaagttcacttataagtggatacc
F-LL LDH.FOR	gaaggagatatacatatggctgataaacaacgtaagaaagttatcct
F-LL-LDH.REV	atgcctctagagtcattagtttttaactgcagaagcaaattcttctttagc
V-LL.REV	atgtatatctccttcttaaagttgttaaccgtga
V-LL.FOR	tgactctagaggcatcaaataaaacgaaagg

3.3 Growth and fermentation media

3.3.1 LB and SOC medium

The LB medium (lysogeny broth) was routinely used to cultivate *E. coli*. LB medium contained 10 g/L tryptone, 5 g/L yeast extract and 10 g/L NaCl. For LB solid medium, 15 g/L agar was added. The medium was autoclaved at 121 ºC for 20 minutes.

Appropriate antibiotics were added into the medium after sterilization according to its purpose. The routine working concentrations of antibiotics were: kanamycin 30 mg/L, ampicillin 100 mg/L and chloramphenicol 34 mg/L. The prepared medium was stored at 4 ^{o}C.

The SOC (Super optimal broth with catabolite repression) medium was used for the regeneration of *E. coli* after heat shock transformation or electroporation. SOC medium contained 20 g/L tryptone, 5 g/L yeast extract, 0.584 g/L NaCl, 0.186 g/L KCl, 3.6 g/L glucose and 2.47 g/L $MgSO_4$. All components except for glucose and $MgSO_4$ were dissolved and sterilized. Glucose and $MgSO_4$ were autoclaved separately. All components were mixed after sterilization and the final volume was adjusted to 1 liter with sterilized water.

3.3.2 Fermentation medium for 1,3-PDO production

For 1,3-PDO production in shake flask, the fermentation medium I (FM I) was used and given in Table 3.6, as described by Chen et al. (2015). Notably, 30 g/L $CaCO_3$ was added to the FM I for buffering pH during the cultivation, 5 g/L L-homoserine was added to assure enough substrate for SerC in the medium, and 1 g/L L-threonine was added due to the threonine-dependent host strain used in this study.

Table 3.6: Components of fermentation medium I.

Components	Concentration (g/L)
Glucose	20
$(NH_4)_2SO_4$	16
KH_2PO_4	1
$MgSO_4$	1
Yeast extract	2
$FeSO_4 \cdot 7H_2O$	0.01
$MnSO_4 \cdot 7H_2O$	0.01
L-Homoserine	5
L-Threonine	1
Vitamin B_1	0.01
$CaCO_3$	30

To prepare FM I, components of $(NH_4)_2SO_4$, KH_2PO_4 and yeast extract were dissolved in deionized water and autoclaved. Glucose, $MgSO_4$ and $CaCO_3$ were autoclaved separately. All autoclaved components were mixed and added with filter-sterilized $FeSO_4 \cdot 7H_2O$, $MnSO_4 \cdot 7H_2O$, L-homoserine, L-threonine and Vitamin B_1. The final volume was adjusted to 1 liter with sterilized water and the pH was kept to 7.0 with 5 M NaOH.

Fermentation medium II (FM II, Table 3.7) and fermentation medium III (FM III, Table 3.8) were used for 1,3-PDO production in fed-batch fermentations. FM II and FM III were modified from those described by Chen et al. (2017), respectively. 2 g/L L-threonine was added in both mediums. KH_2PO_4 and K_2HPO_4 were used in FM II for a better buffering system in shake flask. The pH of FM II was adjusted to 7.0 with 5 M NaOH.

Table 3.7: FM II in shake flask.

Components	Concentration (g/L)
Glucose	30
$(NH_4)_2SO_4$	4
KH_2PO_4	3
K_2HPO_4	12
$MgSO_4$	1
$FeSO_4 \cdot 7H_2O$	0.01
$MnSO_4 \cdot 7H_2O$	0.01
Yeast extract	2
Monosodium citrate	2
L-Threonine	2

The pH of FM III was kept at 7.4 by titration with NH_4OH during the fermentation. Meanwhile, to achieve high cell density, trace elements were added in FM III. The trace element solution was prepared in 100X stock and stored at 4 ^oC (Table 3.9). Unless otherwise stated, the concentrations of components are same in both fermentation medium and feeding medium, except that the concentration of glucose was 500 g/L in the feeding medium.

Table 3.8: FM III for fed-batch fermentation in bioreactor.

Components	Concentration (g/L)
Glucose	30
$(NH_4)_2SO_4$	4
KH_2PO_4	2
$MgSO_4$	1
Yeast extract	2
Monosodium citrate	2
L-Threonine	2
Biotin	1×10^{-4}
DL-calcium pantothenate	1×10^{-4}
Trace element solution (100X)	10 ml

Table 3.9: Components of trace element solution

Trace element solution	Working concentration (mg/L)
$MnSO_4\cdot H_2O$	12.5
$AlCl_3$	6.9
$FeSO_4\cdot 7H_2O$	50
$CoCl_2\cdot 6H_2O$	8.75
$CaCl_2$	37.75
$ZnSO_4\cdot 7H_2O$	2.5
$CuCl_2\cdot 2H_2O$	1.25
H_3BO_3	0.625
$Na_2MoO_4\cdot 2H_2O$	2.5

3.3.3 Fermentation medium for BT production

The production of BT was performed in modified M9 minimal medium (20 g/L glucose, 6.78 g/L Na_2HPO_4, 3.0 g/L KH_2PO_4, 0.5 g/L NaCl, 1.0 g/L NH_4Cl, 1 mM $MgSO_4$, 0.1 mM $CaCl_2$, 10 mM $NaHCO_3$, 10 μg/mL thiamine, 1 g/L L-threonine and 100 mM MOPS) (Li et al., 2014). The MOPS was used to improve the buffering capacity. The microaerobic conditions were achieved by piercing the septum with a 23G needle (Becton-Dickenson) after flushing capped anaerobic bottles with nitrogen for at least 5 min.

Fermentations performed in DASGIP bioreactors used modified M9 minimal medium (6.78 g/L Na_2HPO_4, 3.0 g/L KH_2PO_4, 0.5 g/L NaCl, 2.0 g/L NH_4Cl, 1.0 g/L $(NH_4)_2SO_4$,

1 mM $MgSO_4$, 0.1 mM $CaCl_2$, 1 g/L L-threonine) supplemented with 20 g/L glucose (Yim et al., 2011). The pH was kept at 7.0 using 2M NH_4OH (aerobic phase) or Na_2CO_3 (microaerobic phase).

3.4 Computational methods

3.4.1 Systems preparation and molecular dynamics (MD) simulations

Crystal structure of SerC was retrieved from the Protein Data Bank (PDB code: 1BJO). The SerC with the binding of L-phosphoserine and SerC with the binding of L-homoserine were then constructed by altering the side chain of the L-glutamate located in the substrate binding pocket of the crystal structure. The coenzyme pyridoxal phosphate (PLP) exists in each of the structures as given in the PDB file.

Dynamics simulations were run with the NAMD program under the AMBER force field. Each of the complexes was neutralized by adding sodium counter ions randomly and solvated in a rectangular box of TIP3P water molecules with a minimum solute-wall distance of 12Å (Case et al., 2005; Jorgensen 1982). Energy minimizations of the solved system were conducted before the MD simulations. Each system was minimized for 1ns to let protein stay at a comfortable structure. A residue-based cut-off of 9 Å was applied to the non-covalent interactions. No constraint was applied to either the protein or the substrates during MD simulations. The MD simulations were performed under periodic boundary condition in the NPT ensemble at 300 K using Langevin dynamics with a damping coefficient (gamma) of 5 ps-1 and constant pressure of 1 atm. The Shake algorithm was applied to fix all covalent bonds containing a hydrogen atom with a time step of 2 fs.

3.4.2 Decomposition of binding free energy at residue level

The molecular mechanics/generalized Born surface area (MM/GBSA) approach (Kollman et al., 2000), which is implemented in the Amber program, was applied to

compute the binding free energy ($G_{binding}$) of each complex. The $\Delta G_{binding}$ was determined from the free energies of the complex, protein and ligand according to the equation:

$$\Delta G_{binding} = G_{water}(complex) - [G_{water}(protein) + G_{water}(ligand)] \quad (1)$$

The binding free energies of each term were in turn estimated from the absolute molecular mechanical energies (E_{MM}), the solvation free energies (G_{sol}) and the vibration, rotation and translation entropies. Each of these terms was calculated with the following equations:

$$G_{water} = E_{MM} + G_{sol} - TS \quad (2)$$

$$E_{MM} = E_{int} + E_{ele} + E_{vdW} \quad (3)$$

$$G_{sol} = G_{GB} + G_{np} \quad (4)$$

$$G_{np} = 0.0072 * SASA \quad (5)$$

where E_{int} is the internal energy having three contributions: E_{bond}, E_{angle}, and $E_{torsion}$, which represent the strain energy in bonds, angles and torsion angles caused by their deviation from the equilibrium values; E_{ele} and E_{vdW} are the electrostatic and van der Waals interaction energies, respectively; T is temperature; S is the entropy. G_{GB} is the electrostatic solvation free energy obtained by solving the generalized Born equation; G_{np} is the non-polar solvation free energy given by Equation 5; $SASA$ is the solvent accessible area (Sitkoff et al., 1994).

Energy decomposition was performed on the gas phase energies of the system calculated with the GB models in Amber, with respect to the backbone and side chain atoms for each amino acid. Decomposition was performed on a per-residue basis with interaction to either electrostatic or vdW contributions. Dielectricity constant for electrostatic interactions was set as 1.0. Onufriev's GB and ICOSA method (Onufriev et al., 2004; Weiser et al., 1999) were used for SASA calculation. Dielectricity constant for the solvent was 80.0 and solute was 1.0.

3.4.3 Virtual screening of SerC mutants

Site-directed saturation mutagenesis was applied to key residues identified from energy decomposition. The respective position has been mutated to 20 natural amino acids, respectively. Each of the protein and the complex were generated with the above method, respectively. The energy change between the mutant and the wild type was calculated for each mutation according to the following equation:

$$\Delta\Delta G_{binding} = \Delta G_{binding}\text{ (mutant)} - \Delta G_{binding}\text{ (wild type)} \quad (6)$$

3.5 Strain Construction

3.5.1 Preparation of calcium competent *E. coli*

The protocol for the preparation of calcium competent *E. coli* cells was modified from the Hanahan method (Hanahan, 1983). One isolated colony from LB plate was inoculated into 3 mL LB medium for overnight cultivation. The overnight culture was then transferred into 50 mL LB medium in shake flask with 100 dilution. When the OD_{600} of culture reached 0.4~0.5, cells were harvested at 4 ºC at 4000 rpm for 10 minutes. The supernatant was discarded under clean bench and the cell pellets were resuspended gently with 20 mL ice-cold 0.1 M $CaCl_2$ and kept on ice for 30 minutes. Centrifuge again to get rid of the supernatant and resuspend cells in 2 mL ice-cold 0.1 M $CaCl_2$ with 15% glycerol under clean bench. Aliquot the prepared competent cells into 2 mL sterile tubes and store in -80 ºC freezer.

3.5.2 Preparation of electrocompetent cells and electroporation of cells

The procedure for preparation of electrocompetent cells was modified from the method reported by Yu et al. (2000). Cryo-stock cells or isolated colony was inoculated into 3 ml of LB medium for overnight cultivation. The overnight culture was inoculated into 10 ml LB medium in 50 ml conical tube for about 2 hours. When its OD_{600} reached

0.3~0.4, the culture with tube was kept on ice for 15 min. Then centrifuge was performed at 4000 rpm for 10 min to harvest the cells. The cell pellets were resuspended in 1 ml chilled sterile 10% glycerol and spun for 30 sec at 13,000 rpm and 4 °C to remove supernatant. Repeat at least three wash cycles in 10% glycerol. Finally, the cells were resuspended in 400 μl chilled 10% glycerol for electroporation or storage. Add 20 mM L-arabinose for induction during the process if necessary.

The procedure of electroporation was modified from the method reported by Dower et al. (1988). The thawed electrocompetent cells were mixed with DNA (<100 ng) on ice and then the mixture was pipetted into a chilled cuvette. The cells in the cuvette were electroporated using the Gene Pulser™ (Bio-Rad Laboratories, Hercules, CA, USA) at 2.5 kV, 25 μF, with a pulse controller of 200 ohms. After electroporation, SOC medium was added to the cuvette and then the mixture was transferred to a 1.5 ml tube on shaking incubator to recover the cells at 37°C for 1 h. Spread the cells on LB plate containing the appropriate antibiotic and incubate overnight at 37°C.

3.5.3 Genetic modification on the chromosome

The genes *gdh*, *gltB*, *gltD*, *ldhA* and *adhE* were knocked out using λ red recombination or CRISPR/Cas9 methods. Detailed theoretical backgrounds were described in Section 2.3.

A simplified procedure of λ red recombination method:

(1) Transform pKD46 into target strain;

(2) Amplify linear fragment DNA using pKD4 as template;

(3) Make target strain carrying pKD46 electrocompetent;

(4) Electroporate linear DNA into electrocompetent cells of target strain;

(5) Verify by colony PCR;

(6) Remove antibiotic resistance with pCP20;

(7) Verify the loss of antibiotic resistance and absence of pCP20;

(8) Stock desired strain for future work.

A simplified procedure of CRISPR/Cas9 method:

(1) Construct pTarget plasmid containing sgRNA and donor DNA;

(2) Electroporate pCas plasmid into target strain;

(3) Make target strain carrying pCas plasmid electrocompetent;

(4) Electroporate pTarget plasmid into electrocompetent cells of target strain;

(5) Cure pTarget plasmid by inducing pCas plasmid with IPTG;

(6) Verify the deletion of pTarget plasmid using colony PCR;

(7) Cure pCas9 plasmid or go to step (3) for another round of genome editing;

(8) Stock desired strain for future work.

3.6 Plasmids construction

3.6.1 Site-directed mutagenesis of SerC

Mutations for the candidates suggested by the computational method were obtained using the approach of site-directed mutagenesis. Point mutations to change the amino acid sequence of SerC were introduced by PCR (CloneAmp^{TM} HiFi PCR Premix, direct and reverse primers 0.03 μM, template plasmid <100 ng) with plasmid pET28a-SerC(WT) used as the template. The PCR products were treated with *Dpn* I at 37 °C in a heat block for 5 min to remove the intact template plasmids before being transformed into Stellar^{TM} competent cells. The resulting plasmids were further transformed into *E. coli* BL21 (DE3) for overexpression of proteins.

3.6.2 Co-expression of SerC, PDC and YqhD genes

The co-expression plasmids pZA-SerC(R42W-R77W)-PDC-YqhD (referred as pZAX) and pZA-SerC(WT)-PDC-YqhD (referred as pZAWT) were constructed as follows. The genes of SerC(R42W-R77W) and SerC(WT) were amplified from the constructed

vector pET28a-SerC(R42W-R77W) and pET28a-SerC(WT), respectively. Linearized vectors containing the genes of PDC and YqhD were achieved using PCR and the plasmid pZA-GDH-PDC-YqhD (Chen et al., 2016) as template with primers having 15 bp extensions homologous at its ends. The PCR-generated fragment and linearized vectors were set up in an In-Fusion cloning reaction using the In-Fusion HD Cloning Kits (Clontech, TaKara Bio USA Inc., USA).

The co-expression plasmids pZAX and pZAWT were transformed into electroporated *E. coli* MG1655△*thr*B (referred as HOM002, Table 3.1) cells respectively according to Dower *et al*. (1988). The resulting strains HOM002/pZAWT and HOM002/pZAX were obtained.

The co-expression plasmids pZAX and pZAWT were electroporated into HOM002/pMely (referred as S87, Table 3.1) respectively and the resulting strains S87/pZAWT and S87/pZAX were obtained.

3.6.3 Construction of SerC library

The primers using for semi-rational design were designed in NNK form (See Table 3.3). Random mutagenesis was achieved using JBS Error-Prone Kit (Jena Bioscience). The obtained PCR products were treated with *Dpn* I and transformed into Stellar^{TM} competent cells to yield a pool of transformants. The plasmids from this pool were mixed if necessary and transformed into target strains for further screening.

3.7 Enzymatic characterization

3.7.1 Overexpression of SerC

E. coli BL21 (DE3) cells harboring the appropriate plasmid were inoculated in 50 mL LB medium at 37 ^{o}C in shake flask with an initial OD_{600} of 0.1 from an overnight culture. The culture medium contained 50 μg/mL kanamycin. When the OD_{600} reached 0.6∼0.7,

IPTG was added into the culture medium at a final concentration of 0.1 mM for induction. After incubation at 25 ºC for 3 h, cells were harvested by centrifugation (5500 rpm, 4 ºC, 10 min) and washed with 50 mM phosphate buffer (pH7.0) twice. Cell pellets were stored at -20 ºC for further usage.

3.7.2 Purification of SerC

Frozen cell pellets were suspended in 2 mL Resuspension Buffer (50 mM sodium phosphate, pH7.4, 0.1 mM DTT, 0.1 mM PLP) and disrupted using Fastprep-24™ Sample Preparation Instrument (MP Biomedicals/VWR, USA). The cell disruption was processed for 30 seconds at a speed of 5.5 m/s, repeated three times with an interval of 2 min on ice. Cell debris were removed by centrifugation (13,000 rpm, 4 ºC, 20 min) and the supernatant was purified using His SpinTrap column (GE Healthcare Bio-Sciences AB, Uppsala, Sweden) according to the standard protocol. The purity of enzymes was checked by SDS-PAGE analysis. Protein concentration was determined using the Bradford method (Bradford, 1976).

3.7.3 Enzymatic assay

3.7.3.1 Activity assay towards L-homoserine in cuvette

L-homoserine transaminase activity was determined at 30 ºC using a coupled enzymatic assay (Ferrier, 1990). The assay was carried out in a total volume of 1 mL consisting of 200 mM potassium phosphate buffer (pH 8.2), 1 mM α-ketoglutarate, 3 mM L-homoserine, 2 mM acetylpyridine adenine dinucleotide (APAD), 16 U L-glutamate dehydrogenase (GDH) from bovine liver and 9 μg of purified SerC protein. The reaction mixture without purified SerC was prepared and incubated at 30 ºC for 5 min. Then the purified SerC was added to start the reaction. The consumption of APAD was monitored at 375 nm using a spectrophotometer. The activity from the control assay, lacking 1 mM α-ketoglutarate (the amino acceptor), was subtracted from the final activity of SerC. One unit of L-homoserine transaminase activity is the amount of

enzyme required to catalyse the transamination of 1 μmol of L-homoserine per min at 30 ºC and triple measurements were conducted for each sample. APAD has a higher oxidation potential and is a more sensitive cofactor compared to NAD for obtaining better assay precision. And the good stability of the commercial GDH used in the coupled assay system, catalysing the conversion of L-glutamate to α-ketoglutarate, enables a satisfied reproducibility of the assay results.

3.7.3.2 Activity assay towards L-phosphoserine in cuvette

As for the L-phosphoserine transaminase activity, the assay condition and the components in the reaction mixture were the same as that for L-homoserine transaminase, except that 3 mM L-phosphoserine instead of L-homoserine, 90 U GDH and 2 μg purified SerC protein were used.

3.7.3.3 Activity assay towards L-homoserine in 96-well plate

As for the GDH-coupled screening method, the activity assay of crude SerC protein in cell lysates was determined on 96-well plate by monitoring the absorbance change of NADH at 340 nm using a spectrophotometer. The detailed steps are described as follows:

(1) The cell pellets on 96-well deep well plate stored at -80 ºC are taken out and thaw at room temperature for 1h.
(2) Use multi-channel pipette to add 400 μL Cell Lysis Buffer to each well, then vortex the deep well plate to resuspend the cell pellets. The Cell Lysis Buffer contains KPB buffer (100 mM, pH8.2), 0.5 mg/ml lysozyme and 0.7 U/ml Dnase I.
(3) Place the prepared deep well plate at 37 ºC for 1h to disrupt cells.
(4) Centrifuge at 3500 rpm, 4 ºC for 15 min, then carefully transfer 150 μL supernatant (cell lysate) into a new 96-well plate.
(5) Add 50 μL Reaction Buffer to each well. Incubate at 30 ºC for 5 min and then start

to monitor the absorbance change of NADH in plate reader. The Reaction Buffer contains KPB buffer (100 mM, pH8.2), 0.4 mM PLP, 2 mM NAD^+, 8 mM α-ketoglutarate, 40 mM L-homoserine and 4 U GDH.

3.7.3.4 Colorimetric assay towards L-homoserine on 96-well plate

By the detection of produced H_2S, the activity of SerC toward L-homoserine can be easily qualitatively determined. H_2S can react rapidly with iron to form a black iron sulfide precipitate, which is readily observable (Allen and Geldreich, 1975). This method doesn't need spectrophotometer to monitor cofactor NADH formation and can be employed on 96-well plate or on agar plate. Herein is a detailed procedure on 96-well plate:

(1) The cells disruption steps are same with Step (1) ~Step (4) in Section 3.7.3.3. Except that 50 mM Tris-Acetate buffer is used instead of KPB buffer.

(2) 50 μL of Reaction Mixture is added into the cell lysates in each well. And incubate on a 30 ºC thermomixer for reacting in the fume hood. The Reaction Mixture contains 50 mM Tris-Acetate buffer, 8 mM α-ketoglutarate, 8 mM L-cysteine, 10 mM $FeSO_4$ and 4 mM DTT.

3.8 Cultivation conditions

3.8.1 Continuous cultivations with glutamate-dependent auxotrophic strain

The pool of plasmids generated in Section 3.6.3 was transformed into the glutamate-dependent auxotrophic strain, resulting in pooled transformants. The pooled transformants were incubated in 20 mL of modified M9 medium. The modified M9 medium contains 10 mM L-homoserine as nitrogen source. 10 mM of α-ketoglutarate (α-KG) and 0.3 mM L-serine were also added in the culturing medium.

After cultivation for several days at 30 ºC, 10 μL of culture was subcultured into 3 mL fresh modified M9 medium. After several rounds of continuous cultivation, cultures

were streaked on the plate to isolate single colony. The plasmids from the isolated colonies were sequenced, respectively.

3.8.2 Cultivation conditions on 96-well deep well plate

The cultivation conditions are modified from Reetz and Carballeira (2007). First, pre-fill the 96-well deep well plate with 300 µL LB media containing appropriate antibiotics for each well. Then use tips to transfer every single transformant from agar plate into each well. The resulting plate is named as 1st plate. Seal the 1st plate with a gas-permeable seal and shake at 37 ºC, 300 rpm overnight. Second, 50 µL of the overnight culture in the 1st plate is transferred into a 2nd plate for protein overexpression. The 2nd plate is pre-filled with 600 µL LB media containing appropriate antibiotics in each well. The 1st plate is stored at 4 ºC as back-up and the 2nd plate is sealed with a gas-permeable seal and shake at 37 ºC, 300 rpm for 3 hours. Then add 0.1 mM IPTG in each well for induction and continue cultivation at 30 ºC, 300 rpm for 4 hours. The 2nd plate is centrifuged at 3000 rpm for 15 min to harvest cells, which can be stored at -80 ºC for further usage.

3.8.3 Fermentation conditions on DASGIP equipment

Fed-batch fermentations were carried out in a well-controlled DASGIP parallel bioreactor system (Jülich, Germany) with an initial working volume of 500 ml. The pre-culture was performed with 10 mL of LB medium at 37 ºC overnight and then inoculated into the seed culture medium with an initial OD_{600} of 0.2. The initial OD_{600} of fermentation medium was 0.1. The glucose concentration was controlled via supplying feeding medium with a flexible feed rate. The pH of cultures was kept at 7.4 by titration with NH_4OH. The dissolved oxygen was controlled about 30% of air saturation by automated adjustment of the appropriate agitation speed, oxygen content, and the aeration rates. The temperature was kept at 37 ºC from the beginning for cell growth and changed to 30 ºC after induction. Silicone anti-foaming emulsion (Carl Roth, Germany) was used as antifoaming agent during the fermentation.

The conditions of microaerobic fermentation were modified from Yim et al. (2011). The temperature was held at 37 ºC, and the pH was held at 7.0 using 2 M NH_4OH (aerobic phase) or Na_2CO_3 (microaerobic phase). The cultures were added with 0.2 mM IPTG when the OD_{600} reached 10. One hour after induction, the airflow rate was lowered to 0.02 standard liters per minute for microaerobic conditions, and $NaHCO_3$ was added to a final concentration of 10 mM. The agitation rate was 700 rpm. Glucose concentration was kept between 0.5 and 5 g/L.

3.9 Analytic methods

3.9.1 Analysis of 1,3-PDO and intermediates using HPLC

For the measurements of 1,3-PDO in the cultures, filtered samples from fermentation broth were analysed via HPLC with refractive detector using the Aminex HPX-87H column (300 × 7.8 mm) (Bio-Rad, Hercules, USA). The mobile phase was 5 mM H_2SO_4 with a flow rate of 0.6 mL min^{-1}. The working temperature was set at 60 ºC.

For the measurement of L-homoserine and L-methionine concentrations in the culture broth, filtered samples were used for analysis in an Ultimate 3000 HPLC (Dionex/Thermo Fisher) with a FLD 3100 detector and a Kinetex® 2.6 µm C18 100 Å, LC Column of 100 x 4.6 mm, Ea (Phenomenex). The derivatizing reagent was from Waters AccQ-Fluor Reagent Kit. Eluents included Eluent A of 140mM Na-Acetate, 0.1% ACN, pH 4.95, Eluent B of 40% Milli-Q H_2O, 60% ACN, and Eluent C of 95% ACN. The running programs were set as follows: flow rate 1 mL/min, column oven kept at 45 ºC, injection volume 10 µl, and a different gradient concentration of Eluent A, Eluent B and Eluent C over time.

3.9.2 Analysis of 1,3-PDO using GC

For detection of 1,3-PDO in shake flask fermentation, filtered samples from the cultivation cultures were treated with phenylboronic acid in HPLC grade acetone. GC

(Agilent 7890B, USA) was used to quantify the concentration of 1,3-propandiol-phenylboronic acid. The non-polar capillary column used here was HP5ms UI, 30m x 250µm x 0.25µm, and the carrier gas was helium constant at 80kPa. The FID temperature was set to be 350 ºC and the injector temperature was 270 ºC, with 0.2 µL injection volume and 1:5 split. The temperature was held at 100 ºC for 2 min and increased to 270 ºC with a gradient of 20 ºC/min.

3.9.3 Identification of DHB and BT using GCMS

The products of DHB and BT in culture broth samples were derivatized by trimethylsilylation and quantitatively analyzed by GC and GCMS, using a modified procedure adapted from literature (Elliott and Burgess, 2005). 100 µL filtered samples were dried down in a speedvac concentrator (Martin Christ , RVC 2-25 CD-plus) for approximately 1 hour at ambient temperature. Then 20 µL 10 mM cyclohexanol solution (as an internal standard) in dimethylformamide was added. Further, 100 µL N,O-bis(trimethylsilyl)trifluoro-acetimide (BSTFA) with 1% trimethylchlorosilane, was added, and the mixture was incubated at 70 ºC for 30 min. The derivatized samples were centrifuged at full speed for 5 min and then injected into GC or GCMS. A Rtx-5SIL MS capillary column (Restek, 30m x 0.25mm ID x 0.25 µm film thickness) was used.

CHAPTER 4 Rational engineering of SerC for biosynthesis of 1,3-propanediol from L-homoserine in *E. coli*[2]

Herein, a phosphoserine transaminase (SerC) was studied for a novel 1,3-propanediol biosynthetic pathway from glucose via L-homoserine in *E. coli*. The rational design method for altering the substrate preference of SerC from L-phosphoserine to L-homoserine was described in this chapter. The performance of engineered SerC for microbial production of 1,3-propanediol from glucose was studied in shake flask cultivation and fed-batch fermentation.

4.1 Introduction

The natural substrate of phosphoserine transaminase (SerC) from *E. coli*, L-phosphoserine, shares a high similarity in its structure with L-homoserine. This makes SerC a promising candidate to catalyze L-homoserine in the new 1,3-PDO pathway, which starts from extending the homoserine biosynthesis pathway via three heterologous enzymatic reactions (Figure 4.1). SerC catalyzes the crucial deamination of L-homoserine to HOBA, which is the bottleneck step of 1,3-PDO pathway. Compared to the candidates from the class of dehydrogenase, especially the GDH reported by Chen et al., (2015), the transaminase-mediated reaction is uncoupled with the redox balance within the cells and thus its regulation is simple.

Herein, to achieve a higher production of 1,3-PDO, the major task is to improve the performance of SerC towards L-homoserine. SerC belongs to the subgroup IV aminotransferases and it is involved in both pyridoxine and L-serine biosynthesis and catalyzes the reversible conversion of 3-phospho-hydroxypyruvate to L-phosphoserine

[2]The major results of this chapter have been published in Zhang, Y., Ma, C., Dischert, W., Soucaille, P. and Zeng, A. P. (2019) Engineering of Phosphoserine Aminotransferase Increases the Conversion of l-Homoserine to 4-Hydroxy-2-ketobutyrate in a Glycerol-Independent Pathway of 1,3-Propanediol Production from Glucose. Biotechnol. J. DOI: 10.1002/biot.201900003

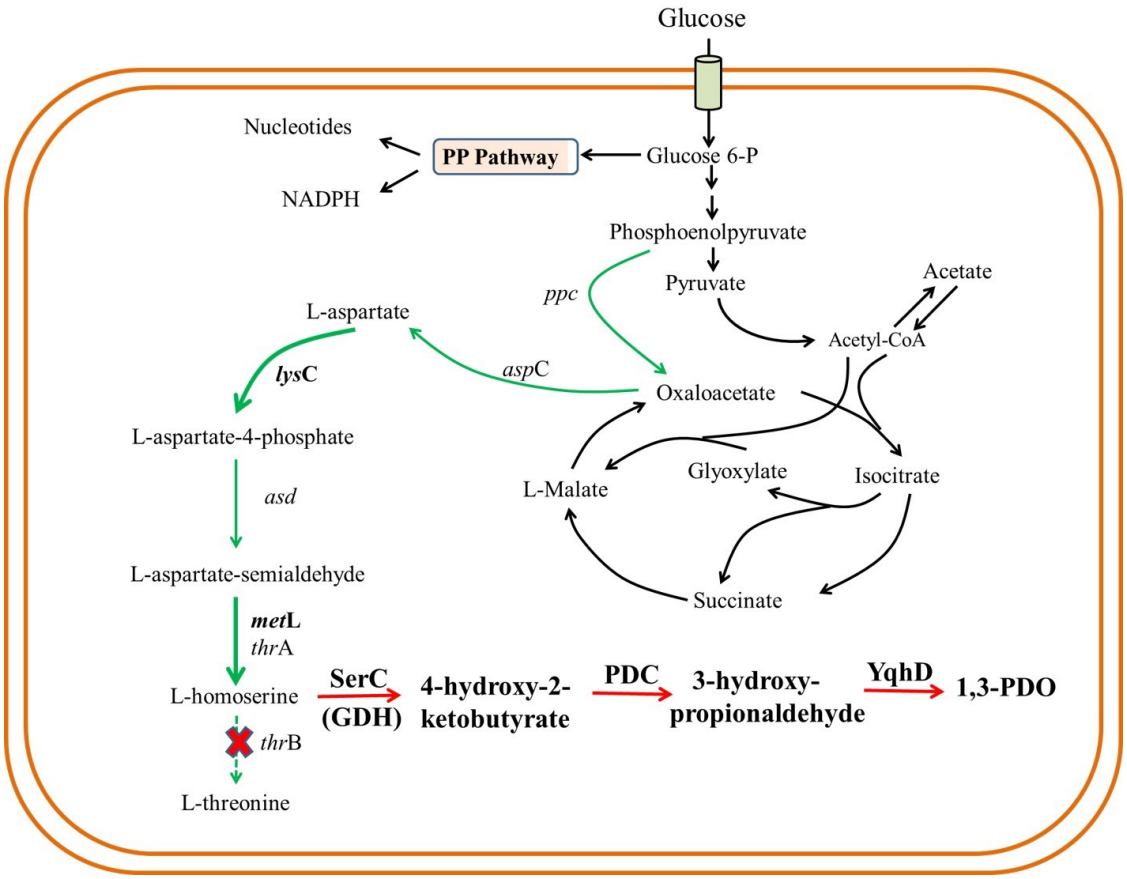

Figure 4.1. The biosynthetic pathway of 1,3-propanediol from glucose via L-homoserine. The natural homoserine-producing pathway in *E. coli* is shown in green line. The biosynthetic pathway for 1,3-PDO production from L-homoserine is given in red line (Adapted from Figure 1 in Zhang et al. 2019).

(Hester et al., 1999; Lam et al., 1990; Drewke et al., 1996). SerC is a homodimer and consists of 361 residues per subunit. Its cofactor PLP is bound through a Schiff base to the active site residue Lys198 (Hester et al., 1999). Since SerC is unable to efficiently bind and transform the desired substrate, L-homoserine, extensive active-site engineering of SerC is necessary. Rational protein engineering has been proven to be a well-established powerful tool for generating novel enzyme variants with altered substrate specificity (Midelfort et al., 2013; Guan et al., 2015). For example, by determining and analysing the crystal structures of LlAdhA and LlAdhA^{RE1}, Liu et al. (2012) finally obtained a new variant (adding N110S to LlAdhA^{RE1}) whose K_m for

isobutyraldehyde, a non-native substrate of LlAdhA, is ~17-fold lower and the catalytic efficiency is higher than the wild type LiAdhA by ~160-fold.

Based on the structural and functional information of SerC, a computation-based rational approach was employed to alter the substrate preference of SerC from L-phosphoserine to L-homoserine. In this approach, residues involved in the substrate binding specificity were identified through calculating binding free energy based on MD simulations and decomposing the energy at the residue level for each complex. Then the site-directed saturation mutagenesis was employed *in silico* for virtual screening. To prove the validity of the improved SerC, a recombinant *E. coli* was constructed by co-expressing the best SerC mutant, PDC and YqhD.

4.2 Results and discussion

4.2.1 Identification of residues determining the substrate binding specificity

SerC is a homodimer and both the coenzyme PLP and the substrate are located at the interface of the two subunits (Hester et al., 1999). In order to identify residues that are responsible for the substrate binding specificity, binding free energy was calculated based on MD simulations and the energy was decomposed at the residue level for each complex.

For each system, the MD simulations lasted 10 ns and their trajectories were recorded at a time interval of 10 ps. To examine the convergence of the MD simulations, the backbone root-mean-square deviations (RMSD) and the backbone root-mean-square fluctuations (RMSF) were calculated from the trajectories using the first configuration as the reference and all coordinate frames from the trajectories were first superimposed on the initial conformation to remove any effect of overall translation and rotation (Figure 4.2).

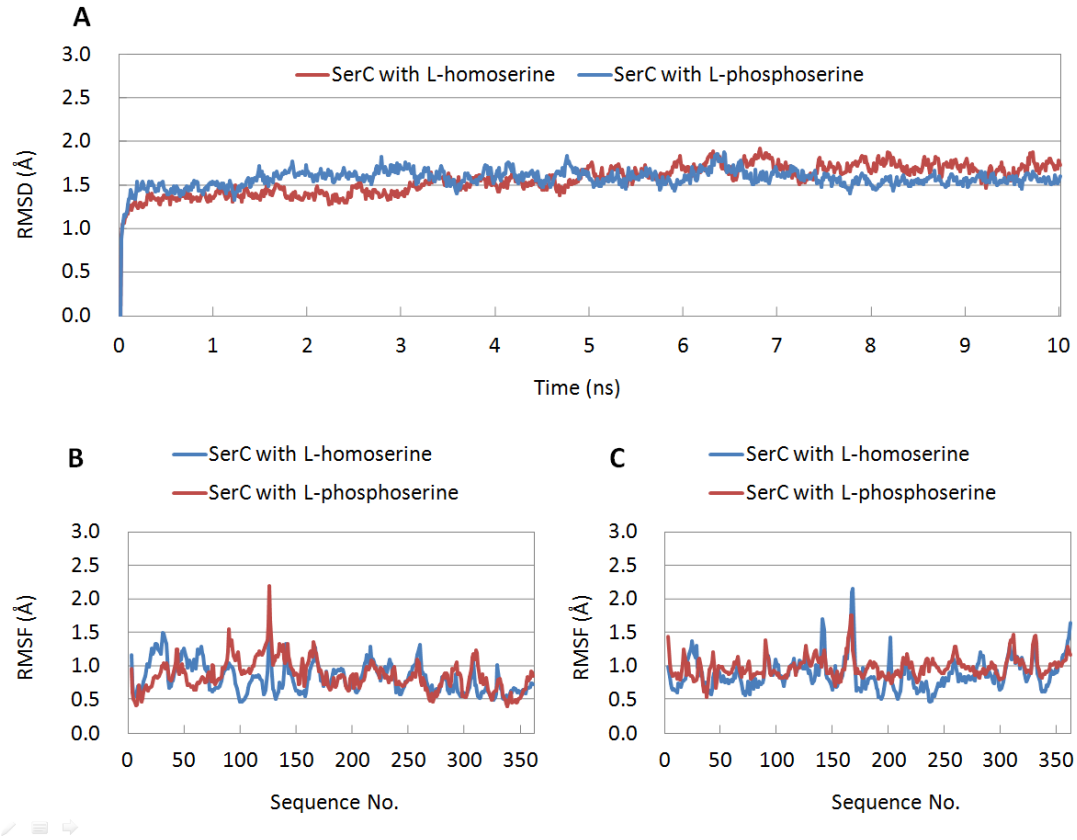

Figure 4.2. A) The backbone root-mean-square deviations (RMSD) of the MD simulations; B) The backbone root-mean-square fluctuations (RMSF) for chain A; C) RMSF for chain B.

It was found that Arg329 from chain A and Arg42 from chain B contribute most to the substrate binding when L-phosphoserine is used as the substrate. Their binding free energies are -23.72 and -23.74 kcal/mol, respectively (Figure 4.3 A and B). When the substrate is replaced by L-homoserine, Lys198 from chain A and Arg42 from chain B contribute most to the substrate binding. Their binding free energies are -11.94 and -20.71 kcal/mol, respectively (Figure 4.3 C and D).

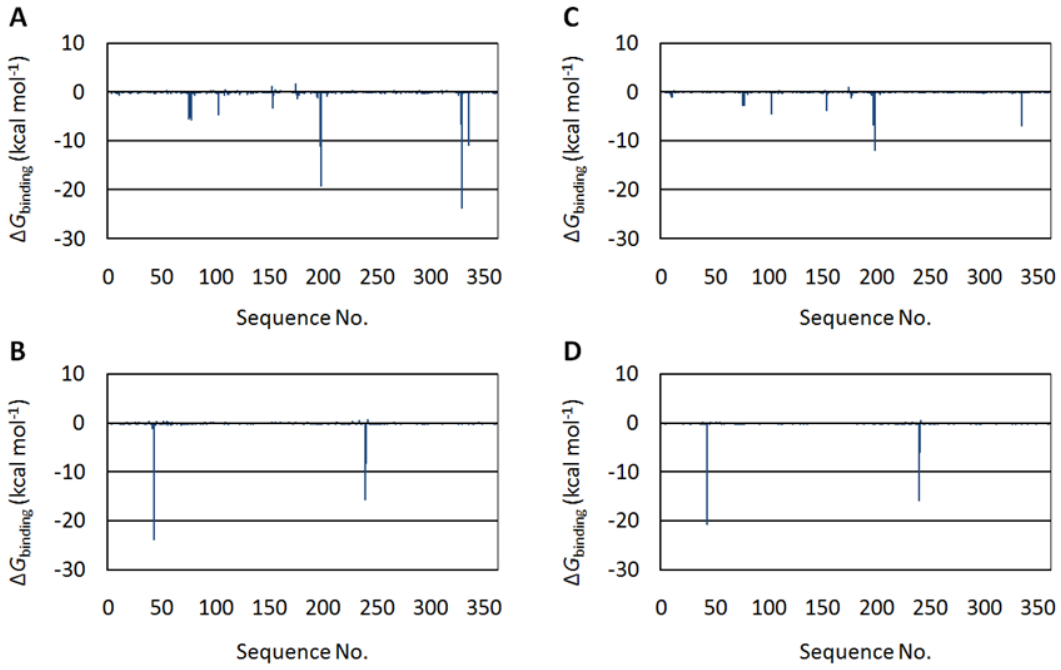

Figure 4.3. Decomposition of binding free energy at residual level for SerC with different substrates. A) Chain A of SerC with L-phosphoserine as the substrate. B) Chain B of SerC with L-phosphoserine as the substrate. C) Chain A of SerC with L-homoserine as the substrate. D) Chain B of SerC with L-homoserine as the substrate.

By decomposition of the binding free energy at residue level, it is possible to compare their contributions for each residue. Because of the fact that the substrate binding specificity for L-phosphoserine and L-homoserine is determined by the difference in their side chains, identification of the key residues responsible for the substrate binding specificity was focused on the regions around the side chains of the substrates. Among the residues, five of them that exhibited large differences in the binding free energy were identified to be involved in the substrate binding preference. Among them, three belong to chain A (Arg77(A), His328(A) and Arg329(A)) and two belong to chain B (His41(B) and Arg42(B)). As shown in Figure 4.4, all of the five residues make great contributions to the substrate binding in the case of L-phosphoserine as the substrate (Figure 4.4 A). However, only three key residues were identified (Arg77(A), His41(B) and Arg42(B)) when the substrate was replaced by L-homoserine (Figure 4.4 B).

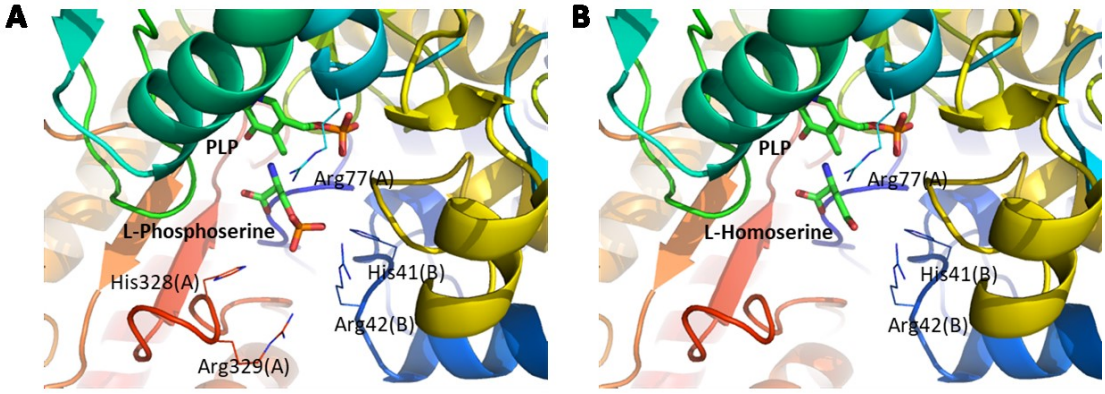

Figure 4.4. Residues involved in the substrate binding specificity of SerC. A) L-Phosphoserine serves as the substrate. B) L-Homoserine serves as the substrate.

4.2.2 Single-site virtual screening and enzyme activity assay of SerC mutants

Based on the results of energy decomposition, virtual screening was conducted on the identified residues. In the first round, single-site saturation mutagenesis was carried out, which resulted in seven mutants that exhibit lower binding free energy for L-homoserine than the wild type SerC, but with relatively high binding free energy for L-phosphoserine (Table 1). It can be seen that all the mutations are found in residues His41 and Arg42, indicating the importance of these two residues in the substrate binding specificity of SerC.

To test the computational results, mutated His-tagged SerC was overexpressed and purified using affinity chromatography. Molecular weight of the purified SerC was determined to be approximately 39 kDa by SDS-PAGE, which is in consistence with the theoretical value of 39.7 kDa. Enzymatic assay of these mutants demonstrated that SerC(R42W) showed the highest activity towards L-homoserine (Table 4.2). Compared with the wild type, the activity of SerC(R42W) was increased by more than twice, whereas its activity towards L-phosphoserine was decreased by over ten times (272 Vs. 3,406 mU/mg).

Table 4.1: Mutation sites suggested by the virtual screening

Rounds	Mutation sites	$\Delta\Delta G_{binding}$ (kcal/mol)		Specific activity (mU/mg)
		L-Homoserine	L-Phosphoserine	L-Homoserine
1st	WT	0.0	0.0	115
	R42W	-0.4	0.7	266
	R42Q	-0.3	0.5	148
	R42K	-0.2	0.3	131
	R42E	-0.3	0.6	22
	H41Q	-0.2	-0.1	51
	H41Y	-0.2	-0.1	31
	H41K	-0.3	-0.4	10
2nd	R42W-R77W	-0.6	0.5	487
	R42W-R77T	-0.6	0.6	273
	R42W-R77S	-0.5	0.5	224
	R42W-R77I	-0.5	0.8	180
	R42W-R77E	-0.5	0.5	58
	R42W-R329H	-0.4	0.8	293
	R42W-R329Q	-0.4	0.7	281
	R42W-R329G	-0.4	0.8	145
3rd	R42W-R77W-H328Y	-0.3	1.3	80
	R42W-R77W-H328L	-0.3	0.7	36
	R42W-R77W-H328E	-0.3	0.8	7
	R42W-R77W-H328K	-0.3	0.5	n.d.[a]

[a)] not detectable

For the residue Arg42, there is a slight increase of activity to L-homoserine when it was replaced by glutamine (R42Q) or lysine (R42K). However, the activity was largely deceased when the positively charged residue was changed to be a negatively charged residue as shown in the case of R42E, although its activity to L-phosphoserine was almost completely diminished (4 mU/mg) due to the reverse of the electrostatic interactions between this residue and the γ-phosphate group of L-phosphoserine. For the residue His41, all of the tested three mutants showed low activity towards L-homoserine. The pairs of His41(B) and Arg42(B), His328(A) and Arg329(A), located next to an α-helix and in a loop between β-strands. These two pairs from different chains are opposite to each other and shaped like a claw to hold the substrate (Figure 4.4). From these results, it can be seen that the position Arg42 exhibited a much higher

flexibility than His41 regarding the alteration of substrate preference.

4.2.3 Double- and triple-site mutagenesis of SerC

Enzymatic results from single-site SerC mutants indicated that SerC(R42W) exhibited the best activity towards L-homoserine. Thus, in the second round of virtual screening, double-site saturation mutagenesis was conducted on Arg42(B) and one of the other four key residues. The mutations exhibiting low binding free energy for L-homoserine and high energy for L-phosphoserine are listed in Table 4.1. Among them, five are the combination of residues Arg42 and Arg77 and the other three are Arg42 and Arg329. Except for R42W-R77E, the specific activity of all the other candidates was increased when L-homoserine was used as the substrate. Especially, the mutant SerC(R42W-R77W) showed obviously improved specific activity of 487 mU/mg towards 3 mM L-homoserine, which was 4.2-fold higher than that of the wild type SerC (Table 4.1). As for its natural substrate L-phosphoserine, SerC(R42W-R77W) almost lost its activity compared to the wild type (79 Vs. 3,406 mU/mg).

To achieve a higher activity towards L-homoserine further, triple-site mutagenesis was carried out in the third round based on the best mutant SerC(R42W-R77W) from the second round and one of the other three key residues. Based on computation the residue His328 was suggested as the best one for the combination. However, the change of binding free energy ($\Delta\Delta G_{binding}$ = -0.3 kcal/mol) is higher than those achieved for SerC(R42W) (-0.4 kcal/mol) and SerC(R42W-R77W) (-0.6 kcal/mol). Experiments also demonstrated that all of the triple-site mutants lost their activity towards L-homoserine when the mutations were introduced into SerC(R42W-R77W) (Table 4.1). Considering the similar results of His41 in the single-site mutagenesis, it was proposed that both His41 and His328 make contributions to the structural stability of the substrate binding pocket, especially the interface composed by the two pairs of His41(B) and Arg42(B), His328(A) and Arg329(A).

The enzyme kinetics of the wild type and best-engineered mutant were determined. As demonstrated by the kinetics parameters (Table 4.2), the K_m value was decreased from 158.50±20.79 for the wild type to 14.15±1.94 mM for the best mutation SerC(R42W-R77W) when L-homoserine was used as the substrate. This is in accordance with the virtual screening which intended to increase the substrate binding affinity. However, the K_m value is still much higher than that for the wild type towards L-phosphoserine (0.12±0.02 mM) although their V_{max} values are similar (1.96±0.05 Vs. 1.86±0.09 μmol/min/mg).

Table 4.2 Kinetic parameters of SerC(WT) and SerC(R42W-R77W) on L-phosphoserine and L-homoserine.

Enzyme	L-phosphoserine			L-homoserine		
	V_{max} (μmol/min/mg)	K_m (mM)	$k$cat/K_m ($s^{-1}mM^{-1}$)	V_{max} (μmol/min/mg)	K_m (mM)	$k$cat/K_m ($s^{-1}mM^{-1}$)
WT	1.86±0.09	0.12±0.02	10.3	3.90±0.16	158.50±20.79	0.02
SerC(R42W-R77W)	n.d.[a]	n.d.[a]	n.d.[a]	1.96±0.05	14.15±1.94	0.09

Data are presented as means ± STDV calculated from at least three replicates.

[a)] not detectable

4.2.4 Production of 1,3-PDO from L-homoserine in shake flasks

L-Homoserine is a precursor for the biosynthesis of L-threonine and L-methionine. The L-homoserine biosynthesis pathway contains three reactions that convert L-aspartate into L-homoserine. The corresponding enzymes in this pathway are intricately regulated and most of them are under repression by both L-methionine and L-threonine. Therefore, to validate the effects of the engineered SerC, *E. coli* MG1655 △*thr*B (HOM002) was used as the host strain and 5 g/L L-homoserine was added into the culture medium (FM I) to enhance the supplement of L-homoserine.

To assure the functionality of 1,3-PDO pathway, three genes (*ser*C, *pdc* and *yqh*D) for the consecutive reactions were assembled in a medium-copy-number plasmid pZA under the control of $P_{LtetO-1}$ operator. The resulting strains HOM002/pZAX and HOM002/pZAWT were cultivated in shake flasks. The wild type strain achieved relatively higher OD_{600} compared to the mutant strain (Figure 4.5). After 48h of cultivation, the mutant strain HOM002/pZAX and the wild type strain HOM002/pZAWT produced 277±20.8mg/L and 5.40±0.78 mg/L of 1,3-PDO, respectively.

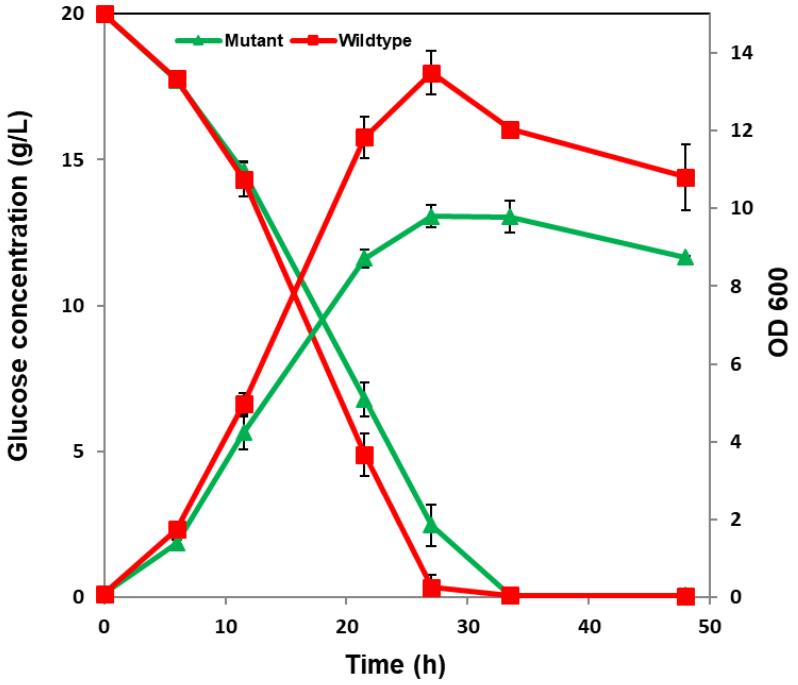

Figure 4.5. Shake flask cultivations of HOM002/pZAWT (wild type) and HOM002/pZAX (mutant) with addition of 5 g/L L-homoserine into the culture medium (FM I). Wild type strain is shown in red square and mutant is in green triangle.

4.2.5 Production of 1,3-PDO from L-homoserine in fed-batch fermentation

To avoid the toxicity of added L-homoserine to the growth of *E. coli* and to explore the potential capacity of the engineered SerC in 1,3-PDO production further, pZAX was transformed into a homoserine-producing strain S87 (see Table 3.1) and fed-batch

fermentations with S87/pZAX were performed in bioreactors using glucose as the carbon source (FM III). As shown in Figure 4.6, the engineered strain achieved a higher cell density compared to the wild type strain S87/pZAWT. After about 17 h of fermentation, glucose was almost completely consumed by both the mutant and the wild type strain. A concentrated glucose stock solution was then added. Surprisingly, the cell growth of the wild type strain went into a stationary phase, while the mutant strain continued growing until its OD_{600} reached 44. The mutant strain was able to produce 3.03 g/L 1,3-PDO after 62 h of fermentation, which is 13-fold higher than the wild type strain (0.24 g/L), and the yield of 1,3-PDO on glucose is also increased by 10 times compared to that of the wild type strain (1.93 % Vs. 0.20 %), indicating the effectiveness of the improved SerC.

Interestingly, the concentration of L-homoserine in the culture of mutant strain was higher than that of the wild type strain, revealing that there is still much room for the utilization of L-homoserine. There are several possible reasons for this. First, the strain embedded with the mutant grew faster than the wild type and thus its OD is higher than that of the wild type. Second, unlike L-homoserine, the concentration of L-methionine in the culture of the wild type is much higher than that of the mutant, which may be another reason for the lower concentration of L-homoserine in the wild type, considering the fact that the pathway of L-methionine from L-homoserine was not blocked in the engineered strain.

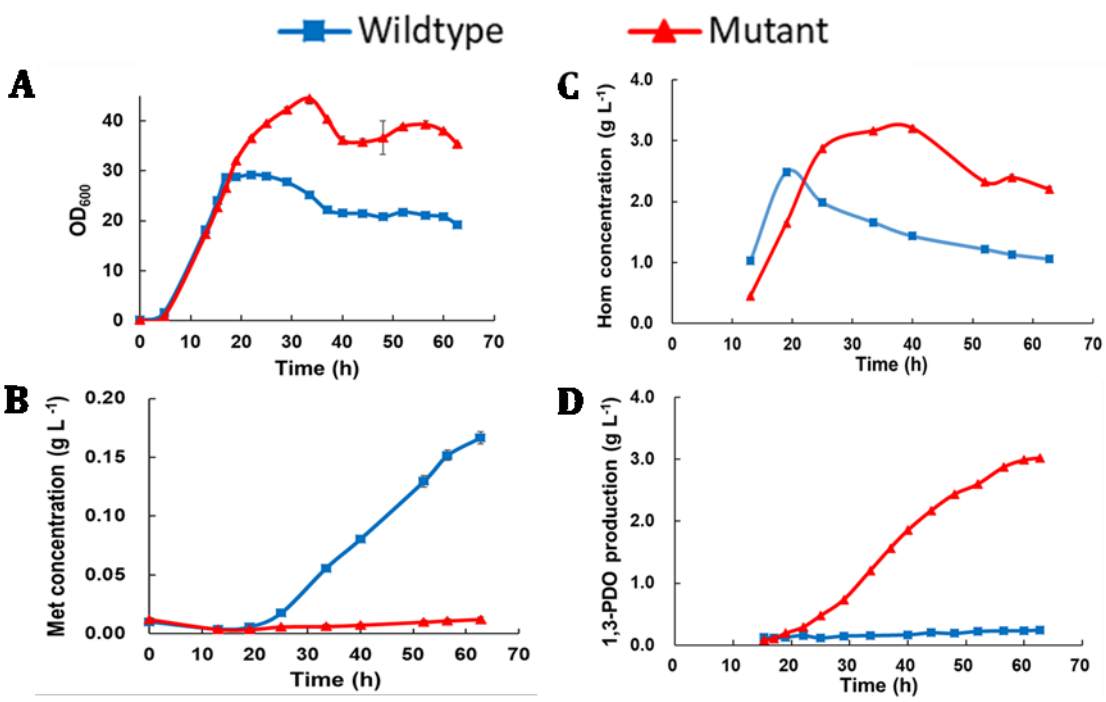

Figure 4.6. The fed-batch fermentation profiles of S87/pZAX (Mutant) and S87/pZAWT (Wild type). Hom: L-homoserine; Met: L-methionine. A) OD_{600}; B) Met concentration (g/L); C) Hom concentration (g/L); D) 1,3-PDO production (g/L). The wild type is shown in blue squares and the mutant in red triangles. Error bars represent standard deviations of the measurements performed in triplicate.

In addition, the formation of byproducts at the end point of fermentations (62 h) has been provided in Figure 4.7. It is clear to see that the strain with the wild type SerC undergoes a process of mixed acid fermentation. Among the acids, acetate is the main byproduct, which is followed by succinate and lactate. As for the strain embedded with the best mutation, it undergoes a process of ethanol fermentation. The concentration of ethanol (47.40 g/L) is much higher that of the acids. No big difference was discovered for the formation of formate.

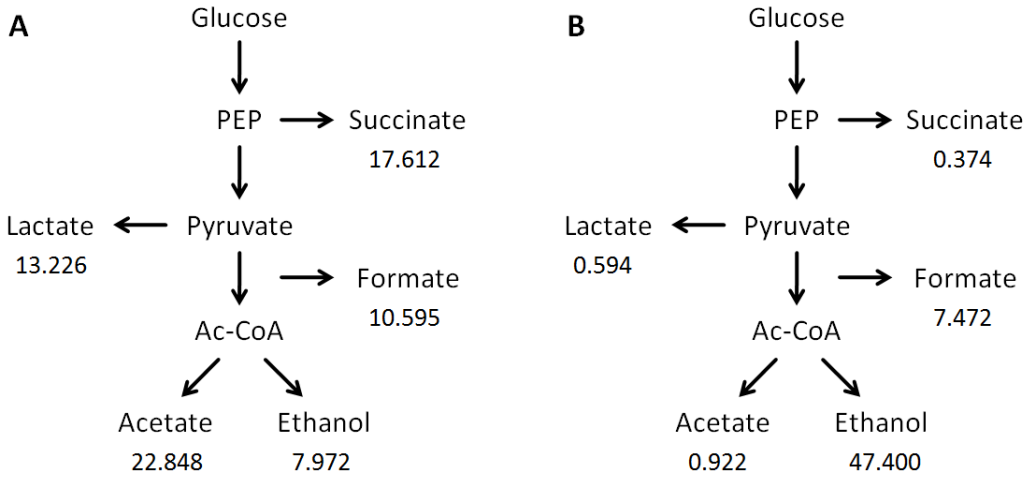

Figure 4.7. Formation of the byproducts (g/L) at the end point of fermentations (62 h). A) S87/pZAWT (Wild type); B) S87/pZAX (Mutant). PEP: phosphoenolpyruvate; Ac-CoA: Acyl-coenzyme A.

The performance of another branched-chain alpha-ketoacid decarboxylase (KDC), which encoded by the *kdc*A gene from *Lactococcus lactis*, was also studied. *E. coli* △*thr*B pMely+pZA-SerC(WT)-KDC-YqhD (wild type strain with KDC) and *E. coli* △*thr*B pMely+pZA-SerC(R42W-R77W)-KDC-YqhD (mutant strain with KDC) were constructed, respectively. In a fed-batch fermentation of both strains (Figure 4.8), the production of 1,3-PDO from the mutant strain with KDC can reach up to 0.60 g/L, higher than that of the wild type strain with KDC (0.38 g/L), but way lower if compared to that of the mutant strain with PDC, which can achieve 3.03 g/L. In summary, the performance of KDC was not as good as PDC in this 1,3-PDO pathway.

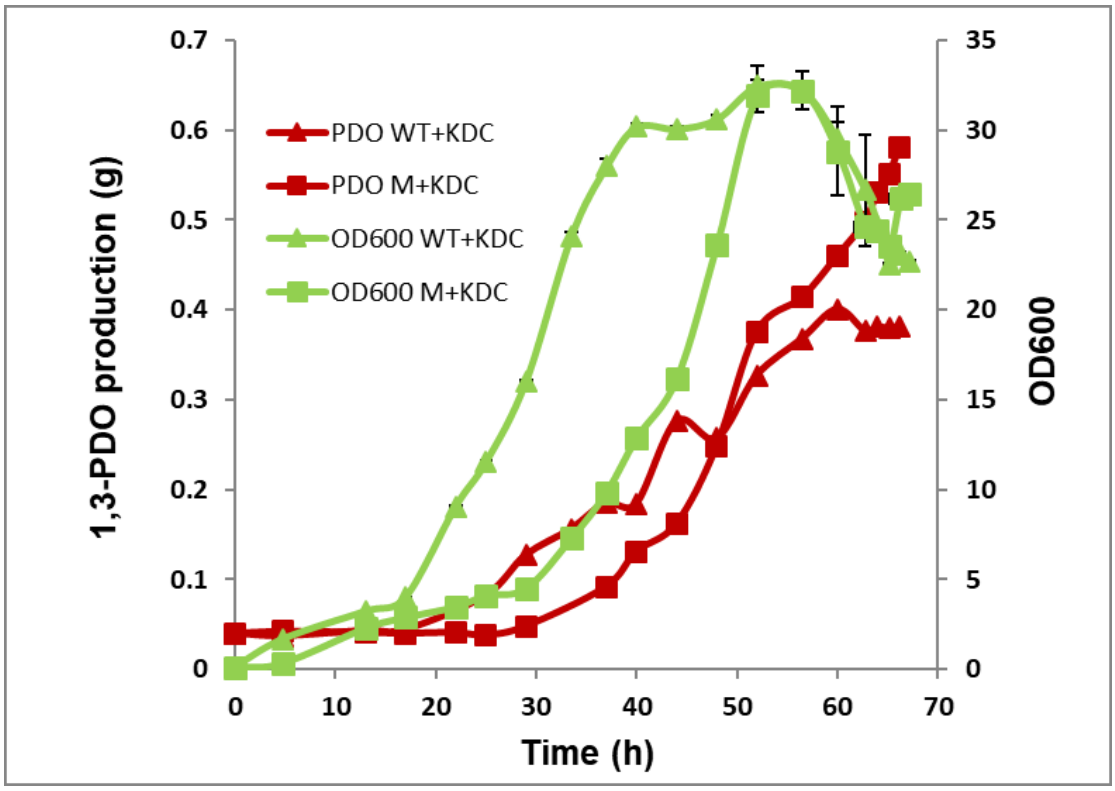

Figure 4.8. Fed-batch fermentation profiles of *E. coli* △*thr*B pMely+pZA-SerC(WT)-KDC-YqhD (wild type strain with KDC) and *E. coli* △*thr*B pMely+pZA-SerC(R42W-R77W)-KDC-YqhD (mutant strain with KDC). The OD_{600} of wild type strain with KDC and mutant strain with KDC is shown in green triangles and green squares, respectively. The 1,3-PDO production by wild type strain with KDC and mutant strain with KDC is shown in red triangles and red squares, respectively.

4.3 Conclusion

In this chapter, a phosphoserine aminotransferase (SerC) was successfully engineered to catalyze the deamination of L-homoserine to HOBA, a key reaction in producing 1,3-PDO from glucose via L-homoserine. The enzyme activity of the best mutant, SerC(R42W-R77W), was improved by 4.2-fold in comparison to that of the wild type when L-homoserine was used as the substrate, while its activity towards the natural substrate L-phosphoserine was completely deactivated. Furthermore, 1,3-PDO production was increased by 50-fold for the mutant strain compared to the wild type

strain in shake flask cultivation. In fed-batch fermentation, after 62 h of cultivation, the mutant strain can achieve up to 3.03 g/L 1,3-PDO, which is 13-fold higher than that of the wild type strain (0.24 g/L). These results indicate that the engineered SerC(R42W-R77W) significantly improved the production of 1,3-PDO in this biosynthetic pathway.

CHAPTER 5 Screening method development for engineering SerC and fermentation verification of mutants

In this section, several screening methods for further improving the performance of SerC towards L-homoserine were investigated. First, a glutamate-dependent auxotrophic strain was constructed and used in a continuous cultivation system to screen a mutant library of SerC *in vivo*. Second, a GDH-coupled photometric detection approach and a colorimetric assay method were studied to screen SerC mutants *in vitro*.

5.1 Introduction

A phosphoserine aminotransferase (SerC) was successfully engineered in the previous study to catalyze the deamination of L-homoserine to HOBA, a key step in the homoserine-derived 1,3-PDO biosynthesis pathway. The activity of the best mutant SerC(R42W-R77W) towards L-homoserine was improved by 4.2-fold. As for the natural substrate L-phosphoserine, SerC(R42W-R77W) almost lost its activity. However, the performance of SerC(R42W-R77W) is still not satisfactory. Considering the limitations of protein rational design, other screening methods were investigated to achieve SerC mutants with a better performance towards L-homoserine.

Directed evolution of enzymes typically generates very large libraries of variants and thus requires extensive high-throughput screening. Therefore, it is vital to have a rapid and sensitive system to screen the mutant libraries. Among the developed screening techniques, the building of an auxotrophic strain based on growth complementation for screening has been proven to be a useful tool (Dietrich et al., 2010). Different from other screening methods which are performed on individual variant, this selection-based method is performed simultaneously on the entire library. Zhang et al. (2010) deleted the transaminase genes *avt*A and *ilv*E from the chromosome of wild type *E. coli* to make it a L-valine auxotrophic. It is known that L-glutamate can be efficiently formed by reductive amination of 2-ketoglutarate with ammonia using glutamate

dehydrogenase (GDH) in the presence of cofactor NADPH. Since the chemical structures of 2-ketobutyrate and 2-ketoisovalerate (the L-valine precursor) are very similar, the authors assume that GDH variants active towards 2-ketoisovalerate could be also active towards 2-ketobutyrate. Therefore, although the constructed *E. coli* L-valine auxotrophic cannot grow in minimal medium, it can be rescued by a mutant GDH aminating the 2-ketoisovalerate. Using this selection strategy, the authors screened pooled transformants (~10^9 cells) in 30 mL of M9 medium. After several rounds of successive subculturing, one best mutant was screened out. The specificity constant $k$cat/K_m of the best mutant towards 2-ketobutyrate is 50-fold higher than that towards the natural substrate 2-ketoglutarate. Herein, we adopted a similar selection strategy by constructing an *E. coli* L-glutamate auxotrophic. The growth of the glutamate-dependent auxotrophic *E. coli* in the modified minimal medium can be rescued by introducing a heterogenous transamination reaction, which catalyzes L-homoserine and α-ketoglutarate into HOBA and L-glutamate. This method can be used to screen large libraries of variants *in vivo*.

Compared to the above *in vivo* screening method, *in vitro* strategy is more observable, easily manipulated and quantitative. The commonly used methods here are visual screening of the colored colonies or an enzyme-coupled screening method. The colorimetric detection can be achieved by forming a detectable product through the reaction of a target chemical with an exogenously added reagent. Alternatively, indirect factors such as product-associated changes in pH (Bornscheuer et al., 1999) or coproduction of H_2O_2 (Zhou et al., 1997) may also be employed for product detection. However, the background noise in the microbial intracellular environment may impede accurate product quantification and the reagent cost may become a significant factor when dealing with a large library size. The first issue can be minimized by increasing production titers. The second issue should be considered and evaluated before employing such a strategy. Photometric assay is another regularly used method for quantification of enzyme cofactors such as ATP and ADP (Koresawa and Okabe, 2004; Kleman-Leyer et al., 2009), reduced or oxidized of NAD and NADP (Molnos et al.,

2003; Smith et al., 2009) and free coenzyme A (Hulcher and Oleson, 1973). When no such cofactors are involved in the target reaction, enzyme-coupled method is an alternative way. The cofactor of the coupled enzyme normally can be monitored continuously through fluorescence change using a microtiter plater reader (Molnos et al., 2003). Herein, we investigated both colorimetric assay method and enzyme-coupled photometric detection strategy for screening mutant library of SerCs *in vitro*.

5.2 Results and discussion

5.2.1 Construction of a glutamate-dependent auxotrophic strain

E. coli has two primary pathways for the synthesis of L-glutamate. One pathway is catalysed by glutamate dehydrogenase (GDH) through the reductive amination of α-ketoglutarate. The other pathway is known as the glutamine synthetase-glutamate synthase (GOGAT) pathway. The L-glutamine synthetase leads to the synthesis of L-glutamine from L-glutamate and ammonia, while the glutamate synthase catalyses L-glutamine and α-ketoglutarate to form two L-glutamate molecules, resulting in a net formation of L-glutamate in the GOGAT pathway. These two pathways play different roles in glutamate synthesis when *E. coli* is under energy or ammonium restriction (Goss et al., 2001; Castaño et al., 1988; Berberich, 1972). Thus, the glutamate auxotrophic strain cannot be achieved by deleting either GDH or glutamate synthase. It is suggested that each of them can produce enough L-glutamate by itself to support the growth of *E. coli*.

To achieve the glutamate-dependent auxotrophic *E. coli*, the genes (*gdh*A, *glt*B, *glt*D) which play great roles in these two primary pathways were deleted from its genome. Gene deletions were performed using lambda red recombination (Datsenko and Wanner, 2000). *E. coli* BL21 (DE3) △*ser*C was used as the starting strain for the deletions of *gdhA*, *gltB* and *gltD* genes. The FRT-flanked kanamycin resistance cassette (*kan*) from pKD4 was generated using primers that had 50bp homologous extension. The PCR

products were transformed into *E. coli* BL21 (DE3) △*ser*C harboring pKD46 which can express lambda red recombinase. Colonies containing the correct deletions were treated with temperature-sensitive plasmid pCP20 to remove the *kan* marker. Finally, the auxotrophic strain *E. coli* BL21 (DE3) △*ser*C △*gdh*A △*glt*BD (S66, see Table 3.1) was obtained.

A heterogenous transamination reaction was then introduced in S66 to substitute the loss of GDH and glutamate synthase (Figure 5.1). This heterogenous transamination reaction is catalysed by SerC to produce L-glutamate from α-ketoglutarate and L-homoserine. Since L-glutamate is required for the growth of *E. coli*, the glutamate-dependent auxotrophic *E. coli* cannot grow in the modified M9 medium. Only those that can produce enough L-glutamate from the heterogenous transamination reaction can grow well during the continuous cultivation.

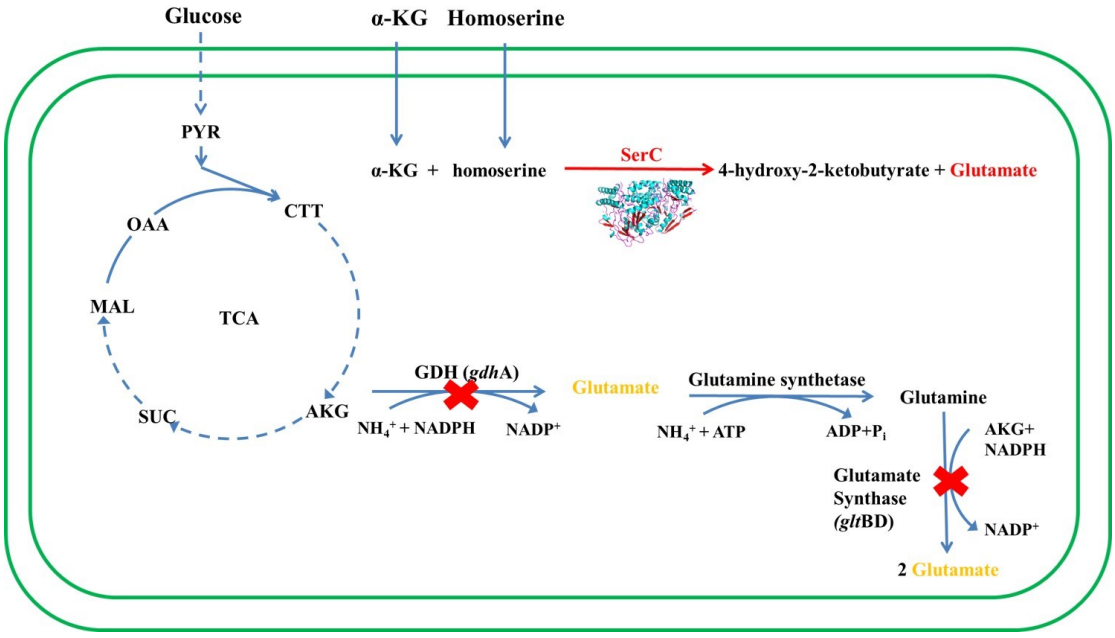

Figure 5.1. Construction of glutamate-dependent auxotrophic *E. coli* used for evolution of SerC. PYR: pyruvate; CTT: citrate; AKG: α-ketoglutarate; SUC: succinate; MAL: malate; OAA: oxaloacetate; Red cross means deleting of genes responsible for the reaction.

5.2.2 Evolving SerC in continuous cultivation

To construct mutant libraries for evolving SerC in a continuous cultivation, both random mutagenesis and semi-rational design were applied. Random mutagenesis was achieved using JBS Error-Prone Kit (Jena Bioscience), which introduces mutations in the gene of SerC by increasing error-rate of the DNA polymerase in a PCR reaction. The rate of mutagenesis achieved by error-prone PCR is in the range of 0.6-2.0%. As for semi-rational design, it is believed that the residues surrounding the substrate binding pocket may have more effects on its activity than those far away from the active site. It was reported that the substrate binding pocket (active site) is situated at the subunit interface (Hester et al., 1999). The two active sites in SerC dimer are situated approximately 20 Å apart from each other. They are formed by residues of both large domains and one small domain at the subunit interface, implying the importance of the complete dimer for activity (John, 1995; Jansonius and Vincent, 1987). The residues of His41, Arg42, His328 and Arg329 in the binding pocket are highly conserved based on a sequence alignment of SerC from diverse sources (Figure 5.2). Changing these conserved residues would undoubtedly decrease its L-phosphoserine catalytic activity dramatically.

Residues of Gy76, Arg77, Tyr101, Trp102, Asn239 and Thr240 from the neighbouring subunit are PLP-binding residues and they are situated at the N-termini of α-helices α3, α4 and α6 respectively (Figure 5.2). The phosphate group of PLP has electrostatic interactions with the positive fields at the N-termini of these α-helical dipoles, especially α3 (Hester et al., 1999). The cofactor of PLP is bound to Lys198 through an aldimine linkage in the active site. In the SerC-AMG complex (PDB:1BJO), AMG (Alpha Methyl-L-Glutamic acid) is covalently bound to PLP as an external aldimine. Ser9 and Arg335 bind the α-carboxylate group of AMG through strong hydrogen bonds

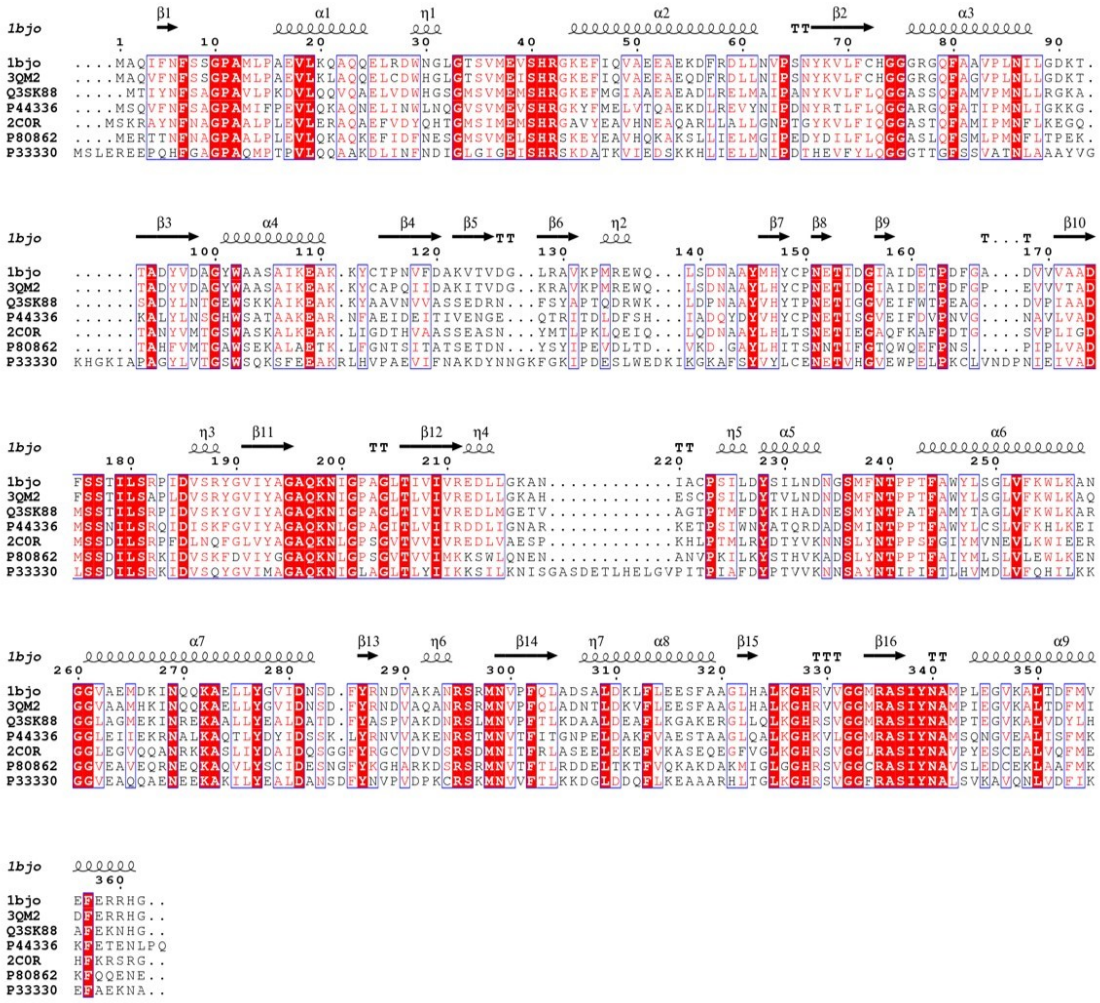

Figure 5.2. Multiple sequence alignment of phosphoserine aminotransferases from different sources. The result was carried out using ClustalW and ESPript 3.0 (Robert and Gouet, 2014). 1BJO from *E. coli* (100%, sequence identity with respect to 1BJO); 3QM2 from *Salmonella typhimurium* (89.50%); Q3SK88 from *Thiobacillus denitrificans* (60.77%); P44336 from *Haemophilus influenza* (52.47%); 2C0R from *Bacillus circulans* (45.05%); P80862 from *Bacillus subtilis* (42.70%); P33330 from *Saccharomyces cerevisiae* (36.71%).

to position AMG in the active site while His41, Arg42 and His328 bind the side chain of AMG (Figure 5.3). Arg77 is involved in binding the AMG side chain indirectly through a solvent molecule and is supposed to position itself during catalysis between the cofactor phosphate group and the substrate side chain. In other words, Arg77 plays

a role in binding the substrate.

In summary, the residues surrounding the substrate binding pocket are likely to be involved in one or more of these possible functions: to bind cofactor of PLP, to bind the

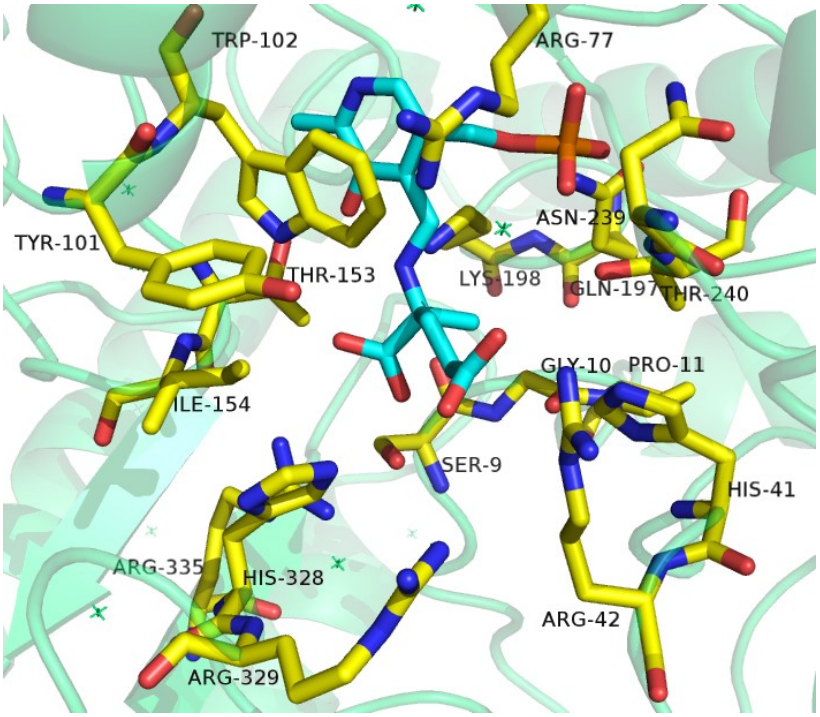

Figure 5.3. The structure of SerC (PDB:1BJO). PLP and AMG are shown in cyan colour. The residues surrounding AMG within 6Å are shown in yellow.

substrate or to play a catalytic role. Therefore, we selected the amino acid residues within a distance of 6 Å from AMG in SerC. They included Ser9, Gly10, Pro11, His41, Arg42, Arg77, Tyr101, Trp102, Thr153, Ile154, Gln197, Lys198, Asn239, Thr240, His328, Arg329 and Arg335 (Figure 5.3). To achieve the mutant library with a high diversity, the primers of these 17 selected residues are designed in NNK form (Table 3.3) (Reetz, 2016). Both pET- and pZA-plasmids carrying *ser*C gene were studied. *Dpn* I was used to get rid of the mother template before transformation.

After several rounds of screening, a few mutants were screened out, such as SerC(R42A) (273 mU/mg), SerC(R42A/R77W) (400 mU/mg) and SerC(R42V) (262 mU/mg). It

was found that the site 42 exists in all of the mutants screened out, once again indicating the importance of this site in the alteration of substrate specificity. Moreover, all triple-site mutations screened, which added another mutation to the double-site mutation R42W-R77W, gave no better mutants compared to SerC(R42W-R77W). The isolated mutants showed unchanged protein sequences after continuous cultivation, but changes at gene level could be noticed.

The results from this screening method were not satisfactory. There are several possible reasons for this. One possible reason is the promiscuity of transaminases. SerC is not the only enzyme that can catalyse this reaction. The loose substrate specificity of both aminotransferase AlaC and AspC suggests that HOBA and L-glutamate might be produced in the wild type *E. coli* (Bouzon et al., 2017; Zhong et al., 2019). Another possibility may be that other compounds derived from L-homoserine can offer nitrogen atom to produce L-glutamate, such as *O*-phospho-L-homoserine and *O*-succinyl-L-homoserine. Both of them can affect the efficiency of this screening method. Besides, the size and diversity of mutant library may also limit the performance of this method.

5.2.3 GDH-coupled photometric detection method

In Section 3.7.3.1, we described the GDH-coupled method for determining the activity of pure protein of SerC by monitoring the formation of APADH at 375 nm in a spectrophotometer. $APAD^+$ is an NAD^+ analog with a higher oxidation potential than NAD^+. It serves as a hydrogen-accepting cofactor in the GDH reaction. The price of $APAD^+$ (1g is 3100 Euro from Sigma-Aldrich) is 41-fold higher than that of NAD^+ (1g is 74.9 Euro from Sigma-Aldrich), which limits its use for screening. NAD^+ is not the best choice for determining the activity of SerC. Considering the experimental cost, NAD^+ was used as cofactor in the GDH-coupled photometric detection method (Figure 5.4). Glutamate dehydrogenase (GDH) from bovine liver was used as the coupled enzyme because it is commercially available and stable, and it has already been successfully applied in numerous continuous coupled assays (Smith et al., 2009; Walton

and Chica, 2013). In this GDH-coupled assay, SerC transfers the amino group of L-homoserine to α-ketoglutarate, resulting in HOBA and L-glutamate. Then L-glutamate is oxidatively deaminated to α-ketoglutarate by GDH, with concomitant formation of NADH. The formation of NADH can be monitored by the change of absorbance at 340 nm.

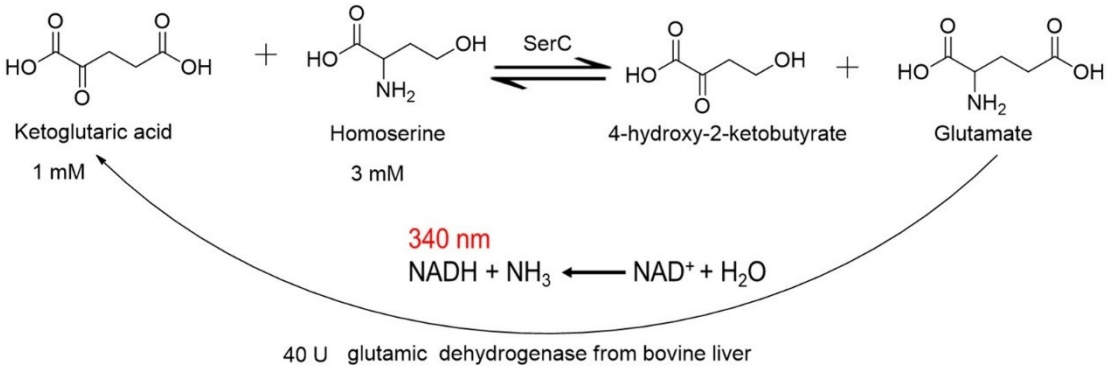

Figure 5.4. Overview of GDH-coupled photometric detection method for SerC screening.

The mutant libraries for screening were constructed as described in Section 3.6.3. 10 mM L-homoserine and 2 mM α-ketoglutarate were used as substrate. The procedure for activity assay is illustrated in Section 3.7.3.3. As seen from Figure 5.5, the activity of SerC from each well can be continuously monitored. The slope in each well is equal to the activity of SerC after calculating from a constant equation. Obviously, the variant of C3 in Figure 5.5 represents the highest activity in this plate.

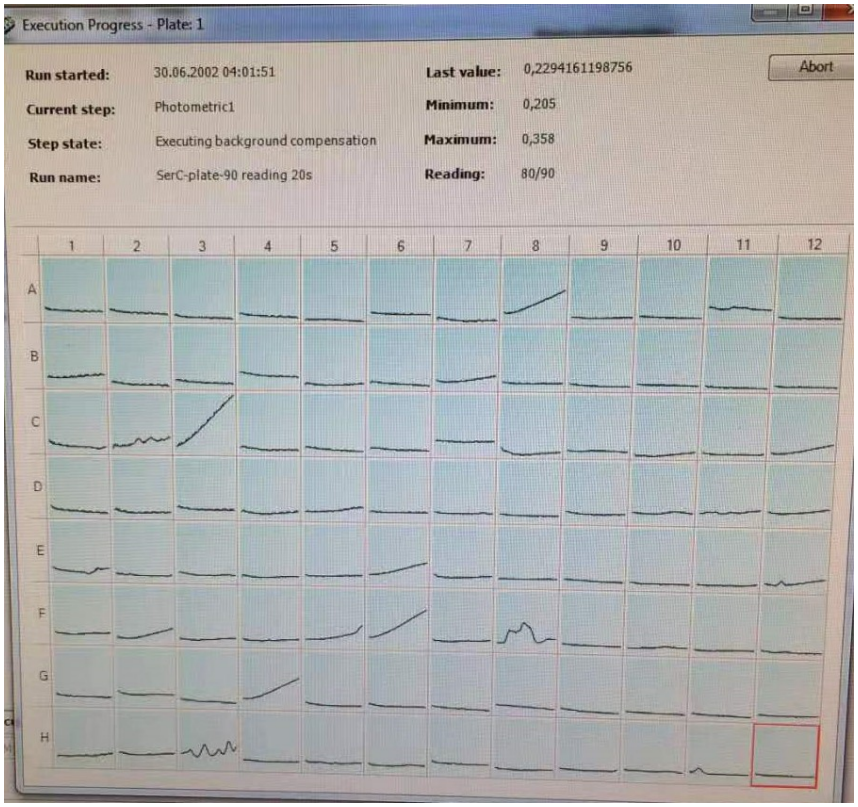

Figure 5.5. A screenshot of real-time graphic of activity assay on a plate reader. Each square means a well on 96-well plate. The plate reader can record the absorbance value of each well every 20 seconds. There are 90 readings for each measurement.

Table 5.1. Activity of mutants screened towards L-homoserine.

	Specific activity (mU/mg)
Mutation	L-Homoserine
SerC (WT)	115
SerC (R42A)	273
SerC (R42V)	262
SerC (R42T)	222
SerC (R42S)	198
SerC (R42V-R77W)	334
SerC (R42S-R77W)	312
SerC (R77T)	184
SerC (R42W-R77W-T240S)	340
SerC (R42W-R77W-F238S)	414
SerC (R42W-R77W-R329P)	632

Though some molecules in the cell lysates, such as NAD(H), L-glutamate/α-

ketoglutarate, ammonia and endogenous SerC, may interfere with the GDH-coupled assay, it is found that the interference from the negative control was negligible (data not shown).

After screening dozens of libraries, some new mutants were screened out (Table 5.1). All of them showed a much higher activity than that of wild type, while few were higher than the previous best mutant SerC(R42W-R77W), which in most cases showed the highest activity in each plate screened. The best one among them, SerC(R42W-R77W-R329P), showed a higher activity towards L-homoserine than that of SerC(R42W-R77W) (632 mU/mg vs 487 mU/mg) and a completely loss of activity towards L-phosphoserine. The kinetic parameters assay demonstrated that the K_m of SerC(R42W-R77W-R329P) towards 3 mM L-homoserine was decreased by 68-fold compared to that of the wild type, which means an increased affinity of SerC towards the substrate L-homoserine. The $k$cat/K_m of SerC(R42W-R77W-R329P) is only 9-fold higher than that of the wild type because of the decrease of Vmax, which means a loss of its catalytic power for L-homoserine.

Table 5.2. Kinetic parameters of mutants and wild type towards L-phosphoserine and L-homoserine.

Enzyme	**L-Phosphoserine**		
	Vmax(μmol/min/mg)	Km (mM)	$k$cat/Km ($s^{-1}mM^{-1}$)
WT	1.86±0.09	0.12±0.02	10.3
SerC(R42W-R77W)	n.d.	n.d.	n.d.
SerC(R42W-R77W-R329P)	n.d.	n.d.	n.d.
Enzyme	**L-Homoserine**		
	Vmax(μmol/min/mg)	Km (mM)	$k$cat/Km ($s^{-1}mM^{-1}$)
WT	3.90±0.16	158.50±20.79	0.02
SerC(R42W-R77W)	1.96±0.05	14.15±1.94	0.09
SerC(R42W-R77W-R329P)	0.621±0.011	2.31±0.18	0.18

n.d.: not detectable

The residues of His328 and Arg329 of the small domain of the same subunit and the residues of His41 and Arg42 of the large domain of the neighboring subunit are oriented

in two pairs and opposite to each other in the active site, and ideally suitable for binding the highly charged and bulky phosphate group of L-phosphoserine. Experimentally, changing the residue of Arg42 would drastically alter the substrate specificity of SerC from L-phosphoserine to L-homoserine. Any changes to His41 and H328 would lead to the loss of activity towards either L-phosphoserine or L-homoserine, indicating their rigidities in the catalytic process. In previous study, the rational designed mutants involving the residue of R329, SerC(R42W-R329H), SerC(R42W-329Q) and SerC(R42W-R329G), showed the activity of 293 mU/mg, 281 mU/mg and 145 mU/mg towards 3 mM L-homoserine, respectively. These results showed that the residue of Arg329 is more flexible than His328 in the catalytic process, which is also proved by the improved activity of SerC(R42W-R77W-R329P).

5.2.4 3-MPST-coupled colorimetric screening method

In recent years, several methods for transaminases screening have been established (Mathew et al, 2013), for example: a) a phenol red assay using alanine as a donor and a combined lactate dehydrogenase and glucose dehydrogenase system (Truppo et al., 2009); b) using *ortho*-xylylenediamine as the amine donor, which on conversion to the aldehyde cyclizes to an more stable aromatic isoindole and then undergoes spontaneous polymerization forming intensely colored derivatives (Green et al., 2014). There is so far no publication of screening method for transaminases ever reported with L-homoserine as the amine donor. Herein, we developed a convenient and inexpensive assay method for rapid screening of SerC activity.

In previous studies, many mutants with improved activity of SerC towards L-homoserine were obtained. It was found that SerC also exhibited activities towards L-serine and L-cysteine, which have similar chemical structures to L-homoserine. Surprisingly, the performances of SerC towards L-homoserine and L-serine shows a linear correlation (Figure 5.6).

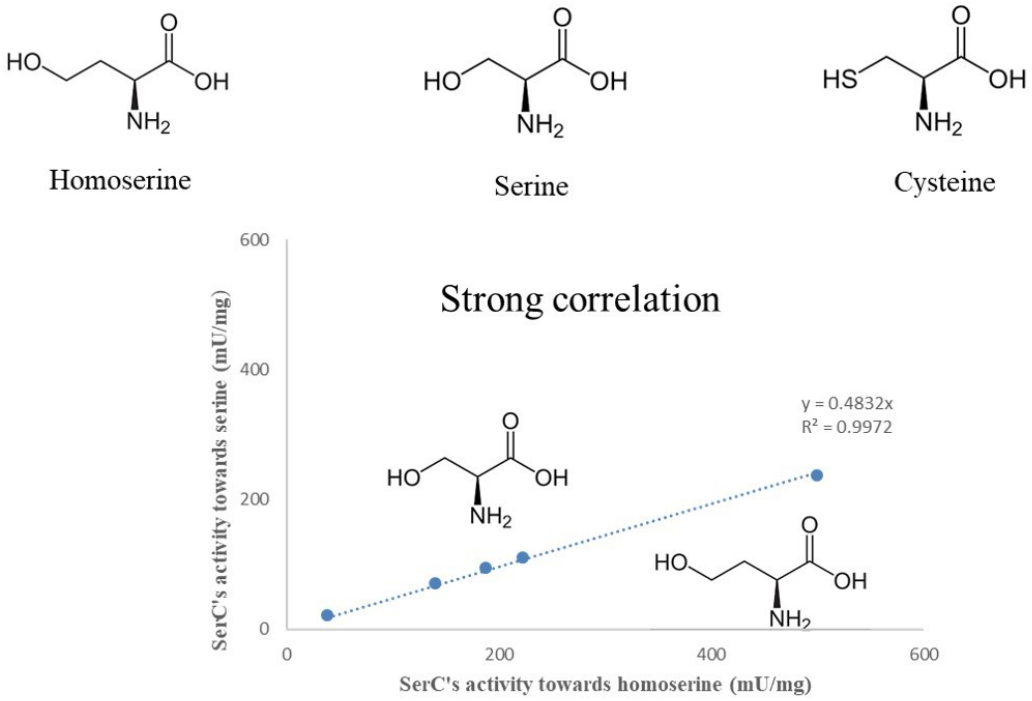

Figure 5.6. Relationship between the activity of SerC towards L-homoserine and L-serine. Each dot means a different mutant. The activities of mutants towards L-homoserine and L-serine were assayed using pure protein according to Section 3.7.3.1.

In Figure 5.6, the activity of SerC towards L-homoserine has a very strong correlation with the activity of SerC towards L-serine. When L-cysteine was used as a substrate, it also showed a similar relationship. Based on these findings, 3-MPST-coupled colorimetric screening method was developed (Figure 5.7).

3-Mercaptopyruvate sulfurtransferase (3-MPST) belongs to an enzyme superfamily of proteins that contain a rhodanese-like domain. It is involved in the endogenous detoxification of cyanide (CN) because it is capable of transferring sulfur from 3-mercaptopyruvate (3-MP) to CN, forming thiocyanate (SCN). The substrate specificity of 3-MPST for 3-mercaptopyruvate is quite high. In one study, three α-keto acids (α-ketoglutarate, α-ketobutyrate and pyruvate) were examined and none of them directly competes with 3-mercaptopyruvate for binding to 3-MPST even though they are structurally very similar to 3-mercaptopyruvate (Porter et al., 1993). It suggests that the

thiol group of 3-mercaptopyruvate is an important determinant of the substrate specificity of 3-MPST.

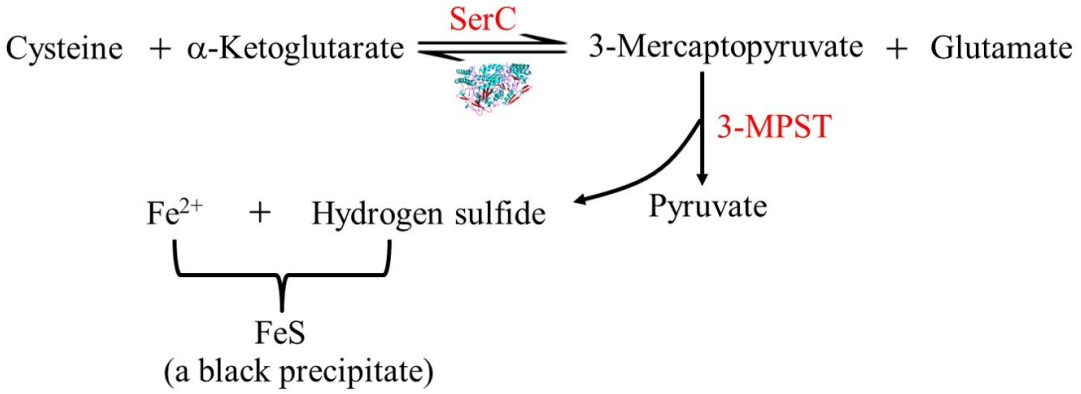

Figure 5.7. Overview of 3-MPST-coupled colorimetric screening method.

In Figure 5.7, SerC transfers the amino group of L-cysteine to α-ketoglutarate, generating 3-mercaptopyruvate and L-glutamate. 3-mercaptopyruvate is further converted by 3-MPST to pyruvate and an enzyme-bound persulfide, which can be released as H_2S in the presence of DTT (dithiothreitol) or physiological substance of DHLA (dihydrolipoic acid) and thioredoxin (Shibuya et al., 2009; Kabil and Banerjee, 2010; Mikami et al., 2011). The produced H_2S can react rapidly with iron to form a black iron sulfide precipitate, which is readily observable (Allen and Geldreich, 1975). Given the low solubility of iron sulfide, this method can detect even a small amount of H_2S.

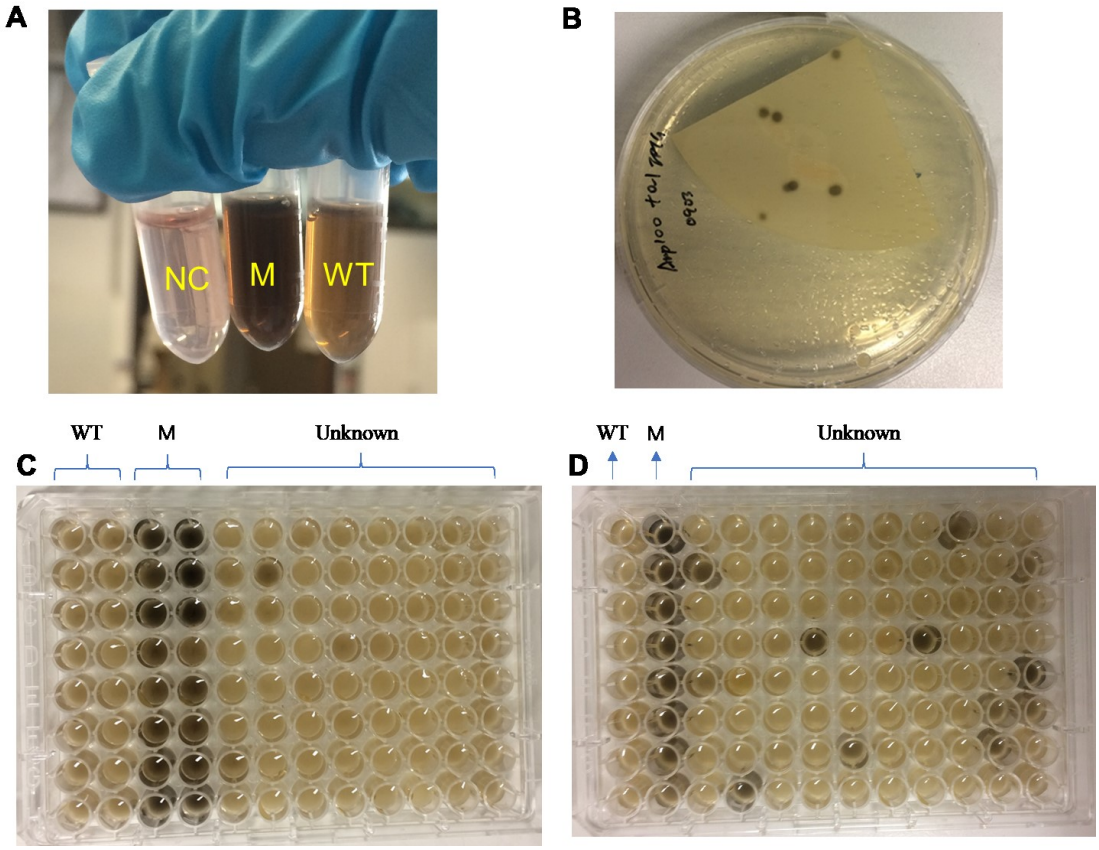

Figure 5.8. 3-MPST-coupled colorimetric screening: A) screening test in liquid; B) screening test on agar plate with mutants; C and D) screening test on 96-well plates. NC: negative control; WT: wild type SerC; M: SerC (R42W-R77W); Unknown: mutants with unknown mutations.

The cultivation conditions used in this method are described in Section 3.8.2. The screening process using 96-well plate is described in Section 3.7.3.4. The 3-MPST-coupled colorimetric screening method was first tested in liquid. As can be seen from Figure 5.8 A, the difference between the wild type and the mutant was very obvious. To achieve a high-throughput screening, this method was tested on agar plate (Figure 5.8 B) and on 96-well plates (Figure 5.8 C and D), respectively. Since the degradation of L-cysteine carried out in *E. coli* can generate hydrogen sulfide, the screening test on agar plate was performed after overexpression of SerC and 3-MPST protein in cells overnight. The paper soaked with a reaction mixture (see Section 3.7.3.4) was put on the colonies on the agar plate to let H_2S-Fe^{2+} react. The produced precipitate in cells

containing high activity of SerC would turn the colony black, just as shown in Figure 5.8 B. The challenge here is the need of an appropriate paper for this goal and the isolation of each colony. Finally, this screening method was employed on 96-well plate. As shown in Figure 5.8 C and D, the wild type and the mutant can be obviously separated by color difference. The variants with a higher activity towards L-cysteine can be easily identified (in the unknown area in Figure 5.8 C and D). After rounds of screening, some mutants were screened out (Table 5.3). The mutants that are the same as those screened out from other methods are not listed in Table 5.3. Among them, the mutant SerC(R42W-R77Q) was the best one, with an activity of 487 mU/mg towards L-homoserine.

Table 5.3. Activity of mutants screened (part).

	Specific activity (mU/mg)
Mutation	L-Homoserine
R42C	187
R42Q	149
R42N	140
R42W-R77Q	487
R42H-R77W	292
R42T-R77W	265
R42A-R77Q	254
R42V-R77T	142
R42V-R329H	198
R42S-R329Q	220

The application of 3-MPST-coupled colorimetric screening method is simple and low-cost. But the activity of SerC cannot be accurately quantified using this method. H_2S from the background noise may also interfere with the screening results.

5.2.5 Performances of different recombinant strains for 1,3-PDO production in shake flasks

L-Homoserine production was enhanced by overexpressing aspartate kinase III (LysC) and homoserine dehydrogenase (MetL) with a medium-copy plasmid. To further

accumulate L-homoserine production in cells, homoserine kinase encoded by *thr*B was deleted (Table 3.1). Lactate dehydrogenase (LDH) from *E. coli*, which is encoded by *ldh*A, has been proven to bear some HOBA reductase activity (Walther et al., 2018) and leads to formation of lactate under oxygen-limited conditions. In addition, alcohol dehydrogenase (AdhE) encoded by *adh*E also results in the production of ethanol under oxygen-limited conditions (Figure 4.7). Thus, both *ldh*A and *adh*E genes were deleted from the genome of *E. coli*.

The plasmid pMely, which can overexpress LysC and MetL, was transformed into *E. coli* △*thr*B △*adh*E △*ldh*A. The resulting homoserine-producing strain was then transformed with the plasmids pZA-SerC(R42W-R77W)-PDC-YqhD and pZA-SerC(R42W-R77W-R329P)-PDC-YqhD respectively, resulting in strains designated as S312 and S317 (Table 3.1). The 1,3-PDO production from these strains (S147, S312, S317 and S318) was determined using FM II culture medium. The FM II culture medium was supplemented with 2 g/L L-threonine to complement the auxotrophy. 30 g/L $CaCO_3$ was added for buffering pH during the cultivation. During the shake flask fermentation process, glucose was completely consumed after 25 h of cultivation, while the OD_{600} of these strains was up to 14 (Figure 5.9), similar to the previous results from shake flask fermentation (Figure 4.5).

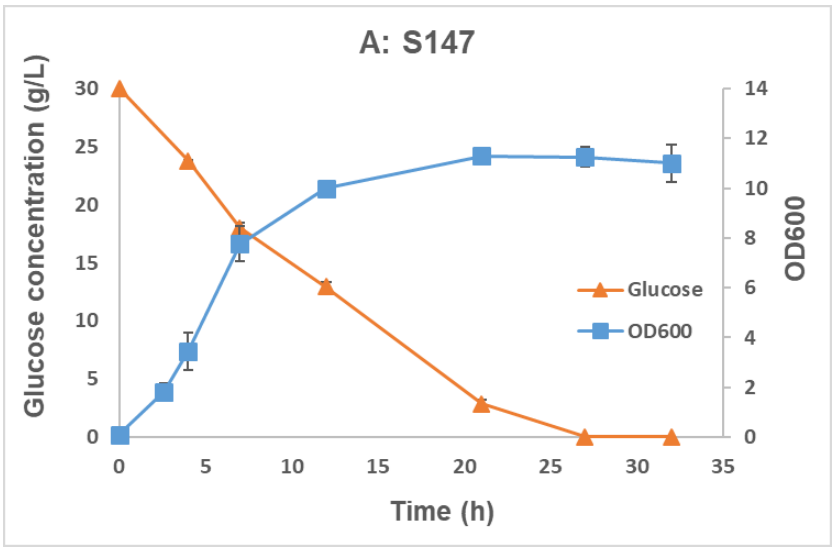

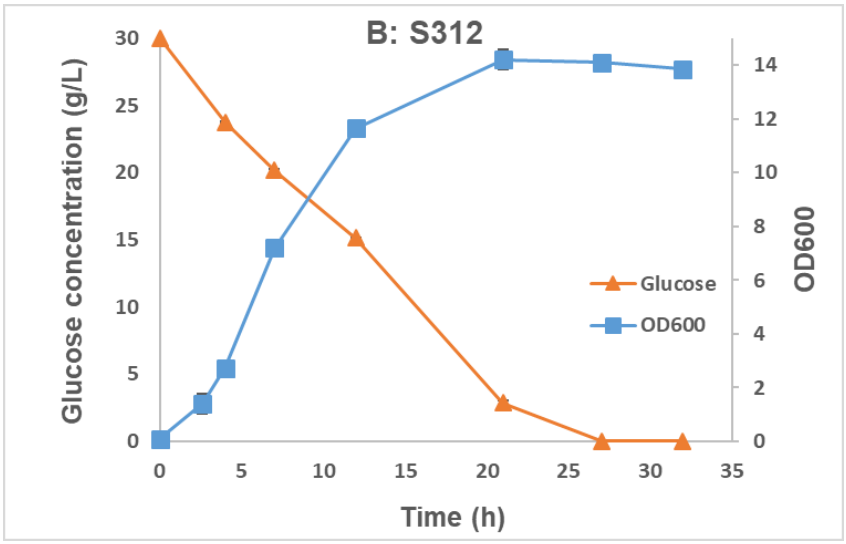

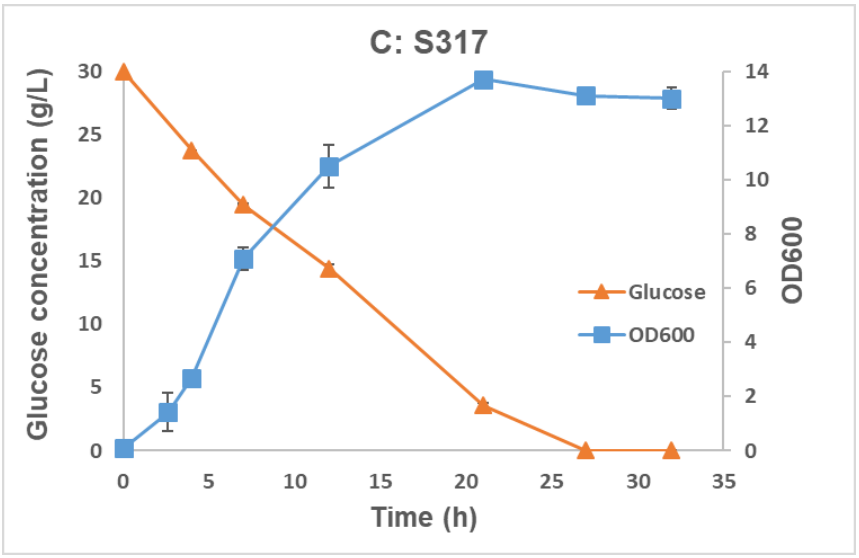

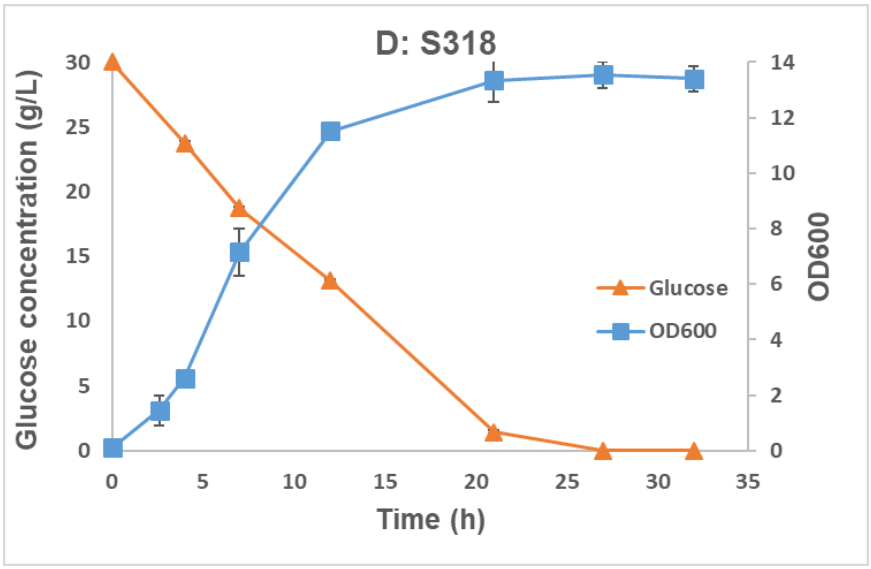

Figure 5.9. Cell growth and glucose consumption of the recombinant strains (S147, S312, S317 and S318).

After 32 h of cultivation, the 1,3-PDO production was measured. Based on the same host strain S87, the 1,3-PDO production from S318 was a relatively higher than that of S147 (179±12 mg/L Vs. 153±3 mg/L). This trend was also observed in another host strain S317, which was better than S312 for 1,3-PDO production (191±10 mg/L Vs. 148±5 mg/L). The strains S318 and S317 harbor the new mutant SerC(R42W-R77W-R329P), while the strains S147 and S312 have the mutant SerC(R42W-R77W). Compared to these results, the addition of 5 g/L L-homoserine in the previous study achieved a higher 1,3-PDO production in shake flasks (277±21 mg/L). Unfortunately, the new constructed strain showed no obvious difference in 1,3-PDO production between the strains S147 and S318 and the strains S312 and S317.

5.3 Conclusion

In this chapter, several strategies were investigated to further engineer SerC for a higher activity towards L-homoserine. These methods include: a) generation and use of glutamate-dependent auxotrophic strain; b) GDH-coupled photometric detection; and c) mercaptopyruvate sulfurtransferase (MPST)-coupled colorimetric screening. A new mutant SerC(R42W-R77W-329P) was identified using these strategies, which has an improved activity towards L-homoserine by 5.5-fold compared to that of the wild type. Its activity towards L-phosphoserine was completely lost. The K_m of SerC(R42W-R77W-R329P) was decreased by 68-fold compared to that of the wild type when 3 mM L-homoserine was used as substrate, which means an increased affinity of SerC for the substrate L-homoserine. The performance of this new mutant was verified in engineered host strains for 1,3-PDO production in shake flask fermentations. The performance of SerC(R42W-R77W-R329P) exhibited a higher 1,3-PDO production compared to that of SerC(R42W-R77W).

CHAPTER 6 Design of a homoserine-derived 1,2,4-butanetriol biosynthetic pathway

In previous studies, SerC mutants exhibiting a high catalytic efficiency towards L-homoserine were obtained. In this section, the engineered SerC was utilized to explore a new biosynthesis pathway for 1,2,4-butanetriol (BT) production from glucose via L-homoserine. To this end, plasmids and host strains were developed. Fed-batch fermentations were carried out to verify the BT biosynthetic pathway.

6.1 Introduction

Biobased production of BT from renewable substrates is increasingly attracting attention. Microbial synthesis of BT from pure xylose was firstly achieved by Niu et al. (2003), and was further improved using a series of genetic engineering strategies (Cao et al., 2005; Lu et al., 2016; Wang et al., 2017; Jing et al., 2018). A novel BT pathway from glucose was firstly reported by Li et al. (2014). In this pathway, glucose is converted to malate by glycolysis and then malate as the starting material is transformed to BT via six enzymatic reactions, including two CoA-dependent reactions. Due to the involvement of low efficiency CoA-dependent reaction and substantial metabolic burden for *E. coli*, the BT production from this non-natural heterologous BT biosynthetic pathway can only achieve 120 ng/L. Since the addition of 100 mM 2,4-dihydroxybutarate (DHB, an intermediate in this pathway) to the cultures of the recombinant *E. coli* can lead to 55 mg/L BT production, the authors speculated that the bottleneck of the entire pathway was the first step, a CoA-dependent reaction from malate to malyl-CoA catalyzed by malate thiokinase. Considering that the engineered SerC can significantly improve the production of 1,3-PDO through the crucial deamination step of L-homoserine in our previous study, a homoserine-derived BT pathway was proposed and studied here (Figure 6.1).

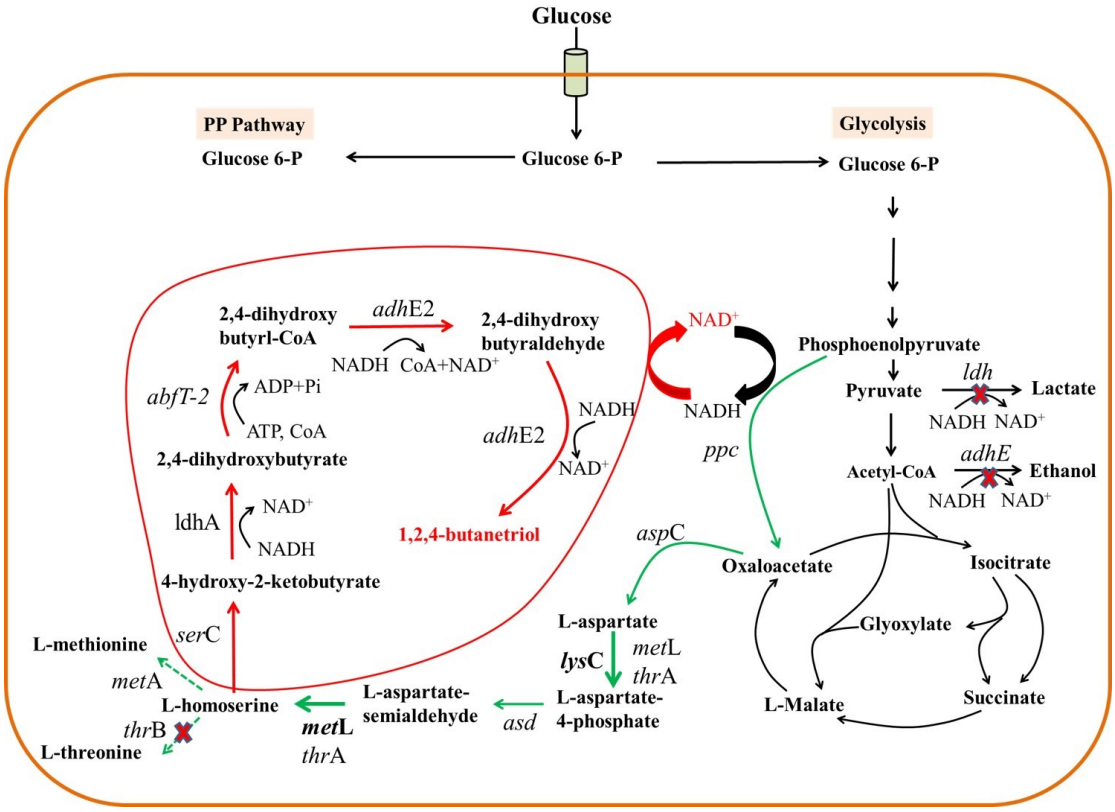

Figure 6.1. Overview of a new metabolic pathway for the production of BT from glucose over homoserine. In this figure, the five reactions starting from L-homoserine, which are boxed inside the purple colored shape, represents the homoserine-derived new BT pathway. The intracellular level of L-homoserine was enhanced by overexpressing the LysC (encoded by gene *lys*C) and MetL (encoded by *met*L) genes and deleting the *thr*B (encodes for homoserine kinase) gene from the *E. coli* genome (Green lines). Further, in order to block the diversion of carbon flux to common fermentation products like lactate and ethanol, the respective genes, *ldh* and *adh*E, were deleted from the *E. coli* genome.

The homoserine-derived BT pathway involves five consecutive enzymatic reactions, which are catalyzed by four heterologous enzymes, including an engineered phosphoserine aminotransferase (SerC), a lactate dehydrogenase (Ldh), a 4-hydroxybutyrate CoA-transferase (AbfT-2) and an aldehyde/alcohol dehydrogenase (AdhE2). To prove the validity of homoserine-derived BT pathway, all of the genes that encode corresponding enzymes were assembled into the expression vector pDPHL or

pZA (a medium-copy number), generating the recombinant plasmid pDPHL-SerC(R42W-R77W)-LdhA(Q85C)-AbfT2-AdhE2 (pDPHL-SLAA) and pZA-SerC(R42W-R77W)-LdhA(Q85C)-AbfT2-AdhE2 (pZA-SLAA), respectively. The resulting plasmids were then transformed into the homoserine-producing strain.

To achieve a successful construction of biosynthesis pathway for alcohols, in addition to the activity of enzymes involved in the pathway itself, the yield of target product also depends on the concentration of precursors and cofactors in the cells (Zhao et al., 2017). As a starting material in the BT pathway, L-homoserine was enhanced by overexpressing the genes of *lys*C and *met*L with the plasmid pMely. Since the involved $LdhA_{Q85C}$ and AdhE2 are responsible for three redox steps which consume NADH, eliminations of the competing lactate and ethanol pathways were implemented to provide a more reductive environment for BT production.

6.2 Results and Discussion

6.2.1 Thermodynamic feasibility of the homoserine-derived BT pathway

The thermodynamic feasibility was analyzed based on the estimated standard Gibbs free energy of formation for every non-natural product in the entire BT pathway. The group contribution method (Jankowski et al., 2008) was used here. According to this method, some simple aspects of the structures within the compounds are always the same in different molecules. Thus, the molecular structure of a single compound can be decomposed into a set of smaller substructures. Then the contributions from each of the substructures (or groups) are summed up to estimate the standard Gibbs free energy of formation ($\Delta_f G'^{\circ}$) of the compound. Similarly, the standard Gibbs free energy of reaction ($\Delta_r G'^{\circ}$) is estimated by summing the contribution of each structural group created or destroyed during the reaction (Jankowski et al., 2008). The contribution values used here are from Jankowski's work. Jankowski and his coworkers estimated the Gibbs free energy contribution values for 74 substructures and 11 interaction factors

using multiple linear regressions against a training set of reactions and compounds. The standard error for these fitted values was 1.9 kcal/mol. The standard error involved in these estimations is 2.22 kcal/mol after cross-validation analysis in estimation of the $\Delta_f G'^{\circ}$ and $\Delta_r G'^{\circ}$ of compounds and reactions. The detailed calculations of the standard Gibbs free energy are shown in Figure 6.2.

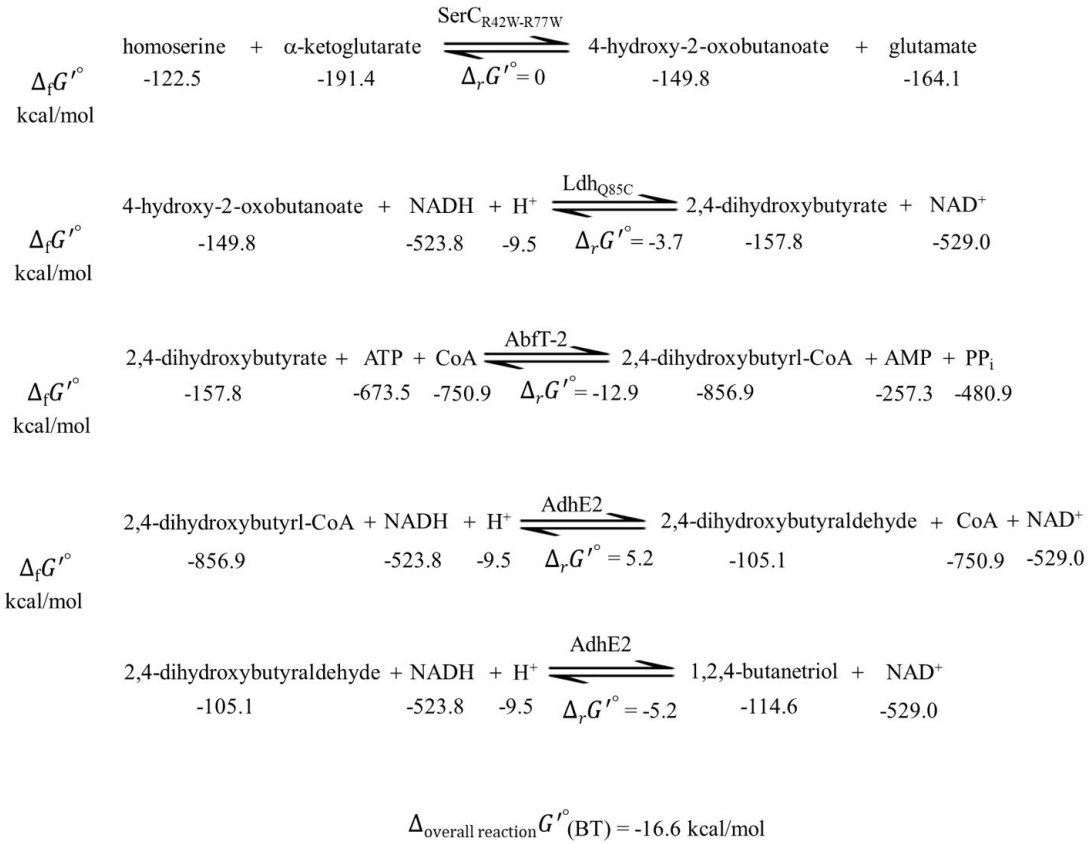

Figure 6.2. The $\Delta_f G'^{\circ}$, $\Delta_r G'^{\circ}$ and $\Delta_{\text{overall reaction}} G'^{\circ}$ of the BT pathway. The standard Gibbs free energy of formation ($\Delta_f G'^{\circ}$) were given in the figure. The standard Gibbs free energy of every reaction ($\Delta_r G'^{\circ}$) and overall reaction ($\Delta_{\text{overall reaction}} G'^{\circ}$) were calculated according to the group contribution method from Jankowski et al. (2008).

The calculated total standard Gibbs free energy change of the four reactions for BT production from L-homoserine was -16.6 kcal/mol, suggesting that the homoserine-derived BT pathway was thermodynamically feasible.

6.2.2 Construction of the plasmids pDPHL and pZA

6.2.2.1 Upstream pathway: biosynthesis of DHB from glucose

The route to DHB starts from the intermediate L-homoserine, which is also a precursor for the biosynthesis of L-methionine and L-threonine. The pathway consists of two consecutive reactions catalyzed by an engineered phosphoserine transaminase, encoded by *ser*C gene, and an engineered lactate dehydrogenase LdhA. To construct the plasmid pZA-SerC(R42W-R77W)-LdhA(Q85C) for the conversion of L-homoserine to DHB, the vector backbone was amplified from the plasmid pZA-SerC(R42W-R77W)-PDC-YqhD, using the primer pair V-LL.FOR / V-LL.REV (Table 3.5). Further, the insert fragment LdhA(Q85C) was amplified from the plasmid pET28a-LdhA(Q85C), which was provided by Jie Ren, with the primer pair F-LL LDH.FOR/ F-LL LDH.REV (Table 3.5). The gene of LdhA(Q85C) in the pET28 plasmid was codon optimized and the Gln85Cys point mutation showed increased activity towards 4-hydroxy-2-oxobutanoate and decreased activity towards the natural substrate pyruvate (Walther et al., 2018).

The purified vector pZA-SerC(R42W-R77W) and the insert fragment LdhA(Q85C) were ligated using the InFusion method. As a result, the plasmid pZA-SerC(R42W-R77W)-LdhA(Q85C) was obtained.

6.2.2.2 Downstream pathway: conversion of DHB to BT in *E. coli*

The conversion of DHB to BT requires two reduction steps, catalyzed by dehydrogenases (Figure 6.1). Li et al. (2014) and his coworkers tested several CoA-transferases and dehydrogenases and found that the 4-hydroxybutyrate CoA-transferase AbfT-2 from *Porphyromonas gingivalis* and the bifunctional aldehyde/alcohol dehydrogenase AdhE2 from *C. acetobutylicum* can work together to synthesize BT from DHB.

To achieve the downstream of BT pathway from DHB to BT, the *abf*T2 gene with 15 base pair homologous ends was amplified from the genomic DNA of *Porphyromonas gingivalis* (purchased from DSMZ) using the primer pair AbfT2-fragment.FOR/ AbfT2-fragment.REV. The vector backbone was amplified from pZA-SerC(R42W-R77W)-LdhA(Q85C) using primers V-LL.FOR/ AbfT2-vector.FOR. The amplified *abf*T2 gene was then cloned into the vector backbone via Infusion reaction to obtain the plasmid pZA-SerC(R42W-R77W)-LdhA(Q85C)-AbfT2. The *adh*E2 gene with 15 bp homologous ends was amplified from *Clostridium acetobutylicum* (purchased from DSMZ) using primers AdhE2-fragment.FOR/ AdhE2-fragment.REV. Its vector backbone was amplified from the obtained plasmid pZA-SerC(R42W-R77W)-LdhA(Q85C)-AbfT2 using the primers V-LL.FOR/ AdhE2-Vector-REV. Further, the amplified vector backbone and the AdhE2 fragments were mixed for Infusion reaction. Finally, the resulting plasmid pZA-SerC(R42W-R77W)-LdhA(Q85C)-AbfT2-AdhE2 (referred as pZA-SLAA) was obtained (Figure 6.3, A).

Apart from constructing a medium copy number pZA plasmid, the pDPHL vector was also investigated. Using primer pairs pDPHL-Fra.FOR/pDPHL-Fra.REV and pDPHL-Vec.FOR/pDPHL-Vec.REV, the fragment SerC(R42W-R77W)-LdhA(Q85C)-AbfT2-AdhE2 and the vector backbone of pDPHL were cloned from the corresponding plasmids using PCR reaction, respectively. Finally, the plasmid pDPHL-SerC(R42W-R77W)-LdhA(Q85C)-AbfT2-AdhE2 (referred as pDPHL-SLAA) was obtained (Figure 6.3, B).

To prove the validity of BT pathway in *E. coli*, plasmids pZA-SLAA and pDPHL-SLAA were introduced into the homoserine-producing strain S310 to generate recombinant strain S313 and S314, respectively.

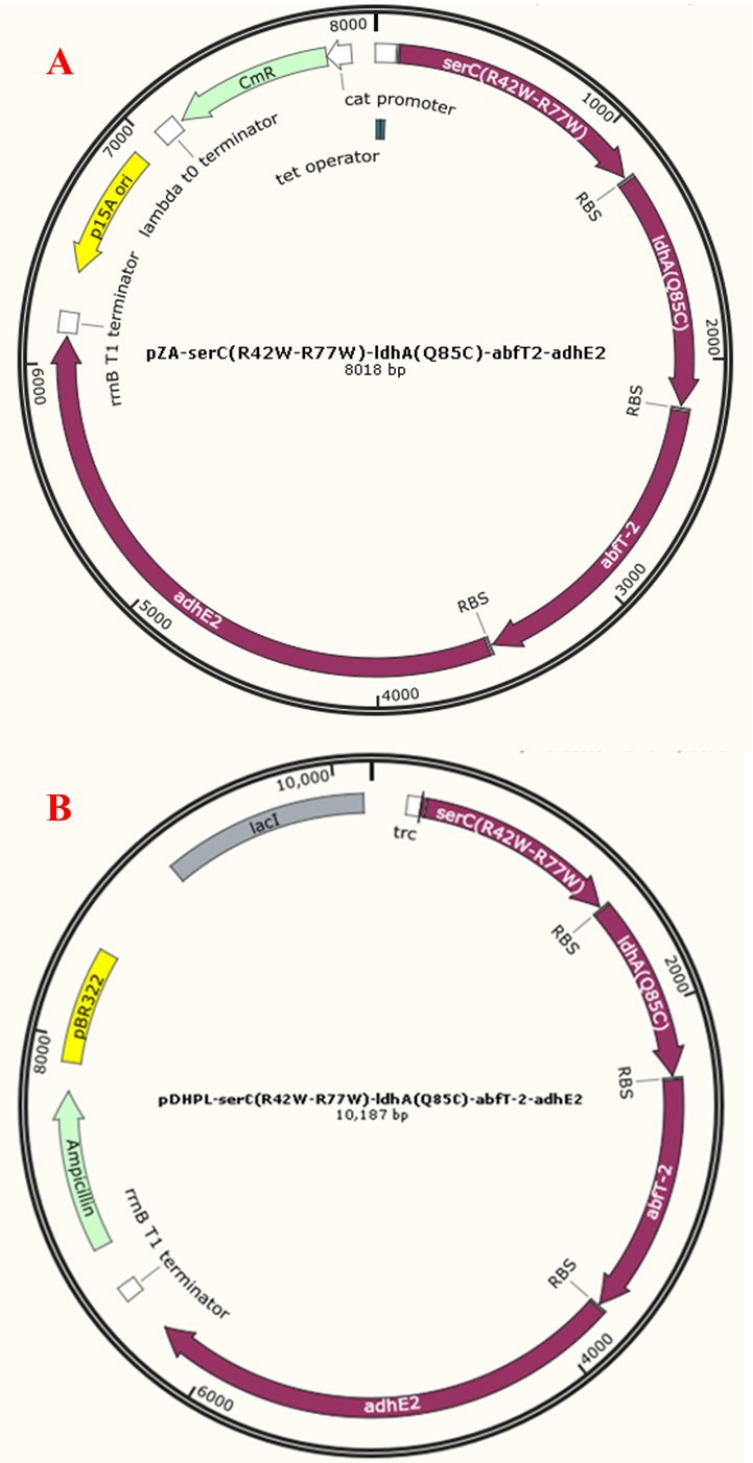

Figure 6.3. The maps of plasmids pZA-SLAA (A) and pDPHL-SLAA (B) (generated with Snapgene).

6.2.3 Production of BT by the recombinant strains

To verify the capability of the homoserine-derived BT pathway for BT production *in vivo*, the recombinant strain S313 and S314 (Table 3.1) were investigated using glucose as the sole carbon source. The strain S310 (Table 3.1) harboring no any BT biosynthetic pathway was used as the control strain. In the biosynthesis of BT route, the upstream pathway from L-homoserine to DHB involves two engineered enzymes, SerC(R42W-R77W) and LdhA(Q85C), which have already been proved to exhibit a good catalytic efficiency toward L-homoserine and HOBA in our previous work and in the literature, respectively (Zhang et al., 2019; Walther et al., 2018). However, the other two enzymes, AbfT2 and AdhE2, involved in the downstream pathway from DHB to BT, show poor performances and are the rate-limiting steps in BT pathway. As a proof, Li et al. (2014) showed a low bioconversion efficiency of the downstream pathway, producing 55 mg/L BT under microaerobic fermentation with the addition of 100 mM DHB. In our study, there was no detectable BT (only the level of mg/L can be tested in our lab) produced in batch fermentations, which were implemented in anaerobic bottles containing modified M9 medium. A needle was kept in the bottle during the cultivation to keep microaerobic conditions (Yim et al., 2011).

The enzyme AbfT2 encoded by *abf*T2 gene from *Porphyromonas gingivalis* exhibited 4-hydroxybutyryl-CoA transferase activity when implemented as part of a pathway to produce 1,4-butanediol (Yim et al., 2011), but its activity towards the non-natural intermediate DHB was rarely reported. The enzyme AdhE2 from *C. acetobutylicum* is oxygen sensitive and contains a highly conserved iron-binding site. Imlay et al. (2016) observed that when enzymes containing iron-sulfur clusters are exposed to molecular oxygen or reactive oxygen species like superoxide ($O2^{-}$) (Lambertz et al., 2011), the iron in the iron-sulfur clusters are getting oxidized which results in the release of an iron atom from the cluster. Such a release of the iron atom would lead to the destabilization of the cluster and the damaged iron-sulfur clusters would later result in the entire degradation of the enzyme complex. Therefore, the uncontrollable oxygen level in the environment may severely affect the activity of AdhE2.

To better validate the effects of BT biosynthetic pathway, fed-batch fermentations of the recombinant strains S310, S313 and S314 were implemented. As depicted in Figure 6.4 (A), there was no detectable BT produced from the control strain S310, which met our expectation, since no relevant BT pathway was in the cells. The production of BT by strains S313 and S314 reached 19.6 ± 5.9 mg/L and 8.9 ± 0.4 mg/L in the fed-batch fermentation, respectively (Figure 6.4 B and C). The DHB concentration in the culture was detected to be 625.1 ± 8.1 mg/L and 745 ± 10.8 mg/L by strains S313 and S314, respectively (Figure 6.5). The samples were also sent for GC-MS analysis and showed similar results (Figure 6.4 A', B' and C').

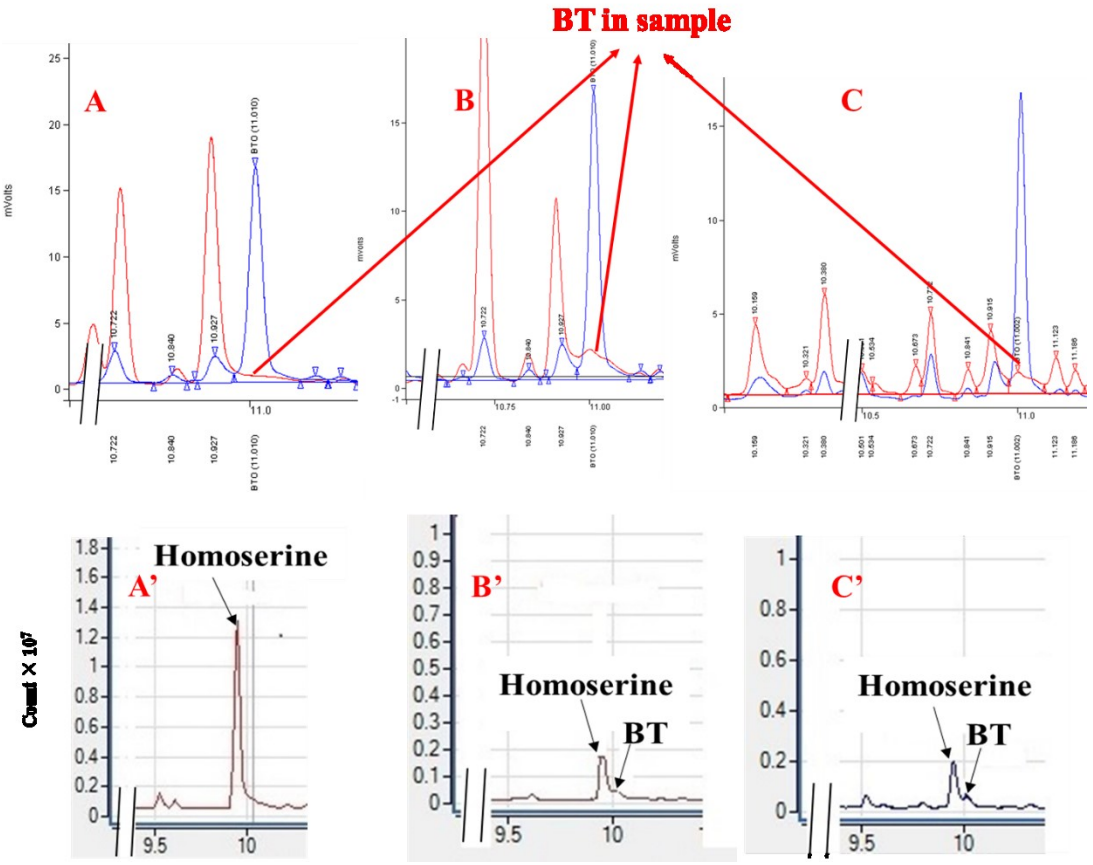

Figure 6.4. GC analysis of BT in the samples from fed-batch fermentations. (A, A'): recombinant strain S310; (B, B') recombinant strain S313; (C, C') recombinant strain S314; A, B and C were measured using GC-FID in our lab, the retention time of BT was 11.00 min; A', B' and C' were measured using GC-MS in the central laboratory, the retention time of BT was 10.05 min. It is noteworthy that the blue line in A, B and

C is BT standard, the red line is sample.

Though a relatively high concentration of DHB was achieved in this study, the accumulation of the key intermediate DHB was limited by the poor overexpression of LdhA(Q85C) in the cells. Recently, an engineered malate dehydrogenase from *E. coli* was reported by Frazão et al. (2018). The employment of this engineered malate dehydrogenase instead of LdhA(Q85C) could result in a two- to three- fold higher DHB titer, which would help to increase the concentration of the key intermediate DHB and be beneficial to achieve a higher BT production.

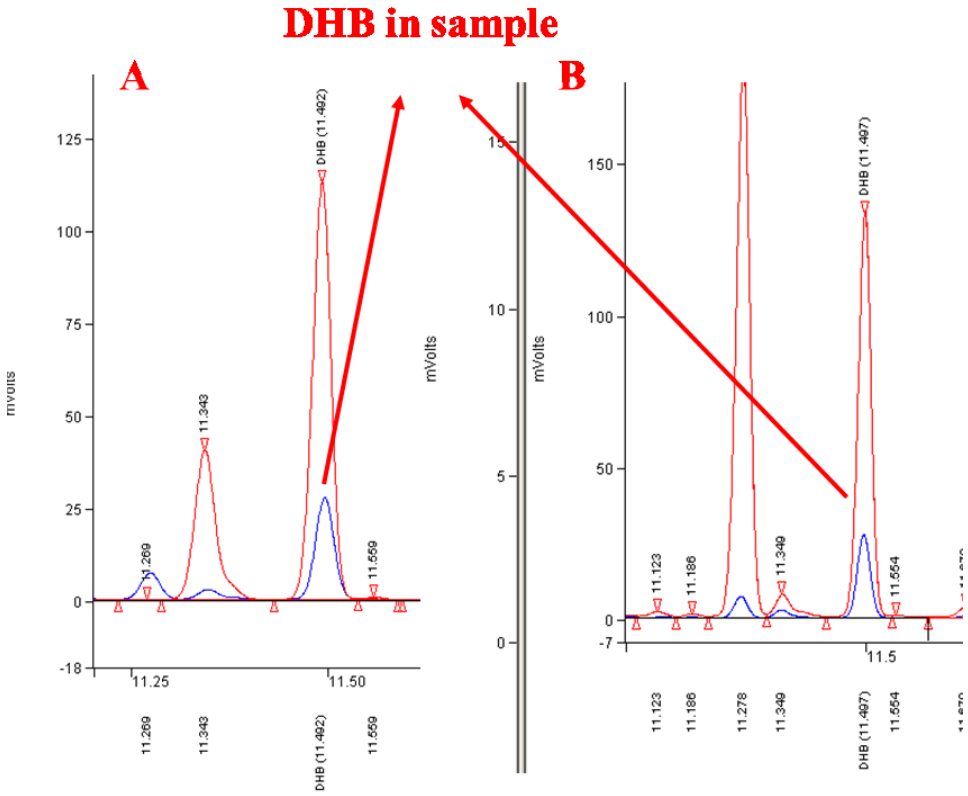

Figure 6.5. GC analysis of DHB in the samples from fed-batch fermentations. (A): recombinant strain S313; (B) recombinant strain S314; A and B were measured using GC-FID in our lab, the retention time of DHB was 11.50 min; It is noteworthy that the blue line in A and B is DHB standard, the red line is sample.

In the total ion chromatogram obtained from GC-MS analysis (Figure 6.4, A', B' and

C'), the BT is observed as a small shoulder peak next to L-homoserine, which is too small to give an accurate concentration (<20 mg/L) due to the limitation of analytic method and equipment. For a better resolution of BT titers, selected ion monitoring with mass spectroscopy for increased sensitivity should be used. On the other hand, re-engineering of the relevant enzymes in the BT pathway and optimization of the conditions for fed-batch fermentations are alternative ways to achieve a higher BT production.

6.3 Conclusion

In this study, a new five-step sequential enzymatic reaction was designed for the biosynthesis of BT from L-homoserine. This pathway was evaluated to be thermodynamically feasible as the standard Gibbs free energy for the overall reaction was estimated to be -16.6 kcal/mol. Considering that the expression of four genes under a strong promoter in multiple copy may result in a substantial metabolic burden on the cells, both medium-copy number plasmid pZA and pDPHL with different promoters were tried. To produce BT from glucose, this non-natural heterologous BT biosynthetic pathway was introduced into an engineered recombinant strain S310. The resulting strains S313 and S314 were able to produce 19.6 ± 5.9 mg/L and 8.9 ± 0.4 mg/L, respectively. The result is much higher than that of BT pathway from malate reported in literature (120 ng/L). This study shows the validity of a novel BT biosynthetic pathway from glucose via L-homoserine.

CHAPTER 7 Summary and Outlook

Summary of this thesis

In this thesis, efforts have been made to develop a new homoserine-derived 1,3-PDO pathway from glucose in *E. coli*. This homoserine-derived pathway was achieved by extending the natural L-homoserine biosynthesis pathway via three heterologous enzymatic reactions: deamination of L-homoserine to HOBA using SerC; decarboxylation of HOBA into 3-hydroxypropionaldehyde using PDC and reduction of 3-hydroxypropionaldehyde into 1,3-PDO using YqhD. In this biosynthetic pathway, the bottleneck is the capability of SerC to catalyse L-homoserine.

To obtain a suitable SerC for the deamination of L-homoserine, a computation-based rational approach was employed to alter the substrate specificity of SerC from L-phosphoserine to L-homoserine. To this end, the structural information of SerC (PDB code: 1BJO) was utilized. Molecular dynamics simulations and virtual screening were combined to predict possible mutation sites for desirable variants. These predicted variants were further verified *in vitro* experimentally. After three rounds of screening, the best mutant, SerC(R42W-R77W), was selected and confirmed in the 'glucose-homoserine-PDO' pathway. The specific activity of SerC(R42W-R77W) towards 3 mM L-homoserine was 487 mU/mg, which was improved by 4.2-fold in comparison to the wild type, while its activity towards the natural substrate L-phosphoserine was almost completely deactivated (79 Vs. 3,406 mU/mg). To confirm the performance of SerC in the 1,3-PDO pathway, three genes (*ser*C, *pdc* and *yqh*D) for the consecutive reactions were assembled in a medium-copy-number plasmid under the control of $P_{LtetO-1}$ operator. The results from shake flask fermentation showed that the mutant strain achieved an increased 1,3-PDO production by 50-fold in comparison to the wild type strain (277±20.8mg/L Vs. 5.40±0.78 mg/L) with the addition of 5 g/L L-homoserine as the starting substrate in the culture. To achieve a high production of 1,3-PDO from this

homoserine-derived pathway, overexpressions of LysC and MetL were complemented by a medium-copy plasmid for producing more L-homoserine in the cells. The homoserine kinase encoded by *thr*B was deleted in order to avoid unwanted consumption of L-homoserine. Fed-batch fermentations of the mutant strain containing SerC(R42W-R77W) and the wild type strain gave a better understanding for the role of SerC in this homoserine-derived 1,3-PDO pathway. With SerC(R42W-R77W), the homoserine-producing strain achieved 3.03 g/L 1,3-PDO after 62 h of cultivation, which is 13-fold higher than that of the wild type strain (0.24 g/L). Replacing PDC with KDC for the decarboxylation step did not show any beneficial improvements, which only achieved 0.6 g/L of 1,3-PDO production.

Since the activity of SerC towards L-homoserine was still not satisfactory, other strategies were employed to further engineer SerC. Directed evolution and semi-rational approach were used to build large and diverse mutant libraries, which increased the chance of obtaining desired variants. Different high-throughput screening and selection methods were investigated to deal with the libraries of variants constructed. Firstly, growth complementation based on high-throughput selection method was tried. The glutamate-dependent auxotrophic strain was constructed and the heterologous transamination reaction of SerC was introduced into this strain. Only strains expressing SerC with a higher activity towards L-homoserine can survive in the selective medium by producing enough L-glutamate to support its growth. Secondly, GDH-coupled photometric assay method was developed. The amino group of L-homoserine was transferred by SerC to α-ketoglutarate, generating HOBA and L-glutamate. The produced L-glutamate was oxidatively deaminated to α-ketoglutarate by GDH, with concomitant formation of NADH which can be monitored at 340 nm in a plate reader. Thirdly, 3-MPST-coupled colorimetric screening on 96-well plate was studied. L-Cysteine instead of L-homoserine was used as the amino donor for SerC. 3-Mercaptopyruvate and L-glutamate were produced from L-cysteine and α-ketoglutarate by SerC. The 3-mercaptopyruvate was further catalyzed by 3-MPST to pyruvate and H_2S. The latter can react rapidly with iron to form a black iron sulfide

precipitate, which is readily observable with eyes. Many variants were screened using these strategies. Among them, the best mutant SerC(R42W-R77W-329P) was identified, whose activity towards L-homoserine was improved by 5.5-fold compared to that of the wild type. Its activity towards L-phosphoserine was completely lost. The K_m of SerC(R42W-R77W-R329P) towards 3 mM L-homoserine was decreased by 68-fold compared to that of the wild type (2.31±0.18 mM Vs. 158.50±20.79 mM), which means an increased affinity of SerC towards L-homoserine. *Ldh*A and *adh*E genes were also deleted from the genome in order to increase the production of 1,3-PDO under oxygen-limited conditions. In shake flask fermentations, the new strain containing SerC(R42W-R77W-R329P) showed a relatively higher 1,3-PDO production compared to that of the previous one that contains SerC(R42W-R77W) (191±10 mg/L Vs. 148±5 mg/L).

In addition, by taking the advantage of SerC(R42W-R77W), a novel homoserine-derived BT pathway was designed and approved. The new BT pathway contains five sequential enzymatic reactions starting from L-homoserine, involving an engineered phosphoserine aminotransferase (SerC), a lactate dehydrogenase (LdhA), a 4-hydroxybutyrate CoA-transferase (AbfT-2) and an aldehyde/alcohol dehydrogenase (AdhE2). The standard Gibbs free energy for the overall reaction was evaluated to be thermodynamically feasible. The enzymes involved in the homoserine-derived BT pathway were assembled in the plasmids pZA and pDPHL, respectively. The plasmids constructed were then transformed into a homoserine-producing strain. The resulting strain S313 can produce as high as 19.6 ± 5.9 mg/L BT from glucose in fed-batch fermentation, indicating the validity of this novel BT biosynthetic pathway.

Outlook for future work

As a high-throughput selection method, growth complementation is very powerful for engineering protein when the cell survival is linked tightly with the desired enzyme property. The screening size is only limited to the transformation efficiency. In this work, we tried to build a glutamate-dependent auxotrophic *E. coli* to realize the link of

improved activity of SerC towards L-homoserine and the cell survival in a selective medium. In other words, only SerC with a higher activity towards L-homoserine can produce enough L-glutamate for cell growth. Although the *E. coli* constructed becomes glutamate-dependent after deleting the genes *gdh*A, *glt*B and *glt*D, its growth is surprisingly not exclusively dependent on the activity of SerC towards L-homoserine. The promiscuity of transaminases and the important role of L-glutamate in the cellular nitrogen metabolism may have led to a complicated situation. HOBA is absent in any known metabolism in *E. coli*. This means that the production of HOBA exclusively represents the activity of SerC. Therefore, the establishment of a HOBA-dependent essential pathway in *E. coli* may help to screen SerC. An evolved HOBA-based *E. coli* may be obtained by altering canonical metabolism with a few genetic deletions and one heterologous gene insertion and leveraging on natural selection mechanisms (Bouzon et al., 2017).

The microtiter plate-based GDH-coupled photometric assay is the most reliable and direct but labor- and time-consuming method for screening SerC. Based on this method, almost every transformant can be screened by detecting their crude enzyme activities. However, since the cultivation conditions in each well cannot be completely the same, the expression level of SerC in each well may be quite different and this can largely affect the final results. Thus, every step of operations and conditions in the whole process should be strictly the same, in order to lower the interference of operations by human and environment factors to the maximal extent. On the other hand, more analysis of the relationships between the known variants and the structural information of SerC should be done in the future to predict key residues and build more smart mutant libraries for screening.

The 3-MPST-coupled colorimetric screening method is very promising. It can fast screen out SerC mutants which have a high activity towards L-homoserine. However, the activity of SerC cannot be quantified and the threshold of screening is relatively low now. In the future, by means of the obtained variants, the threshold should be improved

for further screening. On the other hand, high-throughput screening using this method should be based on agar plate or microfluidics.

As for the fermentation results, there is still much room for improvement of the L-homoserine utilization. Meanwhile, homoserine-producing strain can be built on the genome level, and the *met*A gene for L-methionine production can be blocked in order to improve the accumulation of L-homoserine. Fed-batch fermentations of the strain S317 should be carried out to study the performance of the new mutant SerC(R42W-R77W-R329P) for 1,3-PDO production.

As for the BT biosynthetic pathway, the high concentration of DHB accumulated in the culture suggested that the bottleneck of the pathway may be the step catalyzed by AdhE2. AdhE2 is an oxygen-sensitive aldehyde/alcohol dehydrogenase from *Clostridium acetobutylicum* and is the only enzyme reported so far to have the ability to catalyze 2,4-dihydroxybutyrl-CoA to 2,4-dihydroxybutyraldehyde, followed by its subsequent reduction to BT. AdhE2 was firstly used in the 1,4-butanediol biosynthesis pathway in *E. coli* (Yim et al., 2011) and then employed in the BT pathway by Li et al. (2014) with a very poor performance. In another study for butanol biosynthesis, two oxygen-tolerant dehydrogenases, CoA-acylating propionaldehyde dehydrogenase (PduP) from *Salmonella enterica* and alcohol dehydrogenase (YqhD) from *E. coli* were used to substitute AdhE2. PduP has the ability to catalyze the reduction of a broad range of acyl-CoAs to their corresponding aldehydes (Wittmann and Liao, 2017). Therefore, PudP and YqhD have the possibility of treating 2,4-dihydroxybutyrl-CoA and 2,4-dihydroxybutyraldehyde as substrates to effectively produce BT. On the other hand, codon optimization of AdhE2 may result in increased expression levels of the enzyme in *E. coli* and lead to a higher product concentration (Yim et al., 2011). Considering the requirement of NADH in the BT pathway, the conditions of microaerobic fermentation should be optimized to ensure the availability of sufficient NADH to drive the BT pathway. An alternative choice is the introduction of heterologous formate dehydrogenase (*fdh*) to recycle NAD^+ to NADH by catalyzing formate to CO_2 and keep

redox rebalance (Ma et al., 2016; Molla et al, 2016). Recently, Frazão et al. (2018) engineered a malate dehydrogenase (Mdh) from *E. coli*. The replacement of LdhA(Q85C) with this engineered Mdh could result in a two- to three- fold higher titer of DHB. The increased DHB concentration would be beneficial for achieving a higher BT production since DHB is a key intermediate in the BT pathway.

References

Abdel-Ghany, S. E., Day, I., Heuberger, A. L., Broeckling, C. D. and Reddy, A. S. (2013) Metabolic engineering of Arabidopsis for butanetriol production using bacterial genes. Metab. Eng. 20, 109-120

Abrahamson, M. J., Vazquez-Figueroa, E., Woodall, N. B., Moore, J. C., Bommarius, A. S. (2012) Development of an amine dehydrogenase for synthesis of chiral amines. Angew. Chem. Int. Edit. 51, 3969-3972

Allen, M. J. and Geldreich, E. E. (1975) Bacteriological Criteria for Ground-Water Quality. Ground Water. 13, 45-52

Báez -Viveros, J. L., Osuna, J., Hernández-Chávez, G., Soberón, X., Bolívar, F. and Gosset, G. (2004) Metabolic engineering and protein directed evolution increase the yield of L-phenylalanine synthesized from glucose in *Escherichia coli*. Biotechnol. Bioeng. 87, 516-524

Bal'zhinimaev, B. S., Paukshtis, E. A., Suknev, A. P., Makolkin, N. V. (2018) Highly selective/enantioselective Pt-ReO_x/C catalyst for hydrogenation of L-malic acid at mild conditions. J. Energy Chem. 27, 903-912

Barbirato, F., Camarasa-Claret, C., Grivet, J. P., Bories, A. (1995) Glycerol fermentation by a new 1,3-propanediol-producing microorganism: *Enterobacter agglomerans*. Appl. Microbiol. Biotechnol. 43, 786-793

Battula, P., Dubnovitsky, A. P., Papageorgiou, A. C. (2013) Structural basis of L-phosphoserine binding to *Bacillus alcalophilus* phosphoserine aminotransferase. Acta Cryst. D69, 804-811

Becker, J., Zelder, O., Häfner, S., Schröder, H., Wittmann, C. (2011) From zero to hero--design-based systems metabolic engineering of *Corynebacterium glutamicum* for L-lysine production. Metab. Eng. 13, 159-168

Benson, D. A., Karsch-Mizrachi, I., Lipman, D. J., Ostell, J., Sayers, E. W. (2010) GenBank. Nucleic. Acids. Res. 38, D46-51

Berberich, M. A. (1972) A glutamate-dependent phenotype in *E. coli* K12: The result of two mutations. Biochem. Bioph. Res. Co. 47, No. 6

Berríos-Rivera, S. J., Bennett, G. N., San, K.-Y. (2002) Metabolic Engineering of *Escherichia coli*: Increase of NADH availability by overexpressing an NAD+-dependent formate

dehydrogenase. Metab. Eng. 4, 217-229

Bhoge, S. M., Kshirsagar, P., Richhariya, S., Singh, K. (2012) Process for the preparation of fosamprenavir calcium. US Patent 9085592B2

Biebl, H. (1991) Glycerol fermentation of 1,3-propanediol by *Clostridium butyricum*. Measurement of product inhibition by use of a pH-auxostat. Appl. Microbiol. Biotechnol. 35, 701-705

Bloom, J. D., Arnold, F. H. (2009) In the light of directed evolution: pathways of adaptive protein evolution. Proc. Natl. Acad. Sci. 9995-10000Boenigk, R., Bowien, S., Gottschalk, G. (1993) Fermentation of glycerol to 1,3-propanediol in continuous cultures of *Citrobacter freundii*. Appl. Microbiol. Biotechnol. 38, 453-457

Boisart, C. (2013) Method for the preparation of 1,3-propanediol. EP2540834A1

Bommareddy, R. R., Chen, Z., Rappert, S., Zeng, A. P. (2014) A *de novo* NADPH generation pathway for improving lysine production of *Corynebacterium glutamicum* by rational design of the coenzyme specificity of glyceraldehyde 3-phosphate dehydrogenase. Metab. Eng. 25, 30-37

Bornscheuer, U. T., Altenbuchner, J., Meyer, H. H. (1999) Directed evolution of an esterase: Screening of enzyme libraries based on pH-indicators and a growth assay. Bioorg. Med. Chem. 7, 2169-2173

Bornscheuer, U. T. and Pohl M. (2001) Improved biocatalysts by directed evolution and rational protein design. Curr. Opin. Chem. Biol. 5, 137-143

Bornscheuer, U. T., Huisman, G. W., Kazlauskas, R. J., Lutz, S., Moore, J. C., Robins, K. (2012) Engineering the third wave of biocatalysis. Nature. 485, 185-194

Bouzon, M., Perret, A., Loreau, O., Delmas, V., Perchat, N., Weissenbach, J., Taran, F., Marlière, P. (2017) A Synthetic Alternative to Canonical One-Carbon Metabolism, ACS Synth. Biol. 6, 1520-1533

Bradford, M. M. (1976) A rapid and sensitive method for the quantitation of microgram quantities of protein utilizing the principle of protein-dye binding. Anal. Biochem. 72, 248-254

Brinkmann-Chen, S., Flock, T., Cahn, J. K. B., Snow, C. D., Brustad, E. M., Mclntosh, J. A., Meinhold, P., Zhang, L., Arnold, F. H. (2013) General approach to reversing ketol-acid reductoisomerase cofactor dependence from NADPH to NADH. Proc. Natl. Acad. Sci. 110,

10946-10951

Brooks, B. R., Bruccoleri, R. E., Olafson, B. D., States, D. J., Swaminathan, S., Karplus, M. (1983) CHARMM: A program for macromolecular energy, minimization, and dynamics calculations. J. Comput. Chem. 4, 187-217

Brown, H. S., Casey, P. K., Donahue, J. M. (2000) Poly(trimethylene terephthalate) polymer for fibers. NF New Fibres

Burk, M. J. and Van Dien, S. (2016) Biotechnology for Chemical Production: Challenges and Opportunities. Trends Biotechnol. 34, 187-190

Cahn, J. K. B., Brinkmann-Chen, S., Arnold, F. H. (2018) Enzyme nicotinamide cofactor specificity reversal guided by automated structural analysis and library design. Synthetic Metabolic Pathways: Methods in Molecular Biology, vol. 1671. DOI: 10.1007/978-1-4939-7295-1_2

Cameron, D. C., Altaras, N. E., Hoffman, M. L., Shaw, A. J. (1998) Metabolic engineering of propanediol pathways. Biotechnol. Prog. 14, 116-125

Cao, Y. J., Niu, W., Guo, J. T., Xian, M., Liu, H. Z. (2015) Biotechnological production of 1,2,4-butanetriol: An efficient process to synthesize energetic material precursor from renewable biomass. Sci. Rep. 5: 18149

Case, D. A., Cheatham, T. E., III, Darden, T., Gohlke H., Luo, R., Merz, K. M. Jr, Onufriev, A., Simmerling, C., Wang, B., Woods, R. J., (2005) The Amber Biomolecular Simulation Programs. J. Comput. Chem. 26, 1668-1688

Castaño I, Bastarrachea, F., Covarrubias A. A. (1988) *glt*BDF operon of *Escherichia coli*. J. Bacteriol. 170, 821-827

Celińska, E. (2015) Fully glycerol-independent microbial production of 1,3-propanediol via non-natural pathway: paving the way to success with synthetic tiles. Biotechnol. J. 10, 242-243

Chae, T. U., Kim, W. J., Choi, S., Park, S. J., Lee, S. Y. (2015) Metabolic engineering of *Escherichia coli* for the production of 1,3-diaminopropane, a three carbon diamine. Sci. Rep. 5:13040

Chang, A., Chau, V., Landas, J., Pang, Y. (2017) Preparation of calcium competent *Escherichia coli* and heat-shock transformation. JEMI methods. 1, 22-25

Chappell, J., Westbrook, A., Verosloff, M., Lucks, J. B. (2017) Computational design of small transcription activating RNAs for versatile and dynamic gene regulation. Nat. Commun. 8:1051

Chávez-Béjar, M., Lara, A. R., López, H., Hernández-Chávez, G., Martinez, A., Ramírez, O. T., Bolívar, F., Gosset, G. (2008) Metabolic engineering of *Escherichia coli* for L-tyrosine production by expression of genes coding for the chorismate mutase domain of the native chorismate mutase-prephenate dehydratase and a cyclohexadienyl dehydrogenase from *Zymomonas mobilis*. Appl. Environ. Microbiol. 74, 3284-3290

Chen, K. and Arnold, F.H. (1993) Tuning the activity of an enzyme for unusual environments: Sequential random mutagenesis of subtilisin E for catalysis in dimethylformamide. Proc. Natl. Acad. Sci. USA 90, 5618-5622

Chen, L. (2016) Rational metabolic engineering and systematic analysis of *Escherichia coli* for L-tryptophan bioproduction. PhD thesis of Technische Universität Hamburg. Verllag Dr. Hut, München

Chen, L. and Zeng, A. P. (2017) Rational design and metabolic analysis of *Escherichia coli* for effective production of L-tryptophan at high concentration. Appl. Microbiol. Biotechnol. 101, 559-568

Chen, M. L., Chen, L., Zeng, A. P. (2019) CRISPR/Cas9-facilitated engineering with growth-coupled and sensor-guided *in vivo* screening of enzyme variants for a more efficient chorismate pathway in *E. coli*. Metab. Eng. Commun. 9, e00094

Chen, R. D. (2001) Enzyme engineering: rational redesign versus directed evolution. Trends Biotechnol. 19, No. 1

Chen, Z., Geng, F., Zeng, A. P. (2015) Protein design and engineering of a *de novo* pathway for microbial production of 1,3-propanediol from glucose. Biotechnol. J. 10, 284-289

Chen, Z., Geng, F., Zeng, A. P. (2016) Erratum: Protein design and engineering of a *de novo* pathway for microbial production of 1,3-propanediol from glucose. Biotechnol. J. DOI: 10.1002/biot.201670103

Chen, Z., Geng, F, Zeng, A. P., Dischert, W., Soucaille, P. (2016) Mutant glutamate dehydrogenase for the conversion of homoserine into 4-hydroxy-2-ketobutyrate. WO/2016/050959

Chen, Z. and Liu, D. H. (2016) Toward glycerol biorefnery: metabolic engineering for the

production of biofuels and chemicals from glycerol. Biotechnol. Biofuels. 9, 205-220

Chen, Z. and Zeng, A.P. (2016) Protein engineering approaches to chemical biotechnology. Curr. Opin. Biotechnol. 42, 198-205

Cherepanov, P. P. and Wackernagel, W. (1995) Gene disruption in *Escherichia coli*: Tc^R and Km^R cassettes with the option of Flp-catalyzed excision of the antibiotic-resistance determinant. Gene. 158, 9-14

Cong, L., Ran, F. A., Cox, D., Lin, S., Barretto, R., Habib, N., Hsu, P. D., Wu, X., Jiang, W., Marraffini, L. A., Zhang, F. (2013) Multiplex Genome Engineering Using CRISPR Cas Systems. Science. 339, 819-823

Cress, B. F., Leitz, Q. D., Kim, D. C., Amore, T. D., Suzuki, J. Y., Linhardt, R. J., Koffas, M. AG (2017) CRISPRi-mediated metabolic engineering of *E. coli* for *O*-methylated anthocyanin production. Microb. Cell Fact. 16:10

Cress, B. F., Trantas, E. A., Ververidis, F., Linhardt, R. J., Koffas, M. AG (2015) Sensitive cells: enabling tools for static and dynamic control of microbial metabolic pathways. Curr. Opin. Biotechnol. 36, 205-214

Datsenko, K. A. and Wanner, B. L. (2000) One-step inactivation of chromosomal genes in *Escherichia coli* K-12 using PCR products. Proc. Natl. Acad. Sci. USA 97, 6640-6645

Deltcheva, E., Chylinski, K., Sharma, C. M., Gonzales, K., Chao, Y., Pirzada, Z. A., Eckert, M. R., Vogel, J., Charpentier, E. (2011) CRISPR RNA maturation by trans-encoded small RNA and host factor RNase III. Nature. 471, 602-607

Dharmadi, Y. and Gonzalez, R. (2005) A better global resolution function and a novel iterative stochastic search method for optimization of high-performance liquid chromatographic separation. J. Chromatogr. A. 1070, 89-101

Dien, B. S., Cotta, M. A., Jeffries, T. W. (2003) Bacteria engineered for fuel ethanol production: current status. Appl. Microbiol. Biotechnol. 63, 258-266

Dietrich, J. A., McKee, A. E., Keasling, J. D. (2010) High-throughput metabolic engineering: advances in small-molecule screening and selection. Annu. Rev. Biochem. 79, 563-590

Dower, W. J., Miller, J. F., Ragsdale, C. W. (1988) High efficiency transformation of *E. coli* by high voltage electroporation. Nucleic. Acids. Res. 16, 6127-6145

Drewke, C., Klein, M., Clade, D., Arenz, A., Müller, R., Leistner, E. (1996) 4-O-Phosphoryl-L-threonine, a substrate of the *pdx*C (*ser*C) gene product involved in vitamin B6 biosynthesis. FEBS Lett. 390, 179-182

Ebert, M. CCJC and Pelletier, J. N. (2017) Computational tools for enzyme improvement: why everyone can – and should – use them, Curr. Opin. Chem. Biol. 37, 89-96.

Elliott, S. and Burgess, V. (2005) The presence of gamma-hydroxybutyric acid (GHB) and gammabutyrolactone (GBL) in alcoholic and non-alcoholic beverages. *Forensic Sci Int.* 151, 289-292

Emptage, M., Haynie, S.L., Laffend, L.A., Pucci, J.P., Whited, G. (2003) Process for the biological production of 1,3-propanediol with high titer. US Patent 6514733B1

Esvelt, K. M., Carlson, J. C., Liu, D. R. (2011) A system for the continuous directed evolution of biomolecules. Nature. 472, 499-503

Ferrier, B. (1990) An enzymatic cycling method for 3-acetylpyridine adenine dinucleotide to increase the sensitivity of enzymatic methods which employ this NAD analog. Anal. Biochem. 186, 229-232

Fox, R. J., Davis, S. C., Mundorff, E. C., Newman, L. M., Gavrilovic, V., Ma, S. K., Chung, L. M., Ching, C., Tam, S., Muley, S., Grate, J., Gruber, J., Whitman, J. C., Sheldon, R. A., Huisman, G. W. (2007) Improving catalytic function by ProSAR-driven enzyme evolution. Nat. Biotechnol. 25, 338-344

Frazão, C. J. R., Topham, C. M., Malbert, Y., François, J. M., Walther, T. (2018) Rational engineering of a malate dehydrogenase for microbial production of 2,4-dihydroxybutyric acid via homoserine pathway. Biochem. J. 475, 3887-3901

Frost, J. W., Niu, W. (2011) Microbial synthesis of d-1,2,4-butanetriol. US Patent 2011/0076730 A1

Geng, F., Ma, C. W., Zeng, A. P. (2017) Reengineering substrate specificity of *E. coli* glutamate dehydrogenase using a position-based prediction method. Biotechnol. Lett. 39, 599-605

Goss, T. J., Perez-Matos, A., Bender, R. A. (2001) Roles of Glutamate Synthase, *glt*BD, and *glt*F in Nitrogen Metabolism of *Escherichia coli* and *Klebsiella aerogenes*. J. Bacteriol. 183, 6607-6619

Green, A. P., Turner, N. J., O'Reilly, E. (2014) Chiral amine synthesis using omega-

transaminases: an amine donor that displaces equilibria and enables high-throughput screening. Angew. Chem. Int. Ed. 53, 10714-10717

Groeger, C., Sabra, W., Zeng, A. P. (2016) Simultaneous production of 1, 3-propanediol and n-butanol by *Clostridium pasteurianum*: In situ gas stripping and cellular metabolism. Eng. Life Sci. 16, 664-674

Guan, L. J., Ohtsuka, J., Okai, M., Miyakawa, T., Mase, T., Zhi, Y., Hou, F., Ito, N., Iwasaki, A., Yasohara, Y., Tanokura, M. (2015) A new target region for changing the substrate specificity of amine transaminases. Sci. Rep. 5:10753

Hanahan, D. (1983) Studies on transformation of *Escherichia coli* with plasmids. J. Mol. Biol. 166, 557-580

Hart, D. J. and Waldo, G. S. (2013) Library methods for structural biology of challenging proteins and their complexes. Curr. Opin. Struc. Biol. 23, 403-408

He, Y., Ma, C., Xu, J., Zhou, L. (2011) A high-throughput screening strategy for nitrile-hydrolyzing enzymes based on ferric hydroxamate spectrophotometry. Appl. Microbiol. Biotechnol. 89, 817-823

Hester, G., Stark, W., Moser, M., Kallen, J., Marković -Housley, Z., Jansonius, J. N. (1999) Crystal structure of phosphoserine aminotransferase from *Escherichia coli* at 2.3 Å resolution: Comparison of the unligated enzyme and a complex with α-methyl-L-glutamate. J. Mol. Biol. 286, 829-850

Hillyar, C. R. T. (2012) Genetic recombination in bacteriophage lambda. Bioscience Horizons. 5, 10.1093/biohorizons/hzs001

Holmgren, A. (1968) Thioredoxin. 6. The amino acid sequence of the protein from *Escherichia coli* B. European J. Biochem. 6, 475–484

Hulcher, F. H. and Oleson, W. H. (1973) Simplified spectrophotometric assay for microsomal 3-hydroxy-3-methylglutaryl CoA reductase by measurement of coenzyme A. J. Lipid Res. 14, 625-631

Ikai, K., Mikami, M., Furukawa, Y., Urano, T., Ohtaka, S. (2005) Process for preparing 1,2,4-butanetriol. US Patent 6949684B2

Imlay, J. A. (2006) Iron-sulphur clusters and the problem with oxygen. Mol. Microbiol. 59, 1073-1082

Jankowski, M. D., Henry, C. S., Broadbelt, L. J., Hatzimanikatis, V. (2008) Group contribution method for thermodynamic analysis of complex metabolic networks. Biophys. J. 95, 1487-1499

Jansonius, J. N. and Vincent, M. G. (1987) Structural basis for catalysis by aspartate aminotransferase. In Biological Macromolecules & Assemblies (Jurnak, F. A. &McPherson, A., eds), vol. 3, Active Sites of Enzymes, pp. 187-285, John Wiley & Sons, New York

Jiang, W. Y., Bikard, D., Cox, D., Zhang, F., Marraffini, L. A. (2013) RNA-guided editing of bacterial genomes using CRISPR-Cas systems. Nat. Biotechnol. 31, 233-239

Jiang, Y., Chen, B., Duan, C., Sun, B., Yang, J., Yang, S. (2015) Multigene editing in the *Escherichia coli* genome via the CRISPR-Cas9 system. Appl. Environ. Microbiol. 81, 2506-2514

Jinek, M., Chylinski, K., Fonfara, I., Hauer, M., Doudna, J. A., Charpentier, E. (2012) A Programmable Dual-RNA–Guided DNA Endonuclease in Adaptive Bacterial Immunity. Science. 337, 816-821

Jinek, M., East, A., Cheng, A., Lin, S., Ma, E., Doudna, J. (2013) RNA-programmed genome editing in human cells. eLife. 2:e00471. DOI: 10.7554/eLife.00471

Jing, P., Cao, X., Lu, X., Zong, H., Zhuge, B. (2018) Modification of an engineered *Escherichia coli* by a combined strategy of deleting branch pathway, fine-tuning xylose isomerase expression, and substituting decarboxylase to improve 1,2,4-butanetriol production. J. Biosci. Bioeng. 126, 547-552

Jocelyn, P. C. (1967) The standard redox potential of cysteine-cystine from the thiol-disulphide exchange reaction with glutathione and lipoic acid. Eur. J. Biochem. 2, 327–331

John, R. A. (1995). Pyridoxal phosphate-dependent enzymes. Biochim. Biophys. Acta 1248, 81-96

Jorgensen, W. L. (1982) Revised TIPS for simulations of liquid water and aqueous solutions. J. Chem. Phys. 77, 4156-4163

Kato, M. and Hanyu, Y. (2018) Colony assay for antibody library screening: outlook and comparison to display screening. http://dx.doi.org/10.5772/intechopen.72149

Kabil, O. and Banerjee, R. (2010) Redox biochemistry of hydrogen sulfide. J. Biol. Chem. 285, 21903–21907

Kaur, G., Srivastava, A. K., Chand, S. (2012) Advances in biotechnological production of 1,3-propanediol. Biochem. Eng. J. 64, 106-118

Kim, S. K., Seong, W., Han, G. H., Lee, D.-H., Lee, S.-G. (2017) CRISPR interference-guided multiplex repression of endogenous competing pathway genes for redirecting metabolic flux in *Escherichia coli*. Microb. Cell Fact. 16:188

Kim, S. J., Sim, H. J., Kim, J. W., Lee, Y. G., Park, Y. C., Seo, J. H. (2017) Enhanced production of 2,3-butanediol from xylose by combinatorial engineering of xylose metabolic pathway and cofactor regeneration in pyruvate decarboxylase-deficient *Saccharomyces cerevisiae*. Bioresour. Technol. 245, 1551-1557

Kleman-Leyer, K. M., Klink, T. A., Kopp, A. L., Westermeyer, T. A., Koeff, M. D., Larson, B. R., Worzella, T. J., Pinchard, C. A., van de Kar, S. A.T., Zaman, G. J.R., Hornberg, J. J., Lowery, R. G., (2009) Characterization and optimization of a red-shifted fluorescence polarization ADP detection assay. Assay Drug Dev. Technol. 7, 56–67

Koebmann, B. J., Westerhoff, H. V., Snoep, J. L., Nilsson, D., Jensen, P. R. (2002) The glycolytic flux in *Escherichia coli* is controlled by the demand for ATP. J. Bacteriol. 184, 3909-3916

Kollman, P. A., Massova, I., Reyes, C., Kuhn, B., Huo, S., Chong, L., Lee, M., Lee, T., Duan, Y., Wang, W., Donini, O., Cieplak, P., Srinivasan, J., Case, D. A., Cheatham, T.E. III, (2000) Calculating structures and free energies of complex molecules: combining molecular mechanics and continuum models. Acc. Chem. Res. 33, 889–897

Koné, F. M.T., Béchec, M. L., Sine, J.-P., Dion, M., Tellier, C. (2008) Digital screening methodology for the directed evolution of transglycosidases. Protein Eng. Des. Sel. 22, 37-44

Koresawa, M. and Okabe, T. (2004) High-Throughput Screening with Quantitation of ATP Consumption A Universal Non-Radioisotope, Homogeneous Assay for Protein Kinase. ASSAY Drug Dev. Techn. 2, 153-160

Kraus, G. A. (2008) Synthetic Methods for the Preparation of 1,3-Propanediol. CLEAN - Soil, Air, Water. 36, 648-651

Kurian, J. V. (2005) A New Polymer Platform for the Future — Sorona® from Corn Derived 1,3-Propanediol. J. Polym. Environ. 13, 159-167

LaCroix, R. A., Sandberg, T. E., O'Brien, E. J., Utrilla, J., Ebrahim, A., Guzman, G. I., Szubin,

R., Palsson, B. O., Feist, A. M. (2015) Use of adaptive laboratory evolution to discover key mutations enabling rapid growth of *Escherichia coli* K-12 MG1655 on glucose minimal medium. Appl. Environ. Microbiol. 81, 17-30

Lam, H.-M., Winkler, M. (1990) Metabolic relationships between pyridoxine (vitamin B6) and serine biosynthesis in *Escherichia coli* K-12. J. Bacteriol. 172, 6518-6528

Lambertz, C., Leidel, N., Havelius, K. G., Noth, J., Chernev, P., Winkler, M., Happe, T., Haumann, M. (2011) O_2 reactions at the six-iron active site (H-cluster) in [FeFe]-hydrogenase. J. Biol. Chem. 286, 40614-40623

Lawrence, F.R. and Sullivan, R.H. (1972) Process for making a dioxane. US Patent 3687981A

Lee, J. H., Sung, B. H., Kim, M. S., Blattner, F. R., Yoon, B. H., Kim, J. H., Kim, S. C. (2009) Metabolic engineering of a reduced-genome strain of *Escherichia coli* for L-threonine production. Microb. Cell Fact. 8:2

Lee, K. H., Park, J. H., Kim, T. Y., Kim, H. U., Lee, S. Y. (2007) Systems metabolic engineering of *Escherichia coli* for L-threonine production. Mol. Syst. Biol. 3:149

Lee, M.J., Brown, I.R., Juodeikis, R., Frank, S., Warren, M.J. (2016) Employing bacterial microcompartment technology to engineer a shell-free enzyme-aggregate for enhanced 1,2-propanediol production in Escherichia coli. Metab. Eng. 36, 48-56

Lee, S. J., Song, H., Lee, S. Y. (2006) Genome-based metabolic engineering of *Mannheimia succiniciproducens* for succinic acid production. Appl. Environ. Microbiol. 72, 1939-1948

Lee, S. Y. and Kim, H. U. (2015) Systems strategies for developing industrial microbial strains. Nat. Biotechnol. 33, 1061-1072

Leemhuis, H., Kelly, R. M., Dijkhuizen, L. (2009) Directed evolution of enzymes: Library screening strategies. IUBMB Life. 61, 222-228

Li, X., Cai, Z., Li, Y., Zhang, Y. (2014) Design and construction of a non-natural malate to 1,2,4-butanetriol pathway creates possibility to produce 1,2,4-butanetriol from glucose. Sci. Rep. 4:5541

Li, Y., Wang, X., Ge, X., Tian, P. (2016) High Production of 3-Hydroxypropionic Acid in *Klebsiella pneumoniae* by Systematic Optimization of Glycerol Metabolism. Sci. Rep. 6:26932

Liu, X., Bastian, S., Snow, C. D., Brustad, E. M., Saleski, T. E., Xu, J. H., Meinhold, P., Arnold,

F. H. (2012) Structure-Guided Engineering of *Lactococcus lactis* Alcohol Dehydrogenase LlAdhA for Improved Conversion of Isobutyraldehyde to Isobutanol. J. Biotechnol. 164, 188-195

Lu, X., He, S., Zong, H., Song, J., Chen, W., Zhuge, B. (2016) Improved 1, 2, 4-butanetriol production from an engineered *Escherichia coli* by co-expression of different chaperone proteins. World J. Microb. Biot. 32:149

Lutz, S. (2010) Beyond directed evolution: semi-rational protein engineering and design. Curr. Opin. Biotechnol. 21, 734-743

Ma, C., Ou, J., Xu, N., Fierst, J. L., Yang, S.-T., Liu, X. (2016) Rebalancing Redox to Improve Biobutanol Production by *Clostridium tyrobutyricum*. Bioengineering. 3, 2. DOI: 10.3390/bioengineering3010002

Malisi, C., Schumann, M., Toussaint, N. C., Kageyama, J., Kohlbacher, O., Höcker, B. (2012) Binding Pocket Optimization by Computational Protein Design. PloS one. 7, e52505

Marisch, K., Bayer, K., Cserjan-Puschmann, M., Luchner, M., Striedner, G. (2013) Evaluation of three industrial *Escherichia coli* strains in fed-batch cultivations during high-level SOD protein production. Microb. Cell Fact. 12:58

Mathew, S., Shin, G., Shon, M., Yun, H. (2013) High throughput screening methods for ω-transaminases. Biotechnol. Bioproc. E. 18, 1-7

Midelfort, K. S., Kumar, R., Han, S., Karmilowicz, M. J., McConnell, K., Gehlhaar, D. K., Mistry, A., Chang, J. S., Anderson, M., Villalobos, A., Minshull, J., Govindarajan, S., Wong, J. W. (2013) Redesigning and characterizing the substrate specificity and activity of Vibrio fluvialis aminotransferase for the synthesis of imagabalin. Protein Eng. Des. Sel. 26, 25-33

Mikami, Y., Shibuya, N., Kimura, Y., Nagahara, N., Ogasawara, Y., Kimura, H., (2011) Thioredoxin and dihydrolipoic acid are required for 3-mercaptopyruvate sulfurtransferase to produce hydrogen sulfide. Biochem. J. 439, 479-485

Molla, G. S., Wohlgemuth, R., Liese, A. (2016) One-pot enzymatic reaction sequence for the syntheses of d-glyceraldehyde 3-phosphate and l-glycerol 3-phosphate. J. Mol. Catal. B-Enzym. 124, 77-82

Molnos, J., Gardiner, R., Dale, G. E., Lange, R. (2003) A continuous coupled enzyme assay for bacterial malonyl–CoA: acyl carrier protein transacylase (FabD). Anal. Biochem. 319, 171–

176

Murphy, K. C. (1991) λ Gam protein inhibits the helicase and chi-stimulated recombination activities of *Escherichia coli* RecBCD enzyme. J. Bacteriol. 173, 5808-5821

Na, D., Yoo, S. M., Chung, H., Park, H., Park, J. H., Lee, S. Y. (2013) Metabolic engineering of *Escherichia coli* using synthetic small regulatory RNAs. Nat. Biotechnol. 31, 170-174

Nakamura, C. E. and Whited, G. M. (2003) Metabolic engineering for the microbial production of 1,3-propanediol. Curr. Opin. Biotechnol. 14, 454-459

Niu, W., Molefe, M. N., Frost, J. W. (2003) Microbial Synthesis of the Energetic Material Precursor 1,2,4-Butanetriol. J. Am. Chem. Soc. 125, 12998-12999

Onufriev, A., Bashford, D., Case, D. A. (2004) Exploring protein native states and large-scale conformational changes with a modified generalized born model. Proteins 55, 383-394

Paddon, C. J., Westfall, P. J., Pitera, D. J., Benjamin, K., Fisher, K., McPhee, D., Leavell, M. D., Tai, A., Main, A., Eng, D., Polichuk, D. R., Teoh, K. H., Reed, D. W., Treynor, T., Lenihan, J., Fleck, M., Bajad, S., Dang, G., Dengrove, D., Diola, D., Dorin, G., Ellens, K. W., Fickes, S., Galazzo, J., Gaucher, S. P., Geistlinger, T., Henry, R., Hepp, M., Horning, T., Iqbal, T., Jiang, H., Kizer, L., Lieu, B., Melis, D., Moss, N., Regentin, R., Secrest, S., Tsuruta, H., Vazquez, R., Westblade, L. F., Xu, L., Yu, M., Zhang, Y., Zhao, L., Lievense, J., Covello, P. S., Keasling, J. D., Reiling, K. K., Renninger, N. S., Newman, J. D. (2013) High-level semi-synthetic production of the potent antimalarial artemisinin. Nature. 496, 528-532

Pahel, G., Zelenetz, A. D., Tyler, B. M. (1978) *glt*B gene and regulation of nitrogen metabolism by glutamine synthetase in *Escherichia coli*. J. Bacteriol. 133, 139-148

Park, H. Y., Kim, J., Cho, J. H., Moon, J. Y., Lee, S. J., Yoon, M. Y. (2011) Phage display screen for peptides that bind Bcl-2 protein. J. Biomol. Screen. 16, 82-89

Park, J. H., Lee, K. H., Kim, T. Y., Lee, S. Y. (2007) Metabolic engineering of *Escherichia coli* for the production of L-valine based on transcriptome analysis and in silico gene knockout simulation. Proc. Natl. Acad. Sci. 104, 7797-7802

Park, S. H., Kim, H. U., Kim, T. Y., Park, J. S., Kim, S. S., Lee, S. Y. (2014) Metabolic engineering of *Corynebacterium glutamicum* for L-arginine production. Nat. Commun. 5:4618

Phillips, J. C., Braun, R., Wang, W., Gumbart, J., Tajkhorshid, E., Villa, E., Chipot, C., Skeel, R. D., Kale, L., Schulten, K. (2005) Scalable molecular dynamics with NAMD. J. Comput.

Chem. 26, 1781-1802

Pleiss, J. (2011) Protein design in metabolic engineering and synthetic biology. Curr. Opin. Biotechnol. 22, 611-617

Pontrelli, S., Chiu, T. Y., Lan, E. I., Chen, F. Y., Chang, P., Liao, J. C. (2018) *Escherichia coli* as a host for metabolic engineering. Metab. Eng. 50, 16-46

Porter, D. W., Maduh, E. U., Nealley, E. W., Baskin, S. I. (1993) The Inhibition of 3-Mercaptopyruvate Sulfurtransferase by Three Alpha-Keto Acids, United States Army Medical Research Institute of Chemical Defense, APG, MD 21010-5425

Porter, J. L., Rusli, R. A., Ollis, D. L. (2016) Directed Evolution of Enzymes for Industrial Biocatalysis. ChemBioChem. 17, 197-203

Prier, C. K. and Arnold, F. H. (2015) Chemomimetic biocatalysis: exploiting the synthetic potential of cofactor-dependent enzymes to create new catalysts. J. Am. Chem. Soc. 137, 13992-14006

Qi, L. S., Larson, M. H., Gilbert, L. A., Doudna, J. A., Weissman, J. S., Arkin, A. P., Lim, W. A. (2013) Repurposing CRISPR as an RNA-guided platform for sequence-specific control of gene expression. Cell. 152, 1173-1183

Reetz, M. T. (2016) What are the limitations of enzymes in synthetic organic chemistry? Chem. Rec. 16, 2449-2459

Reetz, M. T. and Carballeira, J. D. (2007) Iterative saturation mutagenesis (ISM) for rapid directed evolution of functional enzymes. Nat. Protoc. 2, 891-903

Reetz, M. T., Carballeira, J. D., Peyralans, J., Höbenreich, H., Maichele, A., Vogel, A. (2006) Expanding the substrate scope of enzymes: combining mutations obtained by CASTing. Chem. Eur. J. 12, 6031-6038

Reetz, M. T., Wang, L. W., Bocola, M. (2006) Directed evolution of enantioselective enzymes: iterative cycles of CASTing for probing protein-sequence space. Angew. Chem. Int. Ed. 45, 1236-1241

Romero, P. A. and Arnold, F. A. (2009) Exploring protein fitness landscapes by directed evolution. Nat. Rev. Mol. Cell Biol. 10, 866-876

Sato, T., Aoyagi, S., Kibayashi, C. (2003) Enantioselective total synthesis of (+)-azimine and

(+)-carpaine. Org. Lett. 5, 3839-3842

Saxena, R. K., Anand, P., Saran, S., Isar, J. (2009) Microbial production of 1,3-propanediol: Recent developments and emerging opportunities. Biotechnol. Adv. 27, 895-913

Schmitz, R., Sabra, W., Arbter, P., Hong, Y., Utesch, T., Zeng, A. P. (2019) Improved electrocompetence and metabolic engineering of *Clostridium pasteurianum* reveals a new regulation pattern of glycerol fermentation. Eng. Life Sci. 19, 412-422

Schütz, H. and Radler, F. (1984) Anaerobic reduction of glycerol to propanediol-1.3 by *Lactobacillus brevis* and *Lactobacillus buchneri*. System. Appl. Microbial. 5, 169-178

Shams Yazdani, S. and Gonzalez, R. (2008) Engineering *Escherichia coli* for the efficient conversion of glycerol to ethanol and co-products. Metab. Eng. 10, 340-351

Shibuya, N., Tanaka, M., Yoshida, M., Ogasawara, Y., Togawa, T., Ishii, K., Kimura, H. (2009) 3-Mercaptopyruvate sulfurtransferase produces hydrogen sulfide and bound sulfane sulfur in the brain. Antioxid. Redox. Sign. 11, 703-714

Siedler, S., Bringer, S., Bott, M. (2011) Increased NADPH availability in *Escherichia coli*: improvement of the product per glucose ratio in reductive whole-cell biotransformation. Appl. Microbiol. Biotechnol. 92, 929-937

Sitkoff, D., Sharp, K. A., Honig, B. (1994) Accurate Calculation of Hydration Free Energies Using Macroscopic Solvent Models. J. Phys. Chem. 98, 1978-1988

Smith, B. C., Hallows, W. C., Denu, J. M. (2009) A continuous microplate assay for sirtuins and nicotinamide-producing enzymes. Anal. Biochem. 394, 101–109

Solladie, G., Arce, E., Bauder, C., Carreno, M. C. (1998) Enantioselective synthesis of (+)-(2R, 3S, 6R)-decarestrictine L. J. Org. Chem. 63, 2332-2337

Soucaille, P. (2012) Process for the biological production of 1,3-propanediol from glycerol with high yield. US Patent 8236994B2

Soucaille, P., Boisart, C. (2012) Method for the preparation of 1,3-propanediol from sucrose. US Patent 8900838B2

Speight, R. E., Hart, D. J., Sutherland, J. D., Blackburn, J. M. (2001) A new plasmid display technology for the *in vitro* selection of functional phenotype-genotype linked proteins. Chem. Biol. 8, 951-965

Sprenger, G. A. (2007) From scratch to value: engineering *Escherichia coli* wild type cells to the production of L-phenylalanine and other fine chemicals derived from chorismate. Appl. Microbiol. Biotechnol. 75, 739-749

Sun, L., Yang, F., Sun, H., Zhu, T., Li, X., Li, Y., Xu, Z., Zhang, Y. (2016) Synthetic pathway optimization for improved 1,2,4-butanetriol production. J. Ind. Microbiol. Biot. 43, 67-78

Szostak, J. W., Orr-Weaver, T. L., Rothstein, R. J., Stahl, F. W. (1983) The double-strand-break repair model for recombination. Cell. 33, 25-35

Tang, W. L. and Zhao, H. (2009) Industrial biotechnology: tools and applications. Biotechnol J. 4, 1725-1739

Thompson, J. D., Higgins, D. G., Gibson, T. J. (1994) CLUSTAL W: improving the sensitivity of progressive multiple sequence alignment through sequence weighting, position-specific gap penalties and weight matrix choice. Nucleic. Acids. Res. 22, 4673-4680

Tong, I-T., Liao, H. H., Cameron, D. C. (1991) 1,3-Propanediol production by *Escherichia coli* expressing genes from the *Klebsiella pneumoniae dha* regulon. Appl. Environ. Microbiol. 57, 3541-3546

Truppo, M. D., Rozzell, J. D., Moore, J. C., Turner, N. J. (2009) Rapid screening and scale-up of transaminase catalysed reactions. Org. Biomol. Chem. 7, 395-398

Utesch, T., Sabra, W., Prescher, C., Baur, J., Arbter, P., Zeng, A.P. (2018) Enhanced electron transfer of different mediators for strictly opposite shifting of metabolism in *Clostridium pasteurianum* grown on glycerol in a new electrochemical bioreactor. Biotechnol. Bioeng. 116, 1627-1643

Walther, T., Calvayrac, F., Malbert, Y., Alkim, C., Dressaire, C., Cordier, H., François J. M. (2018) Construction of a synthetic metabolic pathway for the production of 2,4-dihydroxybutyric acid from homoserine. Metab. Eng. 45, 237-245

Walther, T., Cordier, H., Dressaire, C., Francois, J.M., Huet, R. (2014) Method for the preparation of 2,4-dihydroxybutyrate. WO/2014/009435

Walton, C. J. and Chica, R. A. (2013) A high-throughput assay for screening L- or D-amino acid specific aminotransferase mutant libraries. Anal. Biochem. 441, 190-198

Wang, C., Ren, J., Zhou, L. B., Li, Z. D., Chen, L., Zeng, A. P. (2019) An aldolase-catalyzed new metabolic pathway for the assimilation of formaldehyde and methanol to synthesize 2-

keto-4-hydroxybutyrate and 1,3-propanediol in *Escherichia coli*. ACS Synth. Biol. DOI: 10.1021/acssynbio.9b00102

Wang, F., Qu, H., Zhang, D., Tian, P., Tan, T. (2007) Production of 1,3-propanediol from Glycerol by Recombinant *E. coli* Using Incompatible Plasmids System. Mol. Biotechnol. 37, 112-119

Wang, H. H., Isaacs, F. J., Carr, P. A., Sun, Z. Z., Xu, G., Forest, C. R., Church, G. M. (2009) Programming cells by multiplex genome engineering and accelerated evolution. Nature. 460, 894-898

Wang, X., Xu, N. N., Hu, S. W., Yang, J. M., Gao, Q., Xu, S., Chen, K. Q., Ouyang, P. K. (2018) D-1,2,4-Butanetriol production from renewable biomass with optimization of synthetic pathway in engineered *Escherichia coli*. Bioresource Technol. 250, 406-412

Weiser, J., Shenkin, P. S., Still, W. C. (1999) Approximate atomic surfaces from linear combinations of pairwise overlaps (LCPO). J. Comput. Chem. 20, 217-230

Wittmann, C. and Liao, J. C. (Eds.) (2017) Industrial biotechnology: Products and Processes. Weinheim: Wiley-VCH Verlag GmbH & Co. KGaA (Advanced Biotechnology Ser). Page 594-602. ISBN: 978-3-527-34181-8. DOI: 10.1002/9783527807833

Xiao, H., Bao, Z., Zhao, H. (2015) High Throughput Screening and Selection Methods for Directed Enzyme Evolution. Ind. Eng. Chem. Res. 54, 4011-4020

Xu, Y., Qian, L., Pontsler, A. V., Mclntyre, T. M., Prestwich, G. D. (2004) Synthesis of difluoromethyl substituted lysophosphatidic acid analogues. Tetrahedron. 60, 43-49

Yang, G. and Withers, S. G. (2009) Ultrahigh-throughput FACS-based screening for directed enzyme evolution. ChemBioChem. 10, 2704-2715

Yim, H., Haselbeck, R., Niu, W., Pujol-Baxley, C., Burgard, A., Boldt, J., Khandurina, J., Trawick, J. D., Osterhout, R. E., Stephen, R., Estadilla, J., Teisan, S., Schreyer, H. B., Andrae, S., Yang, T. H., Lee, S. Y., Burk, M. J., Van Dien, S. (2011) Metabolic engineering of Escherichia coli for direct production of 1,4-butanediol. Nat. Chem. Biol. 7, 445-452

Yu, D., Ellis, H. M., Lee, E. C., Jenkins, N. A., Copeland, N. G., Court, D. L. (2000) An efficient recombination system for chromosome engineering in *Escherichia coli*. Proc. Natl. Acad. Sci. 97, 5978-5983

Zeng, A. P. (2019) New bioproduction systems for chemicals and fuels: Needs and new

development. Biotechnol. Adv. 37, 508-518

Zeng, A. P. and Biebl, H. (2002) Bulk chemicals from biotechnology: the case of 1,3-propanediol production and the new trends. Adv. Biochem. Eng. Biot. 74, 239-260

Zeng, A. P. and Sabra, W. (2011) Microbial production of diols as platform chemicals: recent progresses. Curr. Opin. Biotechnol. 22, 749-757

Zhang, K., Li, H., Cho, K. M., Liao, J. C. (2010) Expanding metabolism for total biosynthesis of the nonnatural amino acid L-homoalanine. Proc. Natl. Acad. Sci. 107, 6234-6239

Zhang, Y., Liu, D. H., Chen, Z. (2017) Production of C2–C4 diols from renewable bioresources: new metabolic pathways and metabolic engineering strategies. Biotechnol. Biofuels. 10, 299-319

Zhang, Y. J., Ma, C. W., Dischert, W., Soucaille, P. and Zeng, A. P. (2019) Engineering of Phosphoserine Aminotransferase Increases the Conversion of l-Homoserine to 4-Hydroxy-2-ketobutyrate in a Glycerol-Independent Pathway of 1,3-Propanediol Production from Glucose. Biotechnol. J. DOI: 10.1002/biot.201900003

Zhao, C., Zhao, Q., Li, Y., Zhang, Y. (2017) Engineering redox homeostasis to develop efficient alcohol-producing microbial cell factories. Microb. Cell Fact. 16:115

Zhao, Z. J., Zou, C., Zhu, Y. X., Dai, J., Chen, S., Wu, D., Wu, J., Chen, J. (2011) Development of L-tryptophan production strains by defined genetic modification in Escherichia coli. J. Ind. Microbiol. Biot. 38, 1921-1929

Zhong, W., Zhang, Y., Wu, W., Liu, D., Chen, Z. (2019) Metabolic Engineering of a Homoserine-Derived Non-Natural Pathway for the *De Novo* Production of 1,3-Propanediol from Glucose, ACS Synth. Biol. 8, 587-595

Zhou, H., Liao, X., Liu, L., Wang, T., Du, G., Chen, J. (2011) Enhanced L-phenylalanine production by recombinant *Escherichia coli* BR-42 (pAP-B03) resistant to bacteriophage BP-1 via a two-stage feeding approach. J. Ind. Microbiol. Biot. 38, 1219-1227

Zhou, L. B. and Zeng, A. P. (2015) Exploring lysine riboswitch for metabolic flux control and improvement of L-lysine synthesis in *Corynebacterium glutamicum*. ACS Synth. Biol. 4, 729-734

Zhou, L. B. and Zeng, A. P. (2015) Engineering a Lysine-ON Riboswitch for Metabolic Control of Lysine Production in *Corynebacterium glutamicum*. ACS Synth. Biol. 4, 1335-1340

Zhou, M. and Panchuk-Voloshima, N. (1997) A One-Step Fluorometric Method for the Continuous Measurement of Monoamine Oxidase Activity. Anal. Biochem. 253, 169-174

Zhou, M., Diwu, Z., Panchuk-Voloshina, N., Haugland, R. P. (1997) A stable nonfluorescent derivative of resorufin for the fluorometric determination of trace hydrogen peroxide: applications in detecting the activity of phagocyte NADPH oxidase and other oxidases. Anal. Biochem. 253, 162–168

Zhu, D. M., Yang, Y., Majkowicz, S., Pan, T. H.-Y., Kantardjieff, K., Hua, L. (2008) Inverting the enantioselectivity of a carbonyl reductase via substrate−enzyme docking-guided point mutation. Org. Lett. 10, 525-528

Lebenslauf

Name	Zhang
Vorname	Yujun
Staatsangehörigkeit	chinesisch
Geburtsdatum	30. April 1990
Geburtsort, -land	Shandong, China

09.1996 – 06.2002	Grundschule in Linyi, Shandong, China
09.2002 – 06.2005	Mittelschule in Linyi, Shandong, China
09.2005 – 06.2008	Oberschule in Linyi, Shandong, China
09.2008 – 06.2012	Studium Bioengineering an der Nanjing Agricultural University, Nanjing, China Abschluss: Bachelor
09.2012 – 06.2015	Studium Biocatalysis Engineering an der East China University of Science and Technology, Shanghai, China Abschluss: Master
10.2015 – heute	Studium Bioprozess- und Biosystemtechnik Engineering an der Technische Universität Hamburg, Hamburg, Deutschland